ABSTRACT

| Title of Dissertation: | HIGHLY SIDEROPHILE ELEMENTS, [187]RE-[187]OS AND [182]HF-[182]W ISOTOPIC SYSTEMATICS OF EARLY SOLAR SYSTEM MATERIALS: CONSTRAINING THE EARLY EVOLUTION OF CHONDRITIC AND ACHONDRITIC PARENT BODIES |
| | |
| | Gregory Jude Archer, Doctor of Philosophy, 2016 |
| Dissertation directed by: | Professor Richard J. Walker, Department of Geology |

Highly siderophile element (HSE) abundances and $^{187}$Re-$^{187}$Os isotopic systematics for H chondrites and ungrouped achondrites, as well as $^{182}$Hf-$^{182}$W isotopic systematics of H and CR chondrites are reported.

Achondrite fractions with higher HSE abundances show little disturbance of $^{187}$Re-$^{187}$Os isotopic systematics. By contrast, isotopic systematics for lower abundance fractions are consistent with minor Re mobilization. For magnetically separated H chondrite fractions, the magnitudes of disturbance for the $^{187}$Re-$^{187}$Os isotopic system follow the trend coarse-metal<fine-metal<silicate.

Ungrouped achondrite NWA 6704 has calculated whole-rock HSE abundances that are nearly chondritic and consistent with limited large-scale differentiation of its parent body. Most likely, this rock formed on a chondritic parent body, and crystallized

from a melt from which little or no metal was removed. Modest variations in the relative HSE abundances among bulk pieces may have been the result of sulfide loss or evolving oxidation state during crystallization. The HSE abundances of ungrouped achondrite NWA 7325 are highly fractionated and depleted, relative to bulk chondrites. Therefore, its parent body must have undergone complex processing, including core formation, late accretion, and igneous processes.

A negative thermal ionization mass spectrometry (N-TIMS) technique was developed to measure the W isotopic compositions of H chondrite metal fractions. This method is capable of measuring $^{182}W/^{184}W$ to an external precision of 5.7 ppm and $^{183}W/^{184}W$ to 6.7 ppm, which is ~2-3x more precise than the most recently published technique capable of measuring $^{182}W/^{184}W$ and $^{183}W/^{184}W$.

The HSE abundances of H chondrite nonmagnetic fractions are too high to reflect equilibration between metals and silicates. There is also no correlation between metamorphic grade and apparent degree of equilibration. The $^{182}Hf$-$^{182}W$ isotopic systematics of H chondrite magnetic separates do not form precise isochrons for most H chondrites, consistent with disequilibrium among the separates. However, the slightly magnetic and nonmagnetic separates from most H chondrites do form precise isochrons. The calculated slope ages are inconsistent with the onion shell thermal model, in which H4 chondrites cooled fastest and H6 chondrites cooled slowest. Instead, the data indicate that the H chondrite parent body must have been disrupted, possibly by impact, early in Solar System history.

HIGHLY SIDEROPHILE ELEMENTS, $^{187}$RE-$^{187}$OS AND $^{182}$HF-$^{182}$W ISOTOPIC
SYSTEMATICS OF EARLY SOLAR SYSTEM MATERIALS:
CONSTRAINING THE EARLY EVOLUTION OF CHONDRITIC AND
ACHONDRITIC PARENT BODIES

by

Gregory J. Archer

Dissertation submitted to the Faculty of the Graduate School of the
University of Maryland, College Park, in partial fulfillment
of the requirements for the degree of
Doctor of Philosophy
2016

Advisory Committee:
 Professor Richard Walker, Chair
 Professor James Farquhar
 Dr. Richard Ash
 Dr. Conel Alexander
 Professor Derek Richardson

# Preface

Chapters 2, 3, and 4 consist primarily of text that is intended for peer-reviewed publications. The text from these chapters are either currently in review, or will be submitted to peer-reviewed journals soon. Here the work that each coauthor contributed to the chapters of this dissertation are detailed.

**Chapter 2** Some sections are included in the following manuscripts:

Hibiya Y., **Archer G.J.**, Tanaka R., Iizuka T., Ozawa K., Walker R.J., and Yamaguchi A. The origin and formation process of the NWA 6704 primitive achondrite: Petrology, highly siderophile element chemistry, and O-Ti isotope systematics, in prep.

Irving A.J., Kuehner S.M., Sharp T.G., Hu J., Ziegler K., Conrey R.M., Chen G., **Archer G.J.**, Walker R.J., Sanborn M.E., Yin Q., Williams N.H., Schönbächler M., Andreason R., Righter M., Lapen T.J., Kleine T., Huber L., Wieler R., Britt D.T., and Jull A.J.T. A unique iron-poor, highly reduced olivine gabbroic achondrite meteorite sample from a differentiated planetary parent body, in prep.

For both of these sections, I collected the highly siderophile element and Re-Os data. With the help of Rich Walker, I also made interpretations of the data, and provided them to the above manuscripts. For the purposes of this dissertation, only the data and the interpretations for HSE abundances and Re-Os systematics are included.

**Chapter 3**

**Archer G.J.**, Mundl A., Walker R.J., Worsham E.A., and Bermingham K. (2016) High-precision analysis of $^{182}W/^{184}W$ and $^{183}W/^{184}W$ by negative thermal ionization mass spectrometry: Per-integration oxide corrections using measured $^{18}O/^{16}O$. *Int. J. Mass Spec.*, in review.

With the help of all coauthors, I developed an improved technique for measuring W via N-TIMS. I collected about 50% of the data, and Andi Mundl collected the other 50%. I wrote the text for the manuscript, and edits were primarily provided by Rich Walker.

**Chapter 4**

**Archer G.J.**, Walker R.J., Kleine T., Blackburn T., Wasson J.T., Kruijer T.S., and Tino J. $^{182}$Hf-$^{182}$W, $^{187}$Re-$^{187}$Os, and Highly Siderophile Elements of H Chondrites: Constraining the Thermal History of the H Chondrite Parent Body, in prep.

I collected all of the Hf-W data for H chondrites, with guidance from Mathieu Touboul, Rich Walker, Thomas Kruijer, and Thorsten Kleine. Jon Tino did the chemical separations of HSE from H4-6 metal and silicate samples with my guidance, and we measured the analytes together. With the help of Rich Walker, I produced the text for the manuscript.

# Foreword

The truth is, most of us discover where we are heading when we arrive.

-Bill Watterson

# Dedication

To my wife, Sara, for her unwavering love and support

We will look back on this time and cherish it

# Acknowledgements

I would like to thank Rich Walker, James Farquhar, Richard Ash, Conel Alexander, and Derek Richardson for being on my PhD committee, reading through this entire dissertation, and providing feedback. I would also like to thank Bill McDonough for being on my PhD proposal committee.

In the six years I have been at the University of Maryland, I have had help and advice from many colleagues and friends. Rich Walker has spent countless hours providing mentorship, reviewing manuscripts, discussing ideas, and sharing professional experience, and I am truly grateful. Rich's influence will shape the way I approach scientific problems long after I graduate. I would also like to thank Richard Ash, Bill McDonough, Igor Puchtel, and James Farquhar for always being willing to share professional experience, analytical expertise, and wisdom. I would like to thank Emily Worsham for her comradery through graduate school. I would also like to thank Katherine Bermingham, Jingao Liu, Andi Mundl, Mathieu Touboul, Jeremy Bellucci, Nick Sharp, Miriam Sharp, Brian Tattich, Mitch Haller, Connor Hilton, and all of my fellow graduate students for their friendship, advice, and moral support. I would like to thank Michelle Montero for guiding me through the PhD defense process.

I met my wife, Sara, at the University of Maryland, and marrying her has been my greatest success. Sara, my parents, brothers, sister, and their spouses have unfailingly supported me, and I wouldn't be the person I am today without their support and love.

# Table of Contents

# List of Tables

# List of Figures

# List of Abbreviations

AGB – asymptotic giant branch

ALHA – Allan Hills

BSE – bulk silicate Earth

CAI – calcium-aluminum-rich inclusion

CCAM – carbonaceous chondrite anhydrous mineral

CRE – cosmic ray exposure

GRA – Graves Nunataks

HED – howardite-eucrite-diogenite

HPA-S – high pressure asher

HSE – highly siderophile elements

IGL – Isotope Geochemistry Lab

MC-ICP-MS – multi collector-inductively coupled plasma mass spectrometry

MSWD – mean square weighted deviation

N-TIMS – negative thermal ionization mass spectrometry

NWA – Northwest Africa

PGM – platinum group minerals

UCLA – University of California Los Angeles

UMd – University of Maryland

USNM – United States National Museum

# Chapter 1: Introduction

## *1.1. General Purpose*

Constraining the early chemical evolution of planetary bodies is fundamental for developing models for the formation of asteroids and rocky planets. However, direct evidence for some of the complex processes that were involved in early planetary evolution are inaccessible for large planetary bodies, like Earth. Therefore, another source of information, meteorites that underwent widespread planetary processes early in Solar System history, must be studied to provide direct evidence for early planetary processes, including thermal alteration and early differentiation. In addition, the investigation and comparison of samples from a variety of undifferentiated and differentiated parent bodies can provide further evidence for the diversity of parent bodies and parent body processes that occurred in early Solar System history.

## *1.2. The Early Solar System and Formation of Planetary Bodies*

The formation of the Solar System was initiated by the collapse of a molecular cloud, possibly because of a nearby supernova (e.g., Cameron, 1962). During the collapse, gravity and conservation of angular momentum drove the formation of a young, T-Tauri star surrounded by a protoplanetary disk of gas and dust (Adams, 2010). The Solar System at this stage is referred to as the solar nebula. Within a few hundred thousand years of the formation of the Solar System defined by the formation of calcium-aluminum-rich inclusions (CAIs), the first stages of planetary growth began.

The growth of planetary bodies after the formation of CAIs occurred in a sequence of stages, and a description of those stages is summarized here from Dauphas and Chaussidon (2012). First, through condensation of nebular gas, solid rocky material formed and was mixed with presolar dust (Fig. 1.1). Dust grains then aggregated through Brownian motion, turbulence, and differential vertical settling into dust agglomerates. Growing dust agglomerates were first compacted by collisions, and then eventually fragmented by further collisions. Perhaps because of gravitational instabilities in a turbulent disk, dust aggregates combined further and were processed into 1-1000 km planetesimals. The ensuing growth of planetesimals resulted in the formation of Moon- to Mars-sized embryos (1,000-5,000 km) at regular intervals in heliocentric orbit. The collisional merging of embryos ultimately led to the formation of terrestrial planets, like Earth.
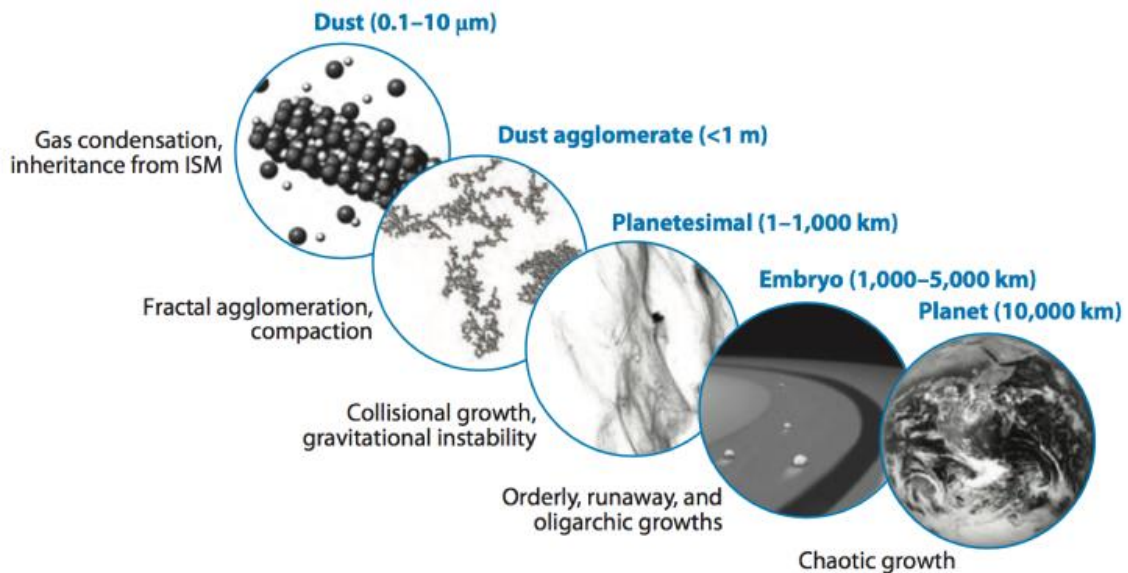


Figure 1.1. The evolutionary stages of matter in the early Solar System. Figure from Dauphas and Chaussidon (2012).

## 1.3. Differentiation of Planetary Bodies

The interiors of some primitive rocky planetary bodies were heated extensively enough to melt and differentiate into outer silicate shells and Fe-rich cores. Differentiation must have been widespread, as all the terrestrial planets and some asteroids are differentiated. A primary heat source for melting early in Solar System history was probably the decay of short-lived $^{26}$Al (e.g., Urey, 1955; Hevey and Sanders; 2006; see section 1.6 for more information about short-lived isotopes). Additional heat sources include the release of kinetic and gravitational energy during impacts and gravitational energy during differentiation, and residual accretionary heat. The amount of heating an early formed parent body experienced and the degree to which it differentiated was likely proportional to the abundance of $^{26}$Al that was still extant in the early Solar System at the time of accretion, and the size of the parent body, as rocky material acted as an insulator.

## 1.4. A Record of the Early Solar System Provided by Meteorites

Meteorites are extraterrestrial objects that survived transit through Earth's atmosphere, and arrived on Earth's surface. They are broadly divided based on their inferred origins from either undifferentiated or differentiated parent bodies (Krot et al., 2014). Here general background information will be provided about some of the broadest classes of meteorites found in meteorite collections.

Some parent bodies were either too small or formed too late to be melted by the decay of $^{26}$Al. Model calculations from Scott et al. (2014) indicate that parent bodies with radii of 50-100 km that formed ~2 million years after Solar System formation may

have experienced enough radiogenic heating (peak temperatures of ~550ºC to ~1050ºC) to cause widespread thermal metamorphism, but not enough heating to cause extensive melting. Samples from parent bodies that did not undergo melting or differentiation are classified as chondrites, and they retain evidence for the processes that occurred in the solar nebula, including high temperature condensation/evaporation. They are aggregates of varying amounts of three main components: refractory inclusions (calcium-aluminum-rich inclusions and ameboid olivine aggregates or AOAs), chondrules, and matrix. The CAIs represent the most refractory and likely oldest material to have formed in our Solar System (e.g., Grossman, 1972; Gray et al., 1973), and their formation, possibly as condensates, is considered to define the beginning of the Solar System. Bouvier and Wadhwa (2010) reported a $^{207}$Pb-$^{206}$Pb age of 4568.2±0.17 for a CAI from a CV3 chondrite. Chondrules are less refractory and may have formed 2-3 million years later, although this has been disputed (Connelly et al., 2012). Matrix is the least refractory material found in chondrites. In addition to these main components, some chondrites also contain varying amounts of Fe,Ni-rich metal, which may have formed during formation of chondrules (Connolly et al., 2001).

Meteorites from parent bodies that underwent melting and differentiation are classified as achondrites, and they provide direct evidence for widespread planetary processes like core formation, crust-mantle formation, and late accretion. Achondrites vary wildly in bulk elemental compositions and textures, and may originate from different regions of multiple planetary bodies. For example, many so called "magmatic" iron meteorite groups are comprised almost entirely of Fe,Ni metal, and likely originated from the cores of planetary bodies. Complementary to the magmatic

iron meteorites are silicate-rich differentiated achondrites, such as members of the Howardite-Eucrite-Diogenite clan, which are thought to have originated from the silicate portion of a planetary body that produced and segregated an iron-rich core (Righter and Drake, 1997a; Day et al., 2012). For a more detailed review of achondrites, see section 2.2.1.

## *1.5. Highly Siderophile Elements and the $^{187}Re$-$^{187}Os$ Isotopic System*

The highly siderophile elements (HSE), including Re, Os, Ir, Ru, Pt, and Pd have geochemical properties that make them useful for examining large-scale planetary processes. Low-pressure experimental studies have reported that the HSE have liquid metal/liquid silicate distribution coefficients (D values) that are $>10^4$ (e.g., Kimura et al., 1974; Newsom, 1990; O'Neill et al., 1995; Borisov and Palme, 1995; Fortenfant et al., 2003; Brenan et al., 2016). The HSE are, therefore, strongly partitioned into metal relative to silicates during equilibration. Further, because of inter-elemental variations in metal-silicate distribution coefficients, the HSE are also fractionated from each other by metal-silicate equilibration.

Because of their siderophile properties, the HSE have been used extensively to investigate metal-silicate equilibration in planetary bodies that have melted and segregated iron-rich cores from silicate outer shells (mantle ± crust). Most iron meteorites are enriched in HSE relative to bulk chondrites (e.g., Smoliar et al., 1996; Walker et al., 2008; McCoy et al., 2011). Differentiated achondrites that are dominated by silicates are complements to magmatic iron meteorites. They were probably derived from the mantles and crusts of differentiated planetary bodies and, therefore, have HSE

abundances that are depleted and fractionated relative to bulk chondrites (e.g., Day et al., 2012; Day et al., 2016).

Although metal-silicate equilibration should effectively strip and fractionate the HSE from the silicate portions of planetary bodies during metal segregation and core formation, the bulk silicate portions of Earth (e.g., Becker et al., 2006; Fischer-Gödde et al., 2011), Mars (Brandon et al., 2012), the Moon (Day et al., 2007), and some differentiated asteroids (e.g., Day et al., 2012; Dale et al. 2012) have relative HSE abundances that are less fractionated and depleted relative to bulk chondrites than predicted by low-pressure metal-silicate partition coefficients. The Earth and Mars have similar HSE abundances that are ~0.007-0.009x CI (Ivuna-type) chondrite, and the Moon has ~0.0002x CI chondrite HSE (Fig. 1.2).
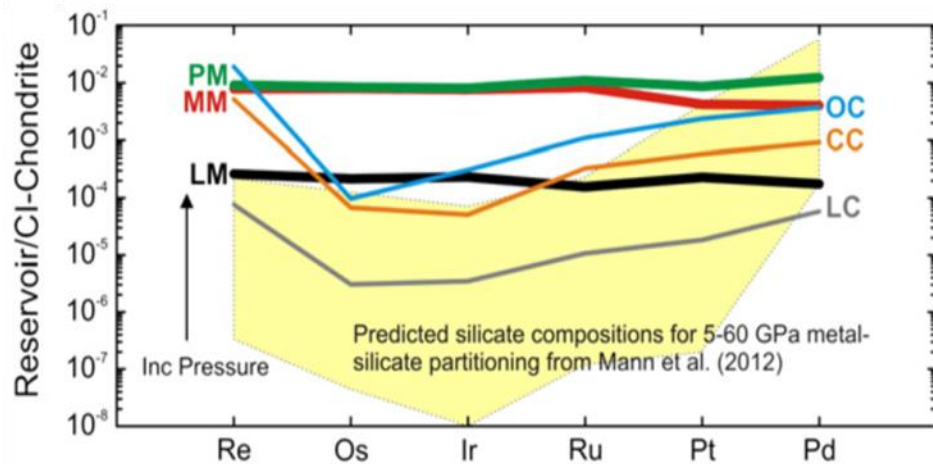


Figure 1.2. Estimated highly siderophile element abundances, normalized to CI chondrites, of different reservoirs from the Moon (LM=lunar mantle; LC=lunar crust), Mars (MM=martian mantle), and Earth (PM=primitive mantle; OC=oceanic crust; CC=continental crust). Highly siderophile elements are arranged from left to right in order of increasing volatility. Yellow field represents range of high-pressure metal-silicate partition coefficients from Mann et al. (2012). Modified from Day (2013).

Some prior studies (e.g., Ringwood, 1977; Murthy, 1991; Righter and Drake; 1997b; Righter et al., 2015) have argued that the abundances of HSE in silicate portions of some planetary bodies could be the result of metal-silicate partitioning at relatively high pressures and temperatures, such as those found at the base of a deep magma ocean. This is based on experimental observations that most HSE become less siderophile with increasing temperatures and pressures (e.g., Mann et al., 2012; Righter et al., 2015). For example, Mann et al. (2012) investigated HSE metal-silicate partitioning under a range of pressure (3.5-18 GPa) and temperature (2423-2773 K) conditions, and they reported a strong temperature and pressure dependence on HSE metal-silicate partitioning (Fig. 1.2). However, they also reported that metal-silicate partitioning, even at pressure and temperature conditions appropriate for the base of a terrestrial magma ocean, cannot account for the HSE abundances of planetary bodies with chondrite-relative HSE abundances, such as observed for the Earth. Nonetheless, the HSE abundances of some differentiated meteorites may retain evidence for metal-silicate partitioning under the pressure and temperature conditions of their respective parent bodies.

Prior studies have argued that late accretion returned HSE to the silicate portions of at least some planetary bodies (e.g., Chou, 1978, Bottke et al., 2010; Brandon et al., 2012; Day et al., 2007; Dale et al., 2012; Day et al., 2012). Late accretion is defined as the mixing of materials (typically with broadly chondritic compositions) into the silicate portions of planetary bodies subsequent to core formation, raising HSE abundances and overprinting HSE fractionations caused by primary metal-silicate equilibration. Walker et al., (2015) compared the estimated HSE

concentrations of bulk silicate Earth (BSE) to those of different chondrite groups. They argued that the last approximately 0.5% of material added to Earth by late accretion had similar relative HSE abundances, except for Ru, to those of enstatite chondrites, resulting in enstatite chondrite-like relative HSE abundances of BSE. Late accretion has also been proposed for the Moon (Day et al., 2007), Mars (Brandon et al., 2012), and some differentiated asteroids (Day et al., 2012).

One additional complexity in the interpretation of primary planetary HSE data is the fact that igneous processes within the silicate portions of planetary bodies can also fractionate HSE. In planetary mantles, the HSE are typically hosted in sulfides and platinum-group minerals (PGM), and have diverse compatibilities (e.g., Barnes and Naldrett, 1985; Walker et al., 1999; Pearson et al., 2004; Puchtel et al., 2004; 2007; Day et al., 2010). For example, during partial melting of the terrestrial mantle, Re, Pt, and Pd typically behave incompatibly, whereas Os, Ir, and Ru typically behave compatibly. However, the compatibilities of some HSE are highly dependent on O fugacity. For example, Re behaves more compatibly in the silicate portions of some other planetary bodies, like the Moon and Mars possibly because of lower O fugacity (Birck and Allégre, 1994). Despite the complexities involved in modeling HSE in silicate systems, the HSE remain useful tools for investigating melting and crystallization processes.

The long-lived $^{187}$Re-$^{187}$Os isotopic system is a radiogenic system comprised of two of the HSE. Through negative beta decay, $^{187}$Re decays to $^{187}$Os ($\lambda$=1.666 x 10$^{-11}$ a$^{-1}$). This system can potentially be used to date the crystallization of early Solar System, HSE-rich materials like iron meteorites (e.g., Smoliar, 1996). In primitive

stony meteorites, limited ranges in Re/Os usually prohibit the use of this system as a precise chronometer, but it can be used to assess secondary processes that have affected some meteorites (open-system behavior), either in their respective parent bodies or by terrestrial alteration (e.g., Becker et al., 2001; Archer et al., 2014). In rocks derived from the silicate portions of some planetary bodies, the system may also be useful for constraining mantle processes if Re is depleted during partial melting (Shirey and Walker, 1998). Constraints on the timing of melt depletion can be made by comparing the $^{187}Os/^{188}Os$ of residual mantle material to models of bulk mantle $^{187}Re$-$^{187}Os$ evolution (e.g., Rudnick and Walker, 2009; Brandon et al., 2012).

In Chapter 2 of this dissertation, the HSE abundances and $^{187}Re$-$^{187}Os$ isotopic systematics of two ungrouped achondrites are used to investigate long-term retention of primary HSE abundances, and then used to generate models for the formation of these achondrites. The HSE abundances of the ungrouped achondrites are compared to the HSE characteristics of various achondrite groups in order to explore the variety of planetary bodies sampled by achondrites. In Chapter 4 of the dissertation, the HSE abundances and $^{187}Re$-$^{187}Os$ isotopic systematics of H chondrites are examined in order to investigate the extent of diffusive exchange of the HSE among phases during thermal metamorphism in asteroidal parent bodies.

## 1.6. Short-lived Isotopic Systems

Short-lived radiogenic isotope systems (e.g., $^{26}Al$-$^{26}Mg$, $^{53}Mn$-$^{53}Cr$, and $^{60}Fe$-$^{60}Ni$) have half-lives of typically less than 100 million years (Wadhwa et al., 2007). Their existence in the early Solar System has been inferred by excesses of their

daughter isotopes in some meteorites. Because they have such short lifespans, their presence indicates that sources of newly synthesized nuclides must have been nearby during the formation of the Solar System. Some sources that have been invoked to produce the parent isotopes include AGB stars (e.g., Wasserburg et al., 2006) and supernovae (e.g., Meyer and Clayton, 2000). Local production of some nuclides by irradiation resulting from an early active stage of the Sun's evolution is also possible (e.g., McKeegen et al., 2000).

Short-lived isotopic systems not only provide information about the local environment feeding the early Solar System, but they can also be used to provide chronological constraints for early Solar System processes. For example, prior studies have used the short-lived $^{26}$Al-$^{26}$Mg isotopic system to constrain the relative formation ages of CAIs (e.g., Bouvier and Wadhwa, 2010; MacPherson et al., 2012) and achondrites (e.g., Spivak-Birndorf et al., 2009).

*1.7. The Short-lived $^{182}$Hf-$^{182}$W Isotopic System*

The short-lived $^{182}$Hf-$^{182}$W isotopic system ($t_{1/2}$ = 8.9±0.09 Ma) is useful for constraining metal-silicate equilibration processes within the first ~50 million years of Solar System history because Hf is lithophile, and W is siderophile (Kleine et al., 2009). For example, the Hf-W system has been used extensively to constrain the ages of core formation by measuring the W isotopic compositions of iron meteorites (e.g., Lee and Halliday, 1995; Harper and Jacobsen, 1996; Kruijer et al., 2014a). Iron meteorite model ages are based on the assumptions of chondritic Hf/W for the parent bodies prior to core segregation, and equilibration between metals and silicates up to the point of metal

separation. For silicate-rich samples with components that contain variable proportions of Hf and W, plots of Hf/W vs. $^{182}$W/$^{184}$W can yield internal Hf-W isochrons that can be used to determine relative formation or closure ages. Prior studies have, consequently, used Hf-W isochrons to calculate formation or isotopic closure ages of bulk chondrites (Kleine et al., 2008), CAIs (Kruijer et al., 2014b), and achondrites (Budde et al., 2015).

The W isotopic compositions of meteorites can also provide information about the degree of isotopic homogenization of W in the early Solar System. Recent studies have reported that some meteorites are characterized by correlated variations in the abundances of $^{182}$W and $^{183}$W (termed nucleosynthetic effects; Burkhardt et al., 2012; Kruijer et al., 2014b) that can be attributed to the inclusion of different proportions of presolar materials with distinct W isotopic compositions into their parent bodies. In order to investigate these effects in meteorites, a high-precision negative thermal ionization mass spectrometry (N-TIMS) method, capable of measuring the abundances of both $^{182}$W and $^{183}$W to external precisions ~5 ppm (2SD), was developed and is reported in Chapter 3. In Chapter 4, the $^{182}$Hf-$^{182}$W of H chondrite magnetic separates are investigated to constrain the thermal histories of H chondrite parent bodies. The new analytical technique is utilized for magnetic (primarily metal) fractions to examine the degree of isotopic homogenization of W in the early Solar System.


*References for Chapter 1*

Adams F.C. (2010) The birth environment of the Solar System. *Ann. Rev. Astron. and Astrophys.* **48**, 47-85.

Archer G.J., Ash R.D., Bullock E.S., and Walker R.J. (2014) Highly siderophile elements and [187]Re-[187]Os isotopic systematics of the Allende meteorite: Evidence for primary nebular processes and late-stage alteration. *Geochim. Cosmochim. Acta* **131**, 402-414.

Barnes S.-J., Naldrett A.J., and Gorton M.P. (1985) The origin of the fractionation of platinum-group elements in terrestrial magmas. *Chem.Geol.* **53**, 302–323.

Becker H., Morgan J.W., Walker R.J., MacPherson G.L. and Grossman J.N. (2001) Rhenium–osmium systematics of calcium–aluminum-rich inclusions in carbonaceous chondrites. *Geochim. Cosmochim. Acta* **65**, 3379–3390.

Becker H., Horan M.F., Walker R.J., Gao S., Lorand J.-P., and Rudnick R.L (2006) Highly siderophile element composition of the Earth's primitive upper mantle: constraints from new data on peridotite massifs and xenoliths. *Geochim. Cosmochim. Acta* **70**, 4528–4550.

Birck J.L. and Allégre C.L. (1994) Contrasting Re/Os magmatic fractionation in planetary basalts. *Earth Planet. Sci. Lett.* **124**, 139–148.

Borisov A. and Palme H. (1998) Experimental determination of osmium metal-silicate partitioning coefficient. *Neues Jb. Miner. Abh.* **172**, 347–356.

Bottke W.F., Walker R.J., Day J.M.D., Nesvorny D., and Elkins-Tanton L. (2010) Stochastic late accretion to Earth, the Moon, and Mars. *Science* **330**:1527–1530.

Bouvier A. and Wadhwa M. (2010) The age of the solar system redefined by the oldest Pb–Pb age of a meteoritic inclusion. *Nature Geosci.* **3**, 637–641.

Brandon A.D., Puchtel I.S., Walker R.J., Day J.M.D., Irving, A.J., and Taylor L.A. (2012) Evolution of the martian mantle inferred from the [187]Re-[187]Os isotope and highly siderophile element abundance systematics of shergottite meteorites. *Geochim. Cosmochim. Acta* **76**, 206-235.

Brenan J.M., Bennett N.R., and Zajacz Z. (2016) Experimental results on fractionation of the highly siderophile elements (HSE) at variable pressures and temperatures during planetary and magmatic differentiation. *Rev. Mineral. Geochem.* **81**, 1–87.

Budde G., Kruijer T.S., Fischer-Gödde M., Irving A.J. and Kleine T. (2015) Planetesimal differentiation revealed by the Hf-W systematics of ureilites. *Earth Planet. Sci. Lett.* **430**, 316–325.

Burkhardt C., Kleine T., Dauphas N., and Wieler R. (2012) Nucleosynthetic tungsten isotope anomalies in acid leachates of the Murchison chondrite: implications for hafnium-tungsten chronometry. *Astrophys. J. Lett.* **753**, L6.

Cameron A.G.W. (1962) The formation of the Sun and planets. *Icarus* **1**, 13-69.

Connelly J., Bizzarro M., Krot A.N., Nordlund A., Wielandt D. and Ivanova M.A. (2012) The absolute chronology and thermal processing of solids in the solar protoplanetary disk. *Science* **338**, 651–655.

Connolly H.C., Huss G.R., and Wasserburg G.J. (2001) On the formation of Fe-Ni metal in Renazzo-like carbonaceous chondrites. *Geochim. Cosmochim. Acta* **65**, 4567–4588.

Chou C.-L. (1978) Fractionation of siderophile elements in the Earth's upper mantle. *Proc. 9th Lunar Planet. Sci. Conf.*, 219–230.

Dale C.W., Burton K.W., Greenwood R.C., Gannoun A., Wade J., Wood B., and Pearson D.G. (2012) Late accretion on the earliest planetesimals revealed by the highly siderophile elements. *Science* **336**, 72–75.

Dauphas N. and Chaussidon M. (2011) A Perspective from Extinct Radionuclides on a Young Stellar Object: The Sun and Its Accretion Disk. *Ann. Rev. Earth Planet. Sci.* **39**, 351-386.

Day J.M.D. (2013) Hotspot volcanism and highly siderophile elements. *Chem. Geol.* **341**, 50–74.

Day J.M.D., Pearson D.G., and Taylor L.A. (2007) Highly siderophile element constraints on accretion and differentiation of the Earth–Moon system. *Science* **315**, 217–219.

Day J.M.D., Pearson D.G., Macpherson C.G., Lowry D. and Carracedo J.C. (2010) Evidence for distinct proportions of subducted oceanic crust and lithosphere in HIMU-type mantle beneath El Hierro and La Palma, Canary Islands. *Geochim. Cosmochim. Acta* **74**, 6565–6589.

Day J.M.D., Walker R.J., Qin L., and Rumble D. III. (2012) Late accretion as a natural consequence of planetary growth. *Nat. Geosci.* **5**, 614–617.

Day J.M.D., Brandon A.D., and Walker R.J. (2016) Highly siderophile elements in Earth, Mars, the Moon, and asteroids. *Rev. Mineral. Geochem.* **81**, 161–238.

Fischer-Gödde M., Becker H., and Wombacher F. (2011) Rhodium, gold and other highly siderophile elements in orogenic peridotites and peridotite xenoliths. *Chem. Geol.* **280**, 365–383.

Fortenfant S.S., Günther D., Dingwell D. B. and Rubie D. C. (2003) Temperature dependence of Pt and Rh solubilities in a haplobasaltic melt. *Geochim. Cosmochim. Acta* **67**, 123–131.

Gray C. M., Papanastassiou D. A. and Wasserburg G. J. (1973) The identification of early condensates from the solar nebula. *Icarus* **20**, 213–239.

Grossman L. (1972) Condensation in the primitive solar nebula. *Geochem. Cosmochim. Acta* **36**, 597–619.

Harper C.L. and Jacobsen S.B. (1996) Evidence for $^{182}$Hf in the early Solar System and constraints on the timescale of terrestrial accretion and core formation, *Geochim. Cosmochim. Acta* **60**, 1131–1153.

Hevey P. J. and Sanders I. S. (2006) A model for planetesimal meltdown by Al-26 and its implications for meteorite parent bodies. *Meteoritics & Planetary Science* **41**, 95-106.

Kimura, K., Lewis, R.S., and Anders, E. (1974) Distribution of gold and rhenium between nickel– iron and silicate melts: implications for the abundance of siderophile elements on the Earth and Moon. *Geochim. Cosmochim. Acta* **38**, 683–701.

Kleine T., Touboul M., Van Orman J.A., Bourdon B., Maden C., Mezger K. and Halliday A.N. (2008) Hf-W thermochronometry: Closure temperature and constraints on the accretion and cooling history of the H chondrite parent body. *Earth Planet. Sci. Lett* **270**, 106-118.

Kleine T., Touboul M., Bourdon B., Nimmo F., Mezger K., Palme H., Jacobsen S.B., Yin Q.Z. and Halliday A.N. (2009) Hf-W chronology of the accretion and early evolution of asteroids and terrestrial planets. *Geochim. Cosmochim. Acta* **73**, 5150-5188.

Krot A.N., Keil K., Scott E.R.D., Goodrich C.A., and Weisberg M.K. (2014) Classification of meteorites and their genetic relationships. In *Treatise on Geochemistry, Vol. 1: Meteorites and Cosmochemical Processes* (ed. A. M. Davis) Elsevier, Oxford. pp. 1–63.

Kruijer T.S., Touboul M., Fischer-Godde M., Bermingham K.R., Walker R.J. and Kleine T., (2014a) Protracted core formation and rapid accretion of protoplanets. *Science* **344**, 1150–1154.

Kruijer T. S., Kleine T., Fischer-Gödde M., Burkhardt C. and Wieler R. (2014b) Nucleosynthetic W isotope anomalies and the Hf-W chronometry of Ca-Al-rich inclusions. *Earth Planet. Sci. Lett.* **403**, 317–327.

14

Lee D.C. and Halliday A.N. (1995) Hafnium–tungsten chronometry and the timing of terrestrial core formation. *Nature* **378**, 771–774.

MacPherson G.J., Kita N.T., Ushikubo T., Bullock E.S. and Davis A.M. (2012) Well-resolved variations in the formation ages for Ca–Al-rich inclusions in the early Solar System. *Earth Planet. Sci. Lett.* **331–332**, 43–45.

Mann U., Frost D.J., Rubie D.C., Becker H., and Audétat A. (2012) Partitioning of Ru, Rh, Pd, Re, Ir and Pt between liquid metal and silicate at high pressures and temperatures- Implications for the origin of highly siderophile element concentrations in the Earth's mantle. *Geochim. Cosmochim. Acta* **84**, 593–613.

McCoy T.J., Walker R.J., Goldstein J.I., Yang J., McDonough W.F., Rumble D., Chabot N.L., Ash R.D., Corrigan C.M., Michael J.R., and Kotula P.G. (2011) Group IVA irons: new constraints on the crystallization and cooling history of an asteroidal core with a complex history. *Geochim. Cosmochim. Acta.* **75**, 6821–6843.

McKeegan K.D., Chaussidon M., and Robert F. (2000) Incorporation of short-lived 10Be in a calcium–aluminum-rich inclusion from the Allende meteorite. *Science* **289**, 1334–1337.

Meyer B. and Clayton D. (2000) Short-Lived radioactivities and the birth of the Sun. *Space Sci. Rev.* **92**, 133-152.

Murthy V. (1991) Early differentiation of the Earth and the problem of mantle siderophile elements; a new approach. *Science* **253**, 303–306.

Newsom H.E. (1990) Accretion and core formation in the Earth: evidence from siderophile elements. In *Origin of the Earth* (eds. H.E. Newsom and J.H. Jones) Oxford Univ. Press, New York, pp. 273–288.

O'Neill H.S.C., Dingwell D.B., Borisov A., Spettel B., and Palme H. (1995) Experimental petrochemistry of some highly siderophile elements at high temperatures, and some implications for core formation and the mantle's early history. *Chem. Geol.* **120**, 255–273.

Pearson D.G., Irvine G.J., Ionov D.A., Boyd F.R., and Dreibus G.E. (2004) Re–Os isotope systematics and platinum group element fractionation during mantle melt extraction: a study of massif and xenolith peridotite suites. *Chem. Geol.* **208**, 29–59.

Puchtel I.S., Humayun M., Campbell A.J., Sproule R.A. and Lesher C.M. (2004) Platinum group element geochemistry of komatiites from the Alexo and Pyke Hill areas, Ontario, Canada. *Geochim. Cosmochim. Acta* **68**, 1361–1383.

Puchtel I.S., Humayun M. and Walker R.J. (2007) Os–Pb–Nd isotope and highly siderophile and lithophile trace element systematics of komatiitic rocks from the Volotsk suite, SE Baltic Shield. *Precambrian Res.* **158**, 119–137.

Righter K., and Drake M.J. (1997a) A magma ocean on Vesta: Core formation and petrogenesis of eucrites and diogenites. *Meteor. Planet. Sci.* **32**, 929-944.

Righter K., and Drake M.J. (1997b) Metal–silicate equilibrium in a homogeneously accreting Earth: new results for Re. *Earth Planet. Sci. Lett.* **146**, 541–553.

Righter K., Danielson L.R., Pando K.M., Williams J., Humayun M., Hervig R.L., and Sharp T.G. (2015) Highly siderophile element (HSE) abundances in the mantle of Mars are due to core formation at high pressure and temperature. *Meteor. Planet. Sci.* **50**, 1–28.

Ringwood A.E. (1977) Composition of core and implications for origin of Earth. *Geochem. J.* **11**, 111–135.

Rudnick R.L. and Walker R.J. (2009) Interpreting ages from Re–Os isotopes in peridotites. *Lithos* **112S**, 1083–1095.

Scott E.R., Krot T.V., Goldstein J.I., and Wakita S. (2014). Thermal and impact history of the H chondrite parent asteroid during metamorphism: Constraints from metallic Fe–Ni. *Geochim. Cosmochim. Acta* **136**, 13-37.

Shirey S.B. and Walker R.J. (1998) The Re–Os isotope system in cosmochemistry and high-temperature geochemistry. *Annu. Rev. Earth Planet. Sci.* **26**, 423–500.

Smoliar M.I., Walker R.J., and Morgan J.W. (1996) Re-Os ages of group IIA, IIIA, IVA and IVB iron meteorites. *Science* **271**, 1099-1102.

Spivak-Birndorf L., Wadhwa M. and Janney P. (2009) $^{26}$Al–$^{26}$Mg systematics in D'Orbigny and Sahara 99555 angrites: implications for high-resolution chronology using extinct chronometers. *Geochim. Cosmochim. Acta* **73**, 5202–5211.

Urey H. C. (1955) The cosmic abundances of potassium, uranium, and thorium and the heat balances of the Earth, the Moon, and Mars. *Proc. Natl. Acad. Sci. U.S.* **41**, 127-144.

Wadhwa M., Amelin Y., Davis A.M., Lugmair G.W., Meyer B., Gounelle M. and Desch S. (2007) From dust to planetesimals: implications for the solar protoplanetary disk from short lived radionuclides. In *Protostars and Planets V* (ed. B. Reipurth). University of Arizona Press, Tucson, pp. 835–848.

Walker R.J., Storey M., Kerr A.C., Tarney J. and Arndt N.T. (1999) Implication of $^{187}$Os isotopic heterogeneities in a mantle plume: evidence from Gorgona Island and Curacao. *Geochim. Cosmochim. Acta* **63**, 713–728.

Walker R.J., McDonough W.F., Honesto J., Chabot N.L., McCoy T.J., Ash R.D., and Bellucci J.J. (2008) Modeling fractional crystallization of group IVB iron meteorites. *Geochim. Cosmochim. Acta.* **72**, 2198–2216.

Walker R.J., Bermingham K., Liu J., Puchtel I.S., Touboul M., and Worsham E.A. (2015) In search of late-stage planetary building blocks. *Chem. Geol*. **411**, 125–142.

Wasserburg G. J., Busso M., Gallino R. and Nollett K. M. (2006) Short-lived nuclei in the early Solar System: Possible AGB sources. *Nuclear Physics A* **777**, 5-69.

# Chapter 2: Highly siderophile elements and $^{187}$Re-$^{187}$Os Systematics of achondrites: Implications for early planetary differentiation

## *2.1. Abstract*

The highly siderophile element (HSE) abundances and $^{187}$Re-$^{187}$Os systematics of two recently recovered achondrites are examined.  Meteorite NWA 6704 is an ungrouped primitive achondrite.  Meteorite NWA 7325 is an ungrouped differentiated achondrite.  The isotopic systematics of metal and bulk pieces from NWA 6704, as well as a fragment from NWA 7325 characterized by high HSE abundances are consistent with limited mobility of HSE since formation, early in Solar System history.  By contrast, the silicate fraction from NWA 6704 and a fragment from NWA 7325 are characterized by low HSE abundances and show evidence for moderate Re mobilization, most likely during terrestrial weathering of these desert meteorites.

NWA 6704 shows clear petrologic evidence for fractional crystallization, yet the HSE abundances of a calculated whole rock composition are similar to bulk chondrites.  This meteorite most likely originated from a parent body that underwent limited differentiation, and crystallized from a melt from which little or no metal was removed.  Modestly heterogeneous absolute HSE abundances among mg-sized bulk pieces are probably the result of the random distributions of the HSE-rich carriers.  Some slight variations in the relative HSE abundances among the bulk pieces were likely the result of sulfide loss, and minor variations in Re/Os may have been caused by an evolving oxidation state during crystallization.  The HSE abundances of the

silicate fraction are too high and unfractionated to reflect equilibration with the metal, and may instead reflect the inclusion of a small fraction of HSE-rich metal or sulfide.

Two bulk fragments from NWA 7325 have HSE abundances that are highly depleted compared to chondritic abundances. The fragment characterized by low HSE abundances also has relative HSE abundances that are fractionated compared to chondritic abundances. This indicates that its parent body underwent complex processing. One formation model that can broadly account for the HSE abundances of the lower HSE abundance fragment includes multiple episodes of metal-silicate equilibration, followed by late accretion. The chondritic-relative HSE abundances of the fragment characterized by high HSE abundances most likely reflect the presence of exogenous chondritic material that was added during or after crystallization by near-surface impacts on the parent body.

## 2.2. Introduction

The transformation of primitive chondritic rocky material into differentiated planetary bodies was undoubtedly complex. Understanding the timing and processes involved in these transformations is critical for developing models for the formation of rocky planets. While direct evidence for some differentiation processes is temporally and spatially inaccessible for large planetary bodies like Earth, the investigation of trace elements from some meteorite groups that record early processes in their respective parent bodies can provide important new insights.

*2.2.1. Achondrites*

Most achondrite meteorites are derived from parent bodies that probably initially accreted as chondritic material, and then underwent complex processing within ~5 million years of Solar System formation (e.g., Nyquist et al., 2009; Koefoed et al., 2016). They are, therefore, resources for exploring the extent and chronology of early planetary processes, such as core-mantle differentiation, crust-mantle differentiation, and late accretion.

Achondrites are broadly classified as *primitive* or *differentiated* based on petrographic and chemical observations (Krot et al., 2004; Weisberg et al., 2006). Primitive achondrites have experienced either extensive metamorphism or at least some degree of melting, but retain broadly bulk chondritic geochemical characteristics. This provides evidence that their parent bodies underwent only limited degrees of chemical fractionation. Such meteorites provide insights into the initial stages of planetary differentiation or, in some instances, local impact-driven processing. By contrast, differentiated achondrites contain clear evidence for more extensive degrees of melting and differentiation in their parent bodies, including major, minor, and trace element abundances that are substantially fractionated relative to bulk chondrites (Krot et al., 2004; Weisberg et al., 2006). Differentiated achondrites, therefore, provide evidence for large-scale, complex processes that produced differentiated planetesimals.

Primitive and differentiated achondrites are further subdivided into groups based on shared petrologic characteristics, bulk chemical compositions, and O isotopic compositions (e.g., Weisberg et al., 2006). The members of any given achondrite group

may have originated from a single, shared parent body, or from closely related parent bodies that formed in the same region of the solar nebula.

Ungrouped achondrites do not share characteristics (e.g., $\varepsilon^{54}Cr$-$\Delta^{17}O$, mineralogy) with any of the major achondrite groups, and probably did not originate from the parent bodies represented by the major achondrite groups. They are sometimes paired with a small number of similar ungrouped achondrites, but appear to have originated from parent bodies that are underrepresented in meteorite collections. However, as with the major achondrite groups, ungrouped achondrites provide information about their respective parent bodies, and every newly discovered ungrouped achondrite can help to expand our understanding of the chemical diversity of the early Solar System.

### 2.2.2. $^{187}Re$-$^{187}Os$ Isotopic Systematics and Highly Siderophile Elements in Achondrites

Because of their partitioning behavior during core formation and igneous processes, the HSE (Re, Os, Ir, Ru, Pt, and Pd) are useful for exploring complex planetary processes (see section 1.5 for a review of HSE behavior during planetary processes). Previous studies have reported $^{187}Re$-$^{187}Os$ systematics and HSE abundances for several different groups of primitive achondrites, including ureilites (ultramafic achondrites; e.g., Warren et al., 2006; Rankenburg et al., 2008), the paired and ungrouped felsic achondrites Graves Nunatak (GRA) 06128 and GRA 06129 (Day et al., 2009, 2012a), and brachinites and brachinite-like achondrites (ultramafic achondrites; Day et al., 2009, 2012a). Other studies have investigated differentiated

achondrites, including diogenites (ultramafic achondrites; Day et al., 2012b; Dale et al., 2013) and angrites (mafic achondrites; Riches et al., 2012). Each of these studies considered HSE abundances and $^{187}$Re-$^{187}$Os systematics to explore multiple differentiation processes that achondrite parent bodies underwent early in Solar System history.

### 2.2.2.1. HSE and $^{187}$Re-$^{187}$Os Systematics of Primitive Achondrites

A literature review of Re-Os isotopic systematics and HSE abundances of primitive and differentiated achondrites follows. Data for the ungrouped achondrites will be compared with major achondrite groups for context.

Ureilites are a major group of ultramafic primitive achondrites containing ~200 known members. They are predominantly comprised of olivine and pyroxene, but also contain minor amounts of other silicates, metals, and sulfides (Weisberg et al., 2006). Although their petrographic textures and mineralogy indicate that they underwent igneous processing, they retain isotopic evidence of their chondritic precursors.

Rankenburg et al. (2008) reported HSE data for ureilites. The HSE abundances of these meteorites are too high to have originated from a parent body that underwent core segregation by the time these samples formed. They reported that whole rock ureilites appear to contain mixtures of two HSE-bearing components. The first end member component is characterized by a mostly flat chondrite-normalized HSE pattern, except for a depletion in Pd relative to the other HSE (Fig. 2.1). They argued that this component formed as a result of the extraction of a S-rich, metallic partial melt from a chondritic precursor. The second component is characterized by much lower

22

absolute abundances, but chondritic relative proportions, of all HSE. Although the genesis of the second component was unclear, the authors suggested that this component may have formed as a result of either the removal of molten metal or chondritic contamination (Fig. 2.1).
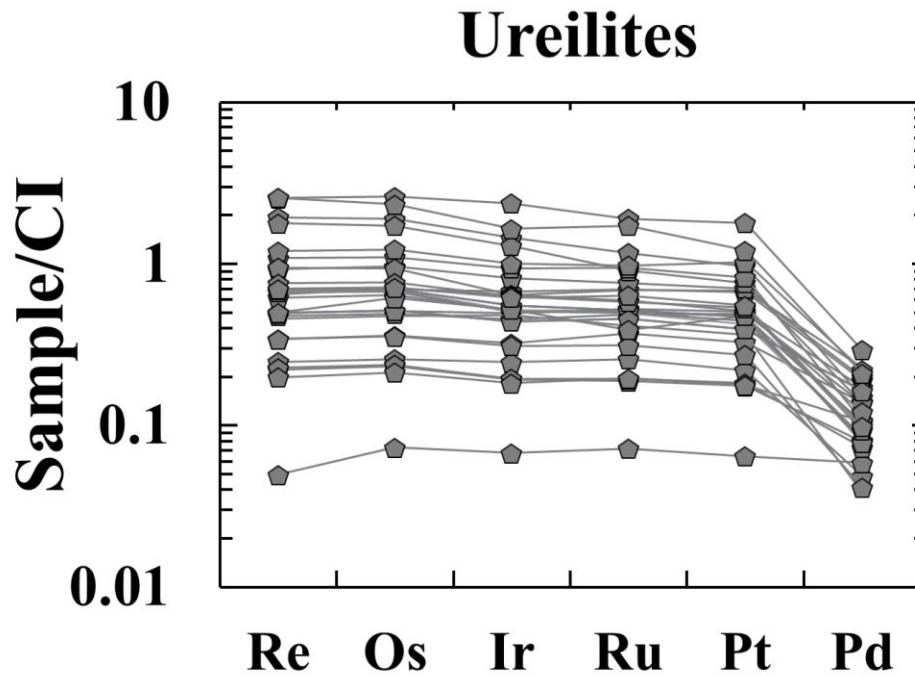
## Ureilites



Figure 2.1. Highly siderophile element abundances of ureilites normalized to CI chondrites, arranged from left to right in order of decreasing 50% condensation temperature. Rhenium abundances were calculated using $^{187}Os/^{188}Os$ and Os abundances. Figure reproduced from Rankeburg et al. (2008).

The GRA 06128/9 achondrites are paired, felsic, primitive achondrites, containing >75% Na-rich plagioclase, as well as olivine, pyroxenes, phosphates, and sulfides. These meteorites probably originated near the surface of their parent body as evolved crustal material (Mikouchi and Miyamoto, 2008). Day et al. (2009, 2012a) reported $^{187}Re$-$^{187}Os$ systematics and HSE abundances for GRA 06128/9 (Fig. 2.2a). The abundances of HSE in GRA 06128/9 are higher than would be expected for

material formed on a parent body that had undergone core segregation. The relative abundances of the HSE are unlike any known chondritic or metal-rich meteorite, and therefore, the HSE abundances are also inconsistent with impact contamination. The calculated initial $^{187}Os/^{188}Os$ for these meteorites are within uncertainty of the initial Solar System ratio, and therefore terrestrial weathering could not have led to the range of Re/Os ratios observed for these samples (or alter the other HSE). The authors concluded that igneous processes, including the partial melting of volatile-rich chondritic material most likely generated the major and trace element compositions found in GRA 06128/9, including their fractionated HSE abundances (Fig. 2.2a).

## GRA 06128/9



## Brachinites
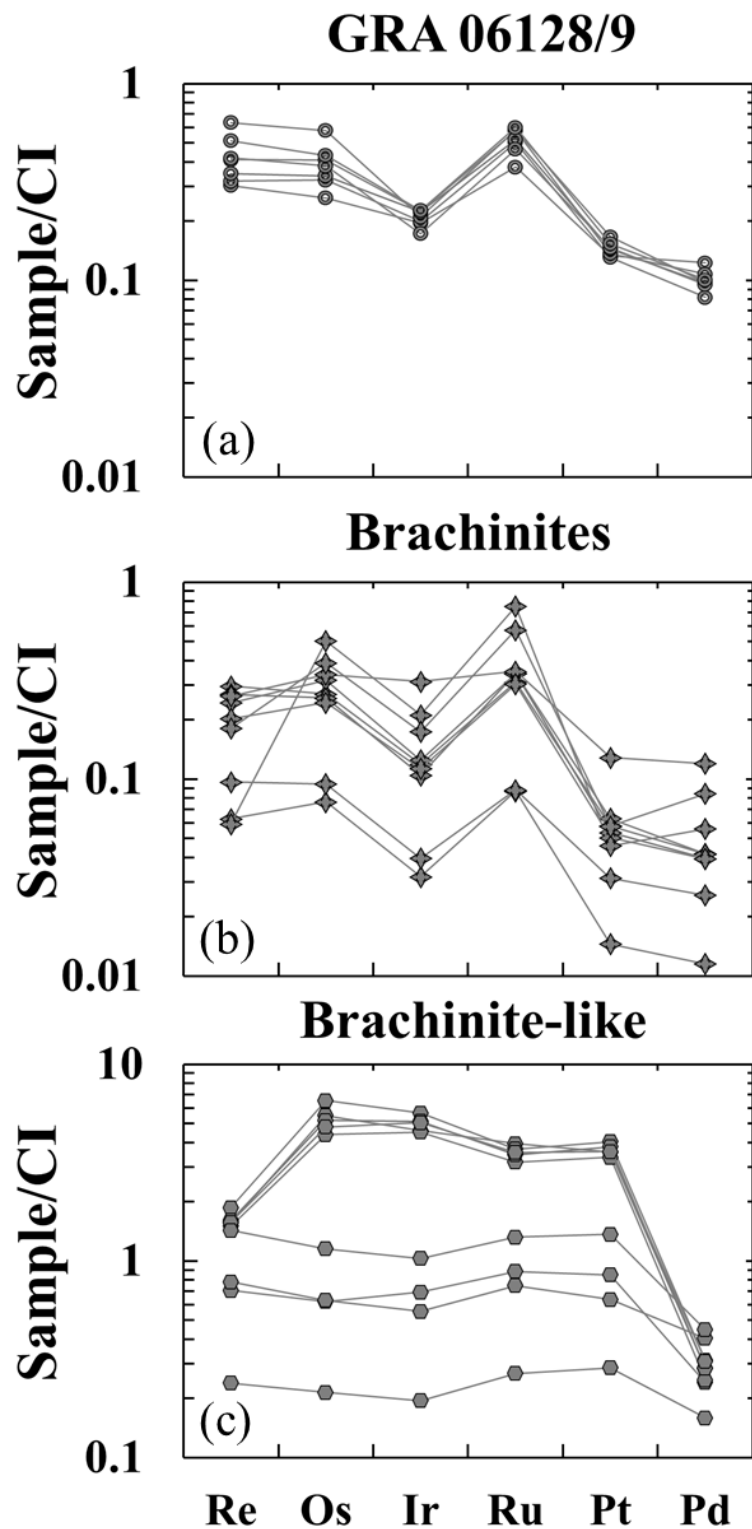


## Brachinite-like



Figure 2.2. Highly siderophile element abundances of (a) GRA 06128/9, (b) brachinites, and (c) brachinite-like achondrites, normalized to CI chondrites and arranged in order of decreasing 50% condensation temperature. Figure reproduced from Day et al. (2012a).

Brachinites are ultramafic primitive achondrites that have O isotopic compositions that overlap with those of GRA 06128/9 (Day et al., 2009, 2012a). Brachinite-like achondrites have similarities with brachinites, including O isotopic compositions and olivine-rich mineralogy. However, brachinite-like achondrites have more Mg-rich silicates and sometimes contain orthopyroxene. Day et al. (2009, 2012a) reported HSE and $^{187}$Re-$^{187}$Os systematics for brachinites and brachinite-like achondrites, and compared them to GRA 06128/9 (Fig. 2.2b and c). Like GRA 06128/9, the absolute HSE abundances of brachinites and brachinite-like achondrites are too high to reflect core formation on their parent bodies. The HSE of brachinites and brachinite-like achondrites are also fractioned relative to bulk chondrites (Fig. 2.2b and c), consistent with igneous processes. Day et al. (2012a) argued, based on shared characteristics, including O isotopic compositions, $^{187}$Re-$^{187}$Os isotopic systematics, and trace element abundances (including the HSE; Fig. 2.2b), that brachinites may represent the complementary melt residue remaining after removal of the partial melt that formed GRA 06128/9. Differences between the HSE characteristics of brachinites and brachinite-like achondrites indicate that they formed by similar processes, but on separate parent bodies.

## 2.2.2.2. HSE and $^{187}$Re-$^{187}$Os Systematics of Differentiated Achondrites

Diogenites are ultramafic differentiated achondrites that may have been derived from the lower crust of their parent body (e.g., Ruzicka et al., 1997). They are one of the groups in the howardite, eucrite, and diogenite (HED) meteorite clan. Based on remote observations from Earth-based instruments (e.g., McCord et al., 1970) and the

Dawn spacecraft (e.g., McSween et al., 2013), prior studies have identified 4 Vesta as a source for the diogenites and the other HED meteorites. Using $^{53}$Mn-$^{53}$Cr data, Day et al. (2012b) reported that diogenites crystallized within 2-3 Myr of calcium-aluminum-rich inclusions (CAIs). They also reported $^{187}$Re-$^{187}$Os systematics and HSE abundances for a suite of diogenites (Fig. 2.3), and most have nearly chondrite relative abundances of the HSE, except for the two lowest abundance samples. The authors argued that a two stage model can account for the HSE abundances of most diogenites. First, metal-silicate equilibration followed by early core-segregation in the HED parent body stripped the majority of the HSE from the mantle. Subsequent to core formation, late accretion added chondritic material to the mantle resulting in the nearly chondritic relative HSE abundances of most diogenites. This two-stage model is similar to some models proposed for the mantles of Earth (e.g., Chou, 1978), Mars (Brandon et al., 2012), and the Moon (Day et al., 2007). The samples with the lowest and most fractionated (relative to CI chondrites) HSE abundances were probably the result of further fractionation during crust-mantle partitioning (Day et al. 2012b).
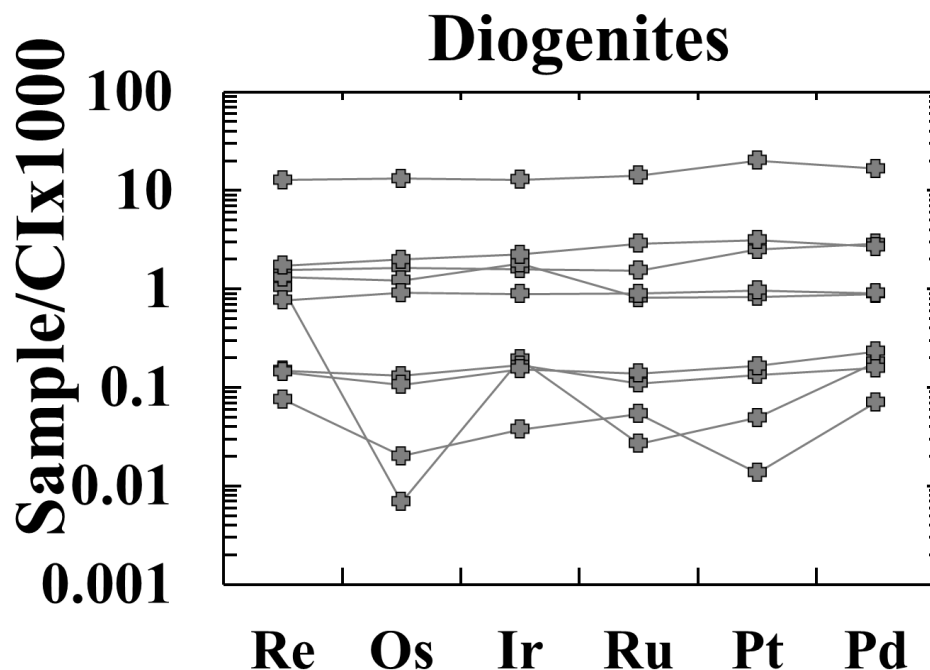
Figure 2.3. Highly siderophile element abundances of diogenites, normalized to CI chondrites and arranged in order of decreasing 50% condensation temperature. Figure reproduced from Day et al., (2012b).

Angrites are basaltic achondrites that formed in the silicate portion(s) of one or more differentiated asteroid parent bodies (Mittlefehldt, 2003) within the first ~2-10 million years after CAI formation (e.g., Markowski et al., 2007). Riches et al. (2012) reported HSE abundances and [187]Re-[187]Os systematics for a suite of angrites (Fig. 2.4), including those with quenched and slowly-cooled textures. They argued that angrites must have crystallized after core-segregation on their parent body, given their low HSE abundances. They also argued that the quenched angrites were crustal materials, and that the chondritic relative abundances of the HSE in these meteorites were caused by late addition of chondritic material that was either assimilated while the rock was crystallizing, or injected by surface impacts. On the other hand, they concluded that HSE abundances of the slowly-cooled angrites NWA 4590 and 4801, with their low Re/Os and Pd/Os, were the result of partial melting of already melt-depleted mantle

28

material.  According to Riches et al. (2012), impact melting most likely generated the elevated and chondritic relative HSE abundances of NWA 4931.
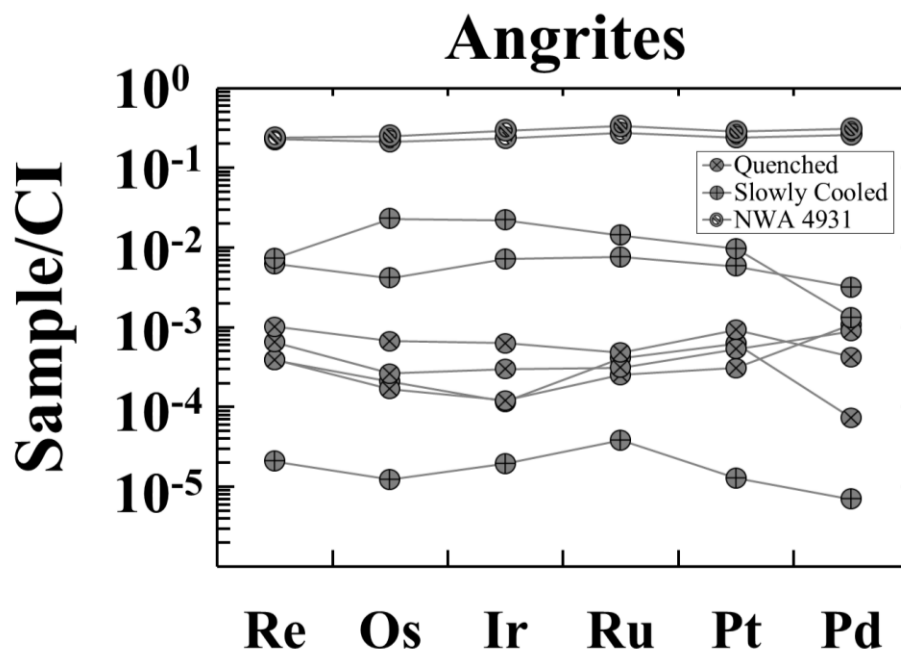


Figure 2.4. Highly siderophile element abundances of NWA 4931, quenched angrites, and slowly-cooled angrites. Data normalized to CI chondrites and arranged in order of decreasing 50% condensation temperature. Figure reproduced from Riches et al. (2012).

### 2.3. Sample Descriptions

#### 2.3.1. NWA 6704

NWA 6704 was found in Algeria in 2010, and has a total mass of 8387g divided among 42 pieces.  It is an ungrouped primitive achondrite, and has been paired with meteorites NWA 6926 and NWA 6693 (Warren et al., 2013).  This sample has an igneous cumulate texture (Irving et al., 2011), and is comprised of low-Ca pyroxene, fayalitic olivine, chromite, sodic-plagioclase, Cr-spinel, sulfides, and awaruite (Irving et al., 2011; Jambon et al., 2012; Hibiya et al., 2016).  Its O isotopic composition is

similar to the O isotopic compositions of acapulcoites and lodranites (Irving et al., 2011). By contrast, the mineral chemistry (Irving et al., 2011) and Cr isotopic composition (Sanborn et al., 2013) differ from those of acapulcoites and lodranites. NWA 6704 has a $^{26}Al$-$^{26}Mg$ age of 4563.48±0.34 Ma (Yin et al., 2013), which is similar to the Pb-Pb age of 4563.34±0.32 Ma (Iizuka et al., 2013).

### 2.3.2. NWA 7325

NWA 7325 is an ungrouped differentiated achondrite that was found in Western Sahara in February 2012, and has a total mass of 345 grams split across 35 pieces. The textures and bulk composition of this achondrite are consistent with an olivine gabbro cumulate (Irving et al., 2013). Prior studies have reported some compositional similarities between NWA 7325 and the surface rocks of Mercury (Irving et al., 2013). A Pb-Pb isochron indicates that NWA 7325 has an age of 4563.4±2.6 Ma, which is consistent with the $^{26}Al$-$^{26}Mg$ age of 4562.8±0.3 (Koefoed et al., 2016).

### 2.4. Methods

From NWA 6704, four bulk fragments and the silicate fraction were crushed into fine powders using an agate mortar and pestle. A metal fraction could not be crushed, and was processed as whole grains. Samples were combined with ~5 mL of a 2:1 mixture of Teflon distilled, concentrated $HNO_3$ and HCl, and appropriate amounts of two isotopic spikes, one enriched in $^{185}Re$ and $^{190}Os$, the other enriched in $^{191}Ir$, $^{99}Ru$, $^{194}Pt$, and $^{105}Pd$. Samples, spikes, and acids were sealed in 8 mL Pyrex™ Carius tubes (Shirey and Walker, 1995) and heated at 260ºC for three days.

Two fragments from a single stone of NWA 7325 were crushed into fine powders using an agate mortar and pestle. Sample powders, ~5 mL of a 2:1 mixture of Teflon distilled, concentrated $HNO_3$ and HCl, and appropriate amounts of two isotopic spikes, one enriched in [185]Re and [190]Os, the other enriched in [191]Ir, [99]Ru, [194]Pt, and [105]Pd, were combined in quartz digestion vessels and sealed with Teflon tape. The samples were then heated in a high-pressure asher (HPA-S, *Anton Paar*[TM]) at 320 °C for 12 hours (Meisel et al., 2003).

Following digestion, both meteorites were processed in a similar manner. Osmium was extracted from the acid by solvent extraction using $CCl_4$, and back extraction into concentrated HBr (Cohen and Waters, 1996). The Os was purified using a microdistillation technique from a dichromate solution into concentrated HBr (Birck et al., 1997). The remaining HSE (Re, Ir, Ru, Pt, and Pd) were separated and purified by anion exchange chromatography using 10 mL *Bio-Rad* columns loaded with ~1 mL of AG1x8 anion exchange resin (Rehkämper and Halliday, 1997).

Purified Os solutions were first dried onto Pt filaments and then a $Ba(OH)_2$ activator was added (Creaser et al., 1991). Osmium was then analyzed by negative thermal ionization mass spectrometry (N-TIMS) on either the UMd *VG Sector 54* or *Thermo-Fisher Triton*, using Faraday cups for all NWA 6704 samples, and ion counters for all NWA 7325 samples. The other HSE were analyzed as solutions by multi collector-inductively coupled plasma mass spectrometry (MC-ICP-MS) on the *Nu Plasma* at UMd using Faraday cups for all NWA 6704 samples, and ion counters for all NWA 7325 samples. Measurements of Ir, Ru, Pt, and Pd for all samples, as well as the Re measurements for NWA 7325 samples, were corrected for mass bias by

interspersing standards with sample measurements. Tungsten was added to Re fractions from all NWA 6704 samples and mass bias corrections were made using $^{184}W/^{186}W = 1.0780$ (Kleine et al., 2004).

Mean (n=3) blanks were 1.0+1.1/-1.0 pg (Re), 1.1±1.0 pg (Os), 0.6±0.4 pg (Ir), 3.2±1.5 pg (Ru), 2.9+3.8/-2.9 pg (Pt), and 11.9+13.2/-11.9 pg (Pd). The Os blank correction was 1.4% for the NWA 6704 silicate fraction, and less than 0.12% for all other NWA 6704 and NWA 7325 samples. Blank corrections for Re, Pt, and Pd were 2.6%, 3.9%, and 1.5%, respectively, for the NWA 6704 silicate fraction. All other blank corrections for NWA 6704 samples, including Ir and Ru blank corrections for the silicate fraction, were less than 0.1%. Blank corrections for Re, Ir, Ru, and Pt were less than 1% for NWA 7325 fragment A, and a correction of ~3% was required for Pd. For NWA 7325 fragment B, blank corrections were < 5% for Ir, Pt, and Pd, and 18% and 18.5% corrections were required for Re and Ru, respectively. Uncertainties arising from blank corrections are included in reported uncertainties. The total uncertainties for HSE concentrations of NWA 6704 bulk and magnetic fractions are ≤ 1%. The total uncertainties for HSE concentrations of the NWA 6704 silicate fraction and both NWA 7325 samples are < 5%.

## *2.5. Results*

### *2.5.1. NWA 6704*

The ~5-34 mg bulk pieces of NWA 6704 have broadly chondritic HSE abundances, ranging from ~0.2x to ~5x CI abundances of Ir (Table 2.1; Fig. 2.5a). The metal fraction has much higher HSE abundances, with ~48x CI Ir. By contrast, the

silicate fraction has much lower HSE abundances than the bulk fractions, with ~0.05x CI Ir. The relative abundances of the HSE in all fractions are only slightly fractionated compared to CI chondrite. CI-normalized Re/Ir, Os/Ir, Ru/Ir, Pt/Ir, and Pd/Ir range from 0.7-1.7, 0.7-1.4, 0.8-1.7, 1.0-1.4, and 0.7-2.2, respectively. To estimate NWA 6704 HSE abundances at the whole-rock scale, the HSE abundances of the milligram-sized bulk pieces were averaged, weighted by mass (Fig. 2.5a).

The $^{187}$Re-$^{187}$Os isotopic systematics for metal and bulk pieces of NWA 6704 were regressed using ISOPLOT (Ludwig, 2001) and define an isochron with an age of 4576±250 Ma. By comparison, the silicate fraction plots below this isochron (Fig. 2.6a). The $^{187}$Re-$^{187}$Os systematics of these samples can be expressed in $\Delta_{Os}$ units (where $\Delta_{Os}$ is the deviation in parts per 10,000 from a primordial 4568 Ma reference isochron, using parameters from Becker et al. (2001) and Archer et al. (2014) ($\Delta_{Os} = 10^4[^{187}Os/^{188}Os_{CAI} - [0.09517 + 0.07908 \times {}^{187}Re/^{188}Os_{CAI}]]$). The $\Delta_{Os}$ of bulk samples and metal range from +0.85 to +6.8, with a typical uncertainty of ~1-2 $\Delta_{Os}$ units. By contrast, the silicate fraction has a $\Delta_{Os}$ value of -24±10 (Table 2.1; Fig. 2.6c). The larger error bars for this fraction are the result of low Re and Os abundances, and consequently, larger blank corrections.

Table 2.1. Highly siderophile element abundances (ppb) and $^{187}$Re-$^{187}$Os systematics of NWA 6704 metal, silicate, and bulk pieces, as well as NWA 6704 fragments

| | Mass (mg) | Re | Os | Ir | Ru | Pt | Pd | $^{187}$Re/$^{188}$Os | 2σ | $^{187}$Os/$^{188}$Os | 2σ | Δ$_{Os}$ | 2σ |
|---|---|---|---|---|---|---|---|---|---|---|---|---|---|
| **NWA 6704** | | | | | | | | | | | | | |
| *Bulk A* | 33.9 | 10.69 | 89.22 | 93.64 | 188.5 | 243.2 | 137.4 | 0.5782 | 0.0008 | 0.14133 | 0.00008 | 4.3 | 0.7 |
| *Bulk B* | 20.3 | 11.69 | 85.78 | 85.49 | 177.3 | 231.3 | 142.6 | 0.658 | 0.0016 | 0.14738 | 0.00012 | 1.8 | 1.2 |
| *Bulk C* | 5.14 | 215.7 | 3242 | 2252 | 2668 | 4200 | 4064 | 0.3203 | 0.0026 | 0.12119 | 0.00076 | 6.8 | 2.2 |
| *Bulk D* | 6.34 | 70.99 | 694.2 | 486.6 | 725.3 | 1135 | 1188 | 0.4932 | 0.0032 | 0.13439 | 0.00025 | 2.1 | 2.5 |
| *Metal* | 6.02 | 3034 | 29820 | 22000 | 32340 | 49270 | 58560 | 0.4906 | 0.0005 | 0.13405 | 0.00018 | 0.85 | 0.4 |
| *Silicate* | 9.96 | 1.474 | 15.42 | 23.47 | 58.37 | 48.38 | 20.36 | 0.461 | 0.013 | 0.12923 | 0.00086 | -24 | 10 |
| | | | | | | | | | | | | | |
| **NWA 7325** | | | | | | | | | | | | | |
| *Fragment A* | 774 | 0.07337 | 0.9133 | 0.9609 | 1.266 | 1.999 | 1.065 | 0.3870 | 0.0043 | 0.12579 | 0.00048 | 0.1 | 3.1 |
| *Fragment B* | 127 | 0.00899 | 0.117 | 0.0899 | 0.100 | 0.0533 | 0.488 | 0.379 | 0.015 | 0.12742 | 0.00087 | 22.8 | 20.1 |

Δ$_{Os}$ is the deviation in parts per 10,000, from a primordial 4568 Ma reference isochron. Uncertainties for $^{187}$Re/$^{188}$Os, $^{187}$Os/$^{188}$Os, and Δ$_{Os}$ are 2σ.
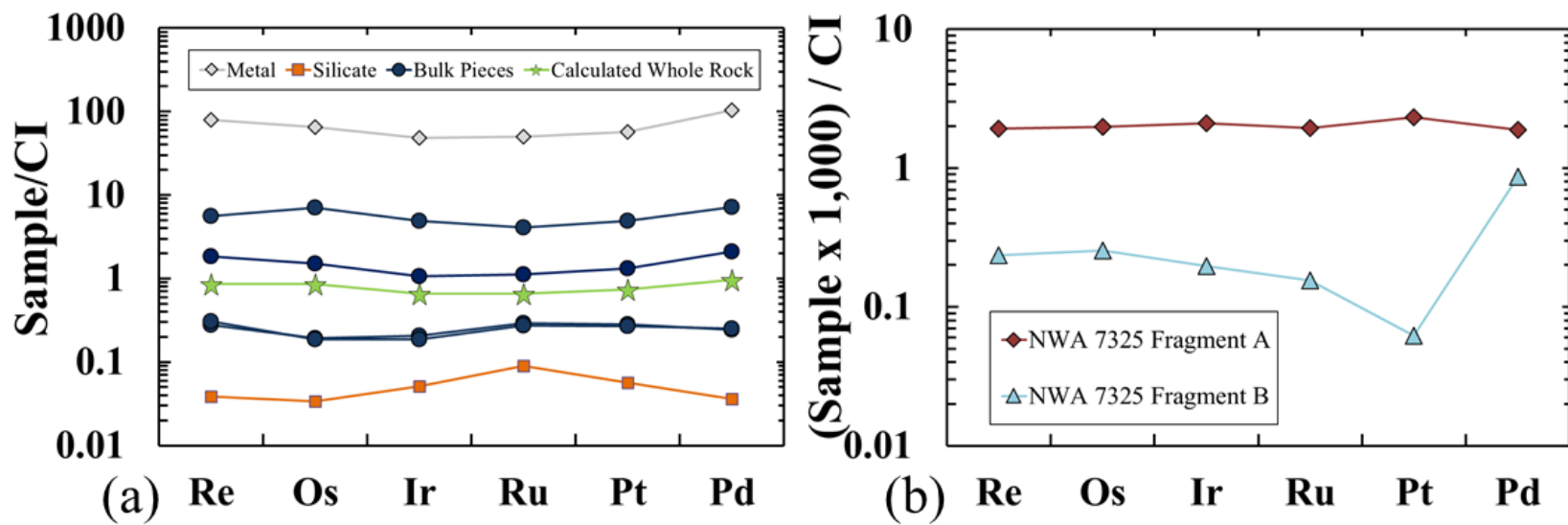
Figure 2.5. CI-normalized (Horan et al., 2003) HSE abundances of (a) NWA 6704 bulk pieces, metal, silicate, and calculated whole rock, and (b) NWA 7325 fragments. Uncertainties are smaller than symbols.
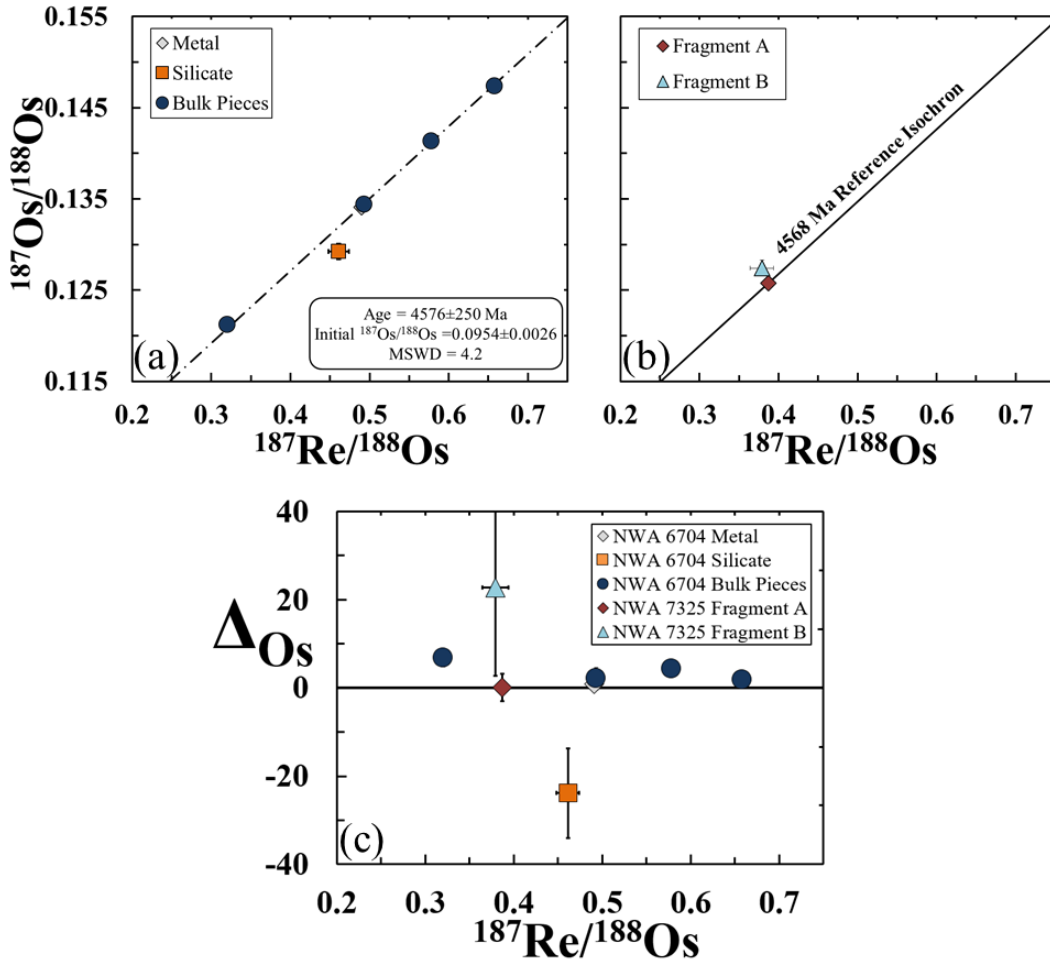
Figure 2.6. $^{187}$Re-$^{187}$Os isotopic systematics of NWA 6704 and NWA 7325. Uncertainties are smaller than symbols unless shown. (a) Re-Os isochron calculated using ISOPLOT (Ludwig, 2001) for NWA 6704 metal and bulk fractions. The silicate fraction is excluded from the regression (b) Re-Os isotopic systematics of NWA 7325 compared to 4568 Ma reference isochron, using parameters from Archer et al. (2014). (c) $^{187}$Re-$^{187}$Os vs. $\Delta_{Os}$ for NWA 6704 and NWA 7325. $\Delta_{Os}$ is the deviation in parts per 10,000, from a primordial 4568 Ma reference isochron.

### 2.5.2. NWA 7325

The HSE abundances of both fragments of NWA 7325 are more than a factor of 100 lower than in CI chondrites (Table 2.1.; Fig. 2.5b). Further, the concentrations of some HSE in the two fragments vary by almost an order of magnitude (Fig. 2.5b;

0.0002 versus 0.002 x CI chondrite Orgueil for Ir in NWA 7325 fragments B and A, respectively).   Despite the strongly subchondritic HSE abundances, NWA 7325 fragment A is characterized by HSE ratios that overlap with the ranges of those observed in bulk chondritic meteorites (Horan et al., 2003; Fischer-Gödde et al., 2010; van Acken et al., 2011).  By contrast, the HSE abundances in NWA 7325 fragment B are significantly fractionated relative to bulk chondrites, with notably subchondritic Pt/Ir and suprachondritic Pd/Ir (Fig. 2.5b).

Sample NWA 7325 fragment A plots within uncertainties of a primordial $^{187}$Re-$^{187}$Os reference isochron. By comparison, sample NWA 7325 fragment B plots slightly above the reference isochron (Fig. 2.6b).  Error bars for this sample are large because of the much lower abundances of Re and Os present in this fragment.  The $\Delta_{Os}$ values of NWA 7325 fragments A and B are 0.1±3.1 and 22.8±20.1, respectively (Table 2.1; Fig. 2.6c).

## 2.6. Discussion

### 2.6.1. NWA 6704: Limited Parent Body Differentiation

The $^{187}$Re-$^{187}$Os systematics of NWA 6704 bulk pieces and the metal fraction are generally consistent with system closure since formation, given that they fall on or near a primordial isochron.  Therefore, these samples are presumed to retain HSE in the absolute abundances present at the time of formation.  The deviation of the silicate fraction from a primordial isochron most likely indicates that a minor amount of Re has been added, probably during terrestrial alteration.  Prior studies have noted similar disturbances of the $^{187}$Re-$^{187}$Os systematics of some achondrite samples from

Northwest Africa (Brandon et al., 2012).  Despite the minor disturbance of the [187]Re-[187]Os systematics, the HSE abundances of the silicate fraction were evidently not affected by secondary processes by more than a few percent.

Multiple processes, including core formation, igneous processing (partial melting and crystallization), and late accretion established the HSE abundances of different parts of planetary bodies.  Immediately following core formation, the HSE concentrations of the silicate portions of planetary bodies were most likely highly depleted and fractionated, relative to bulk chondrites (e.g., Capobianco et al., 1993) given that HSE have high ($>10^4$ under low pressure conditions), but variable metal-silicate partition coefficients (e.g., Kimura et al., 1974; Newsom, 1990; O'Neill et al., 1995; Borisov and Palme, 1995; Fortenfant et al., 2003; Laurenz et al., 2010).  The nearly chondritic absolute HSE abundances of bulk pieces of NWA 6704 are, therefore, inconsistent with significant metal removal.  This, in turn, suggests a parent body that had not segregated metal on a global scale to form a core, by the time this sample formed.

Because of their diverse compatibilities in silicate systems (e.g., Barnes and Naldrett, 1985; Walker et al., 1999; Puchtel et al., 2004; 2007; Day et al., 2010a), the HSE are typically fractionated during silicate differentiation.  Prior studies of some primitive achondrites have reported moderate fractionations of HSE relative to bulk chondrites, and argued that the fractionations resulted from igneous processes, especially when petrologic and other trace element evidence was consistent with those processes (e.g., Day et al., 2009).  The cumulate igneous texture of NWA 6704 (Irving et al., 2011), and subchondritic bulk $MgO/SiO_2$ (Warren et al., 2013) of NWA 6693,

which is paired with NWA 6704, are consistent with fractional crystallization. Despite this, absolute and relative HSE abundances of a calculated whole rock are broadly chondritic (Fig. 2.7). The relative HSE abundances of the calculated whole rock composition are within 2σ of the mean HSE abundances of some bulk chondrites (Fig. 2.7; Day et al., 2016). The HSE of NWA 6704 are also in higher abundance and less fractionated than other primitive achondrites, including ureilites, GRA 06128/9, brachinites, and brachinite-like achondrites (Fig. 2.8). Further, Warren et al. (2013) reported that the relative and absolute abundances of the siderophile elements Fe, Co, Ni, Os, Ir, and Au and nonvolatile lithophile elements of paired NWA 6693 are only minimally fractionated relative to bulk chondrites. They argued that NWA 6693 crystallized from a melt that underwent only minor fractionation. Consistent with the interpretation of Warren et al. (2013), we conclude that the precursor rock to NWA 6704 had chondritic absolute and relative HSE abundances, and that NWA 6704 crystallized from a melt that underwent minor HSE fractionation.
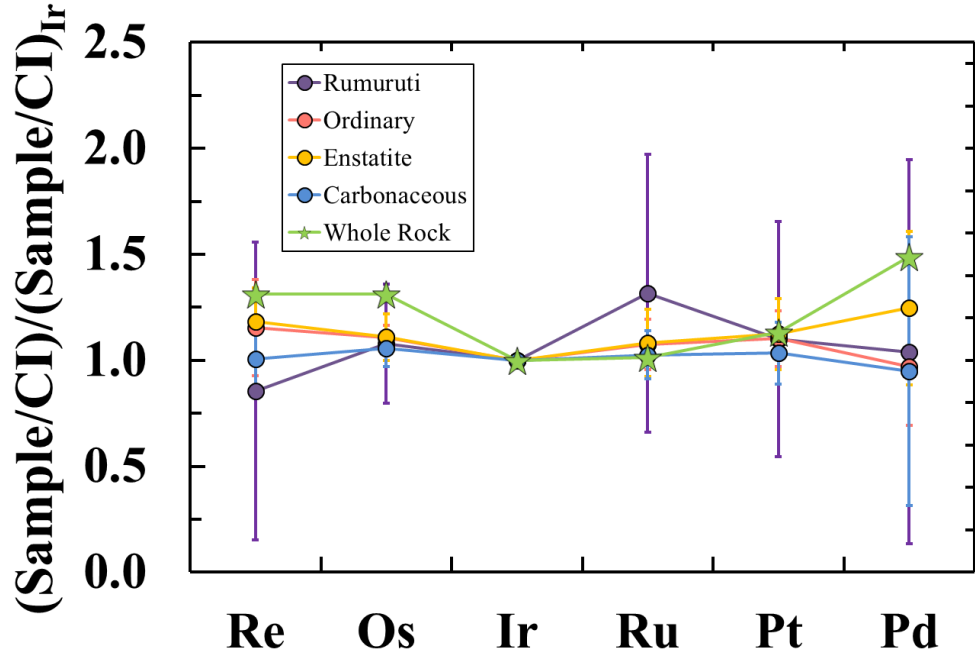
Figure 2.7. Calculated whole rock HSE abundances for NWA 6704, doubly normalized to CI chondrites (Horan et al., 2003) and Ir. For comparison, doubly normalized average and $2\sigma$ of ordinary, carbonaceous, enstatite, and Rumuruti-like chondrites HSE abundances. Chondrite data are from Walker et al. (2002), Horan et al. (2003), Brandon et al. (2005), and Fischer-Gödde et al. (2010).
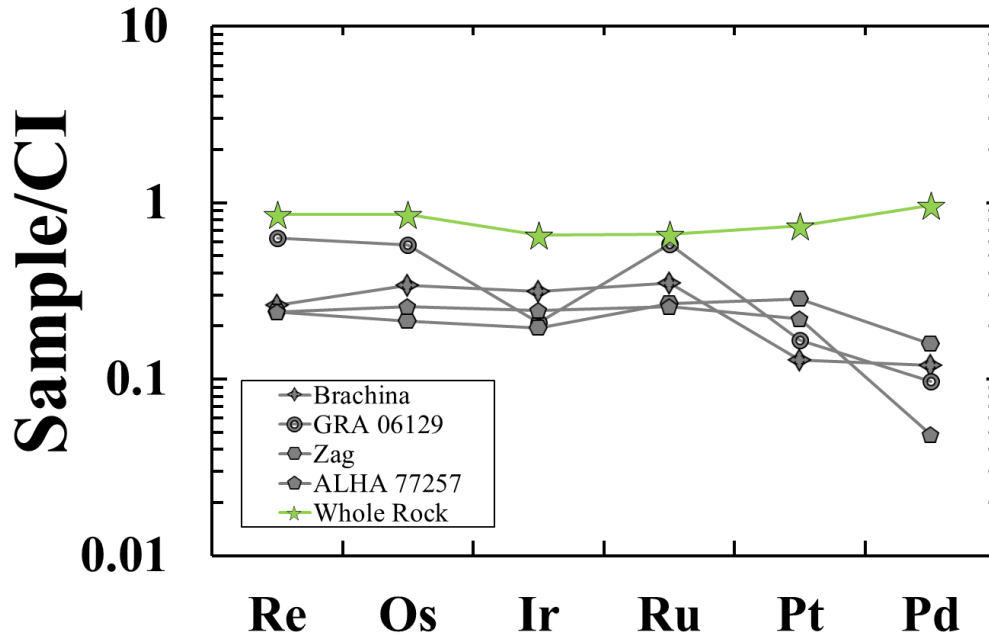


Figure 2.8. CI-normalized (Horan et al., 2003) calculated whole rock HSE abundances from NWA 6704 as well as various primitive achondrites (GRA 06129 from Day et al., 2009; Brachina and brachinite-like achondrite Zag from Day et al., 2012a; ureilite ALHA 77257 from Rankenburg et al. 2008).

Limited HSE fractionations, despite melting and crystallization, indicate that the geochemical effects of the igneous processes must have been different for NWA 6704 compared to other primitive achondrites (e.g., brachinites and ureilites) that are characterized by more fractionated HSE abundances. The large-scale distributions of HSE-rich carriers (primarily metal) in NWA 6704 appear to have been largely unchanged during melting and crystallization. Transport of these carriers must, therefore, have been limited. One possibility is that the NWA 6704 parent body was too small for gravitational separation of metals to occur after melting, and that metal was not segregated by melting/crystallization processes. Alternatively, melting and crystallization may have occurred on a timescale that was too short to allow segregation of metals, such as might occur as a result of near-surface impact melting followed by rapid cooling.

Although the HSE abundances of the calculated whole rock composition are similar to bulk chondrites, there are some HSE fractionations and absolute abundance variations among milligram-sized bulk pieces. The variations in absolute HSE abundances among bulk pieces indicate that the HSE carriers in this rock are heterogeneously distributed. The heterogeneity most likely reflects random distributions of HSE-rich metal carriers, as argued by Warren et al. (2013).

Warren et al. (2013) reported depletions in the abundances of S and chalcophile elements, relative to bulk CI chondrites, in paired NWA 6693. In addition to being primarily siderophile, the HSE, and especially Pd, are also chalcophile. In some cases, sulfides in iron meteorites have Pd abundances that are ~10% of the Pd abundances of coexisting Fe,Ni-rich metal (Carlson and Hauri, 2001). Therefore, sulfide loss may

result in Pd depletions. Bulk pieces of NWA 6704, however, are not characterized by resolvable Pd depletions. Therefore, despite the apparent loss of S and depletion of chalcophile elements, Pd behaved coherently with the other HSE and remained almost wholly retained in the metal. This suggests that, under the formation conditions of NWA 6704, the behavior of Pd was far more siderophile than chalcophile.

Irving et al. (2011) reported that NWA 6704 metal is characterized by high Ni concentrations (75 wt.%; Irving et al., 2011), consistent with formation under highly oxidizing conditions, and oxidative loss of Fe metal. Hibiya (2016) reported olivine reaction rims associated with orthopyroxene and awaruite grains. That study concluded that the reaction rims are consistent with a gradually increasing state of oxidation during the crystallization of NWA 6704. Because Re has the highest oxidation potential of the HSE, some modest Re/Os variations among different bulk fractions may be the result of Re/Os fractionation caused by changing redox states.

Efficient igneous processing should have led to the equilibration of the HSE between metals and silicates. However, the apparent NWA 6704 metal/silicate concentration ratio for Ir is only ~960. Although D values tend to decrease with increasing pressure and temperature for at least some HSE (e.g., Mann et al., 2012), even under P-T conditions appropriate for the terrestrial lower mantle, D values for Ir do not decrease below ~$10^4$. Thus, the HSE abundances of the NWA 6704 silicate fraction either reflect disequilibrium between metals and silicates, or the presence of a small fraction of HSE-rich metal or sulfide in the silicate fraction. Mixing calculations indicate that the presence of only 0.2% of the measured metal in the silicate fraction could broadly account for its HSE abundances. However, the relative HSE abundances

of the metal and silicate fraction are not identical. Therefore, the mixture of metal and sulfide phases in the silicate fraction would have to be characterized by relative HSE abundances that differ from the metal fraction analyzed. Most likely, the sulfide phases present in the silicate fraction have relative HSE abundances that differ from the metal.

### 2.6.2. NWA 7325: Complex Differentiation Processes

The Re-Os isotopic systematics of NWA 7325 fragment A are consistent with system closure since its formation. Thus, the relative abundances of the other HSE in this fragment were likely little modified by subsequent processes. By contrast, the Re-Os isotopic systematics of fragment B deviate slightly from chondritic evolution. Contrary to NWA 6704, the offset likely reflects minor *loss* of Re in the terrestrial environment. Regardless of the cause, the offset from the primordial isochron is minor, and the absolute and relative abundances of the other HSE were probably not affected by shock or terrestrial weathering by more than a few %.

The HSE abundances present in NWA 7325 can be accounted for by a model involving metal segregation, crust-mantle (magmatic) differentiation, and late accretion (e.g., Day et al., 2012a; Brandon et al., 2012). The relatively low HSE concentrations in the two NWA 7325 fragments are generally consistent with HSE depletion of their mantle source by metal segregation, most likely during core formation on the parent body. However, metal-silicate partition coefficients for the relatively low-pressure conditions expected for an asteroid suggest that the HSE abundances should be much lower than observed, if only metal-silicate partitioning was involved. For example, modeling efficient core formation using a metal-silicate D

value of 7 x $10^{15}$ for Pt (Ertel et al., 1999; Walter et al., 2000) results in a concentration of 4.5 x $10^{-13}$ ppb in the silicate portion of the body, assuming the parent body had an approximately chondritic Pt bulk abundance, and an Fe-rich core comprising 30% of the mass of the body. This concentration is much lower than is observed for either of these samples. Further, diverse metal-silicate distribution coefficients for the different HSE should also have resulted in large fractionations among the HSE, as compared to chondritic relative abundances. Instead, the chondrite normalized HSE pattern of fragment A is unfractionated, and even fragment B is characterized by a HSE pattern that is much less fractionated than predicted for metal-silicate partitioning at low pressures. For example, using the metal-silicate D value of 2 x $10^7$ for Pd (Borisov and Palme, 1994; Walter et al., 2000) and the D value for Pt from above, the silicate portion of the parent body would have a Pt/Pd of 4.8 x $10^{-9}$, compared to the measured ratio of 0.11 for fragment B.

The substantial differences in HSE characteristics between the two fragments are diagnostic. It is possible that the melt from which this rock crystallized assimilated regolith with chondritic HSE characteristics, but the assimilant was inefficiently mixed with the melt. However, given the differences in HSE characteristics between fragments A and B, coupled with the small size of the meteorite from which both fragments were taken (0.34 kg), it is difficult to envision an assimilation process that would not affect the entire rock.

High absolute and chondritic relative abundances of HSE in some achondrites have also been attributed to late accretion, the process of continued planetary accretion following cessation of core formation. For example, the chondritic relative abundances

of HSE present in some diogenites were interpreted by Day et al. (2012b) as evidence for uneven late accretionary additions to the mantle or crust of Vesta. Although the absolute and relative abundances of NWA 7325 fragment A are similar to some diogenites, this explanation seems unlikely for NWA 7325. As with assimilation, it is difficult to envision how late accretion could lead to such diverse HSE characteristics in two pieces of rock from the same magmatic system.

The variation in HSE abundances between the two fragments of NWA 7325 most likely indicates mixing of varying proportions of HSE from at least two sources, one of which was probably exogenous, the other endogenous. The relatively high absolute (Ir = 0.9 ppb), and chondritic-relative HSE abundances (Fig. 2.9) present in fragment A are best explained via addition of exogenous chondritic material following crystallization, as a result of near-surface impacts selectively contaminating the rocks. Consistent with this, prior studies have argued that NWA 7325 was shocked, likely during near-surface impacts (Irving et al., 2013; Goodrich et al., 2014). Addition of only ~0.2% of CI-like chondritic material during near-surface impacts could produce the observed abundances. Previous studies have proposed similar models to explain the HSE abundances present in some lunar highland rocks (Day et al., 2010b) and some angrites (Riches et al., 2012).
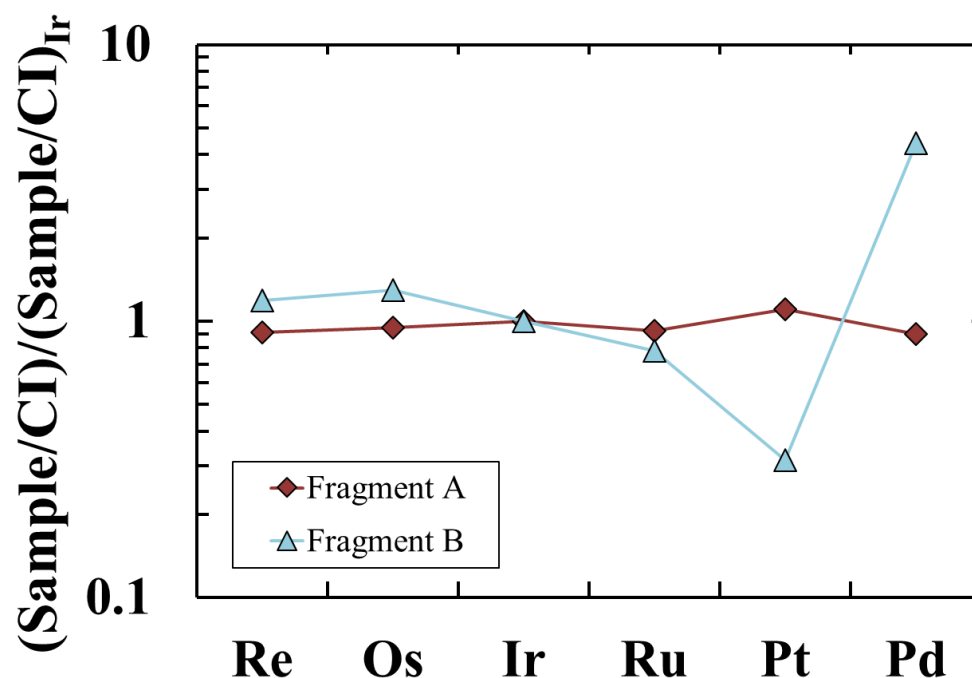
Figure 2.9. HSE abundances of NWA 7325 fragments doubly normalized to CI chondrite abundances and Ir (Horan et al. 2003). Uncertainties are smaller than symbols.

The lower, moderately fractionated HSE abundance pattern of fragment B likely represents more pristine crustal material from the NWA 7325 parent body, with little or no post-crystallization addition of chondritic HSE. The HSE of fragment B may reflect processes including metal segregation, addition of HSE to the mantle of the NWA 7325 parent body via late accretion, and/or silicate differentiation. The effects of these processes are not mutually exclusive, so all three may have factored into the final characteristics of this rock. Given that the HSE characteristics of this sample were evidently not overwhelmed by impact contamination, it is a more valuable sample than fragment A in terms of examining the geochemical characteristics of the parent body.

The HSE characteristics of NWA 7325 fragment B can be broadly generated by a model that combines multiple episodes of metal-silicate equilibration, using

experimentally-derived, low-pressure metal-silicate partition coefficients (Table 2.2), and late accretion.  In the first stage of this model (Table 2.3; Fig. 2.10), metal-silicate equilibration followed by core formation occurrs in an originally chondritic (CI chondrite HSE; Fischer-Gödde et al., 2010) parent body, assuming a 30% Fe-rich metal fraction and a 70% silicate fraction.  In the second stage, a small fraction ($10^{-9}$ wt.% CI) of chondritic material is mixed into the silicate mantle.  In the third stage, a second metal-silicate equilibration occurs in a system comprised of a small fraction of Fe-rich metal grains (10 ppm) and >99.9% silicate from stage 1, followed by metal segregation. Calculated HSE abundances of a rock consisting of 99% silicate containing negligible HSE, and 1% of the metal resulting from the third stage of the model are shown in Fig. 2.10.  In the fourth stage, minor post-crystallization addition of CI-like chondritic material (0.01%) occurs by near-surface impacts, and the final HSE abundances of the model are broadly consistent with the HSE pattern of fragment B.

Table 2.2.  Experimentally-derived metal-silicate bulk partition coefficients (D values) for 1 atm., IW-1 or IW-2, and 1300ºC-1400ºC.  All D values (except Re) originally compiled by Walter et al. (2000).

| Element | Metal-silicate D | Reference |
|---------|------------------|-----------|
| Re | $5 \times 10^{10}$ | Ertel et al. (2001) |
| Os | $6 \times 10^{10}$ | Borisov and Palme (1998) |
| Ir | $>10^{12}$ | Borisov and Palme (1995) |
| Ru | $2 \times 10^{12}$ | Borisov and Nachtweyh (1998) |
| Pt | $7 \times 10^{15}$ | Ertel et al. (1999) |
| Pd | $2 \times 10^7$ | Borisov et al. (1994) |

Core formation and late accretion, the basis of the first two stages of this model, are processes that are commonly invoked to explain the HSE characteristics Earth's mantle (e.g., Chou, 1978), the Moon (Day et al., 2010b), Mars (Brandon et al., 2012),

and some diogenites (Day et al., 2012b). However, the third stage of this model requires the chemical equilibration of a small fraction (10 ppm) of Fe-rich metal with the silicate fraction after the initial core forming metal segregation event. Possible sources of metal include remnant metal, if core formation on the parent body was inefficient (Arculus and Delano, 1981; Jones and Drake, 1986), impactor derived metal, and reduction of FeO within the mantle. The HSE abundances of the metal (even initially HSE-poor metal, if produced by reduction of FeO) are established during equilibration with the surrounding silicate.

This model also requires the segregation of the metal grains and incorporation of those metal grains into the melt that crystallized fragment B. One potential mechanism for the third stage of this model is metal-silicate equilibration of metallic droplets gravitationally settling through a magma ocean (e.g., Rubie et al., 2003). These droplets then collect at a boundary, perhaps the bottom of a magma ocean or pond, and are later brought to the surface, either through magmatism or possibly during mantle overturn. Mantle overturn requires a relatively large planetary (~2,200 km; Brown and Elkins-Tanton, 2009; Elkins-Tanton, 2012). The fourth stage of this model requires addition of CI-like chondritic material. If the HSE abundances of fragment A were set primarily by addition of exogenous chondritic material, it is likely that fragment B also experienced some addition of exogenous chondritic material. However, the addition of material to fragment B must have been relatively minor compared to fragment A.

Table 2.3. HSE abundances (ppb) calculated for progressive stages of planetary differentiation using low-pressure metal-silicate partition coefficients from Table 2.2.

| Stage | Re | Os | Ir | Ru | Pt | Pd |
|---|---|---|---|---|---|---|
| 1. Post Core Formation | $2.71 \times 10^{-9}$ | $2.73 \times 10^{-8}$ | $1.54 \times 10^{-9}$ | $1.15 \times 10^{-9}$ | $4.49 \times 10^{-13}$ | $9.38 \times 10^{-5}$ |
| 2. Late Accretion | $3.12 \times 10^{-9}$ | $3.22 \times 10^{-8}$ | $6.16 \times 10^{-9}$ | $8.03 \times 10^{-9}$ | $9.43 \times 10^{-9}$ | $9.38 \times 10^{-5}$ |
| 3. Metal Seg. and Incorp. | 0.00311 | 0.0321 | 0.00616 | 0.00803 | 0.00943 | 15.6 |
| 4. Minor CI Addition | 0.00718 | 0.0812 | 0.0524 | 0.0768 | 0.104 | 15.7 |
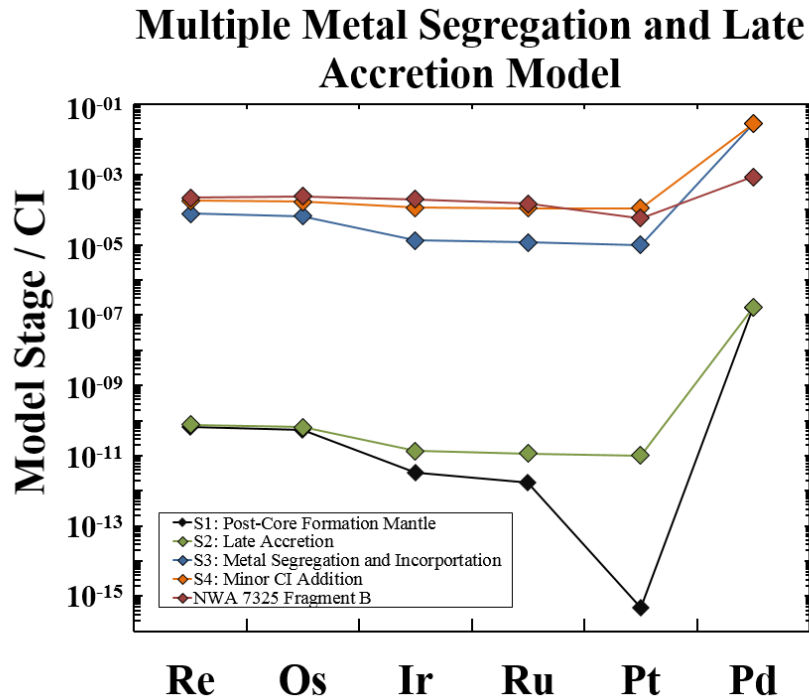


Figure 2.10. HSE abundances at different stages of a planetary body differentiation model using low-pressure metal-silicate partition coefficients. S*x* refers to individual stages described in the text. Data for CI chondrites from Fischer-Gödde et al., (2010). Partition coefficients and references provided in Table 2.2.

The absolute and relative HSE abundances of NWA 7325 fragment B share some similarities with previously published HSE data for some diogenites (Fig. 2.11; Day et al., 2012b). Partial melting of the mantle of the NWA 7325 parent body, containing chondritic relative abundances of the HSE, and crust-mantle partitioning could have led to the HSE fractionations of fragment B, as suggested by Day et al. (2012b) for diogenites with the lowest HSE abundances.

49
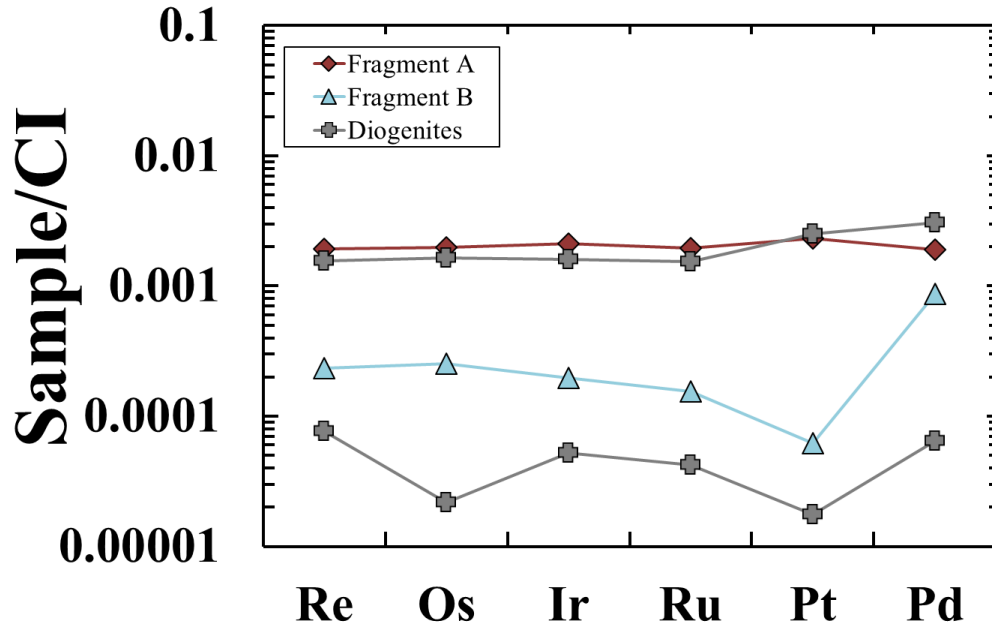
Figure 2.11. CI-normalized (Horan et al., 2003) HSE abundances for NWA 7325 fragments, as well as two diogenites from Day et al. (2012b).

In terrestrial, sulfide-dominated systems Re, Pt, and Pd behave incompatibly, typically producing suprachondritic Re/Ir, Pt/Ir, and Pd/Ir in products of mantle partial melting. In fragment B, Pd/Ir is suprachondritic, whereas Re/Ir is nearly chondritic and Pt/Ir is subchondritic. However, in lunar and martian samples, Re tends to behave compatibly, which has been attributed to the lower O fugacity of those planetary bodies (Birck and Allégre, 1994). NWA 7325 likely also formed under reducing conditions (~IW-4.5; Sutton et al., 2014), and Re would have, therefore, behaved compatibly. However, the subchondritic Pt/Ir cannot be explained by current understanding of crust-mantle partitioning. Nevertheless, the Pt/Ir of diogenite MET 00424, 20, which was interpreted by Day et al. (2012b) to also be the result of crust-mantle partitioning, also is subchondritic. Therefore, it appears that Pt may have behaved compatibly on the HED parent body and the NWA 7325 parent body.

*2.7. Synthesis*

The data reported here for ungrouped achondrites NWA 6704 and NWA 7325 complement the accumulated dataset for HSE and $^{187}$Re-$^{187}$Os systematics of various major primitive and differentiated achondrite groups. NWA 6704 and NWA 7325 crystallized within one million years of each other, and ~5 million years after CAI formation. NWA 7325 originated from a parent body that probably underwent very complex processing, including core formation and late accretion, as well as partial melting. By contrast, NWA 6704 appears to be from a parent body that underwent limited melting. Therefore, contemporary planetary bodies appear to have undergone variable degrees of differentiation in the early Solar System, and the variety is probably a result of size differences, as smaller parent bodies do not retain heat as efficiently as larger parent bodies.

The crystallization ages and HSE abundances of many differentiated achondrites, including angrites, diogenites, and NWA 7325, indicate that their parent bodies produced Fe,Ni-rich cores within the first few million years of Solar System history (Riches et al., 2012; Day et al. 2012b). In addition, at least one sample from the each of the angrite and diogenite groups and NWA 7325 have HSE abundances that have chondritic relative HSE abundances, indicating that these parent bodies were also affected by late accretion. Further, the variability in absolute HSE abundances among different samples from the same parent bodies indicates that the mixing of late-accreted material was incomplete for these parent bodies. Taken together, all of these lines of evidence indicate that i) late accretion was prevalent among parent bodies that produced Fe,Ni-rich cores, ii) late accretion had already begun and was probably

51

ongoing when differentiated achondrites formed, and iii) efficient mixing of late-accreted material in the mantles of these parent bodies did not occur by the time these meteorites formed.

The nearly chondritic absolute HSE abundances of primitive achondrites are inconsistent with core formation having occurred on any of their respective parent bodies by the time these rocks formed. Late accretion may have occurred on primitive achondrite parent bodies, but the chondritic absolute HSE abundances of these meteorites makes it nearly impossible to detect. Based on HSE abundances, only igneous processes appear to have been active on primitive achondrite parent bodies.

The HSE abundances of all primitive and differentiated achondrites indicate that igneous processes were common on parent bodies within the first ~5 million years of Solar System history. For all differentiated achondrite parent bodies and some primitive achondrite parent bodies, melting and crystallization probably took place during mantle-crust differentiation driven by indigenous heating (decay of $^{26}$Al). By contrast, some primitive achondrite parent bodies (like the NWA 6704 parent body) probably experienced melting and crystallization caused by local impact-driven heating.

## 2.A. Appendix

The calculated HSE abundances for a silicate in equilibrium with the measured metal from NWA 6704, using the lowest reported D values for the HSE, are shown in Fig. 2.A.1. Only the measured Pd abundance for the silicate fraction overlaps with the calculated equilibrium abundances (dashed field).
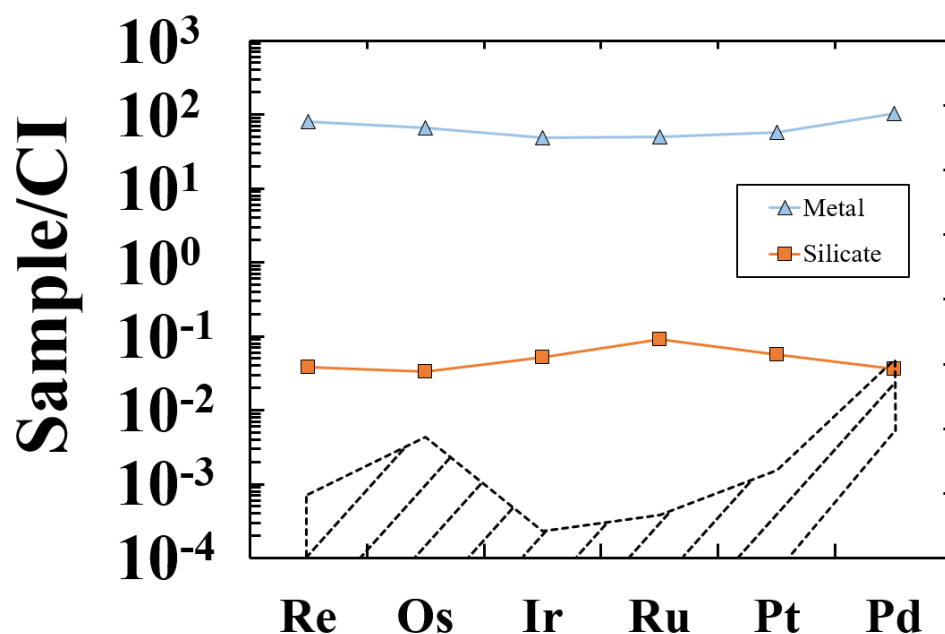
Figure 2.A.1. CI-normalized (Horan et al., 2003) HSE abundances of NWA 6704 silicate and metal fractions. Uncertainties are smaller than symbols. Dashed field indicates calculated HSE abundances of silicate in equilibrium with NWA 6704 metal over a range of temperatures and pressures. Calculations were made using partition coefficients over a range of conditions for Re, Ir, Ru, Pt, and Pd (Mann et al., 2012) and Os (Yokoyama et al., 2009).

*References for Chapter 2*

Archer G.J., Ash R.D., Bullock E.S., and Walker R.J. (2014) Highly siderophile elements and [187]Re-[187]Os isotopic systematics of the Allende meteorite: Evidence for primary nebular processes and late-stage alteration. *Geochim. Cosmochim. Acta* **131**, 402-414.

Arculus R.J. and Delano J.W. (1981) Siderophile element abundances in the upper mantle: evidence for a sulfide signature and equilibrium with the core. *Geochim. Cosmochim Acta* **45**, 1331–1343.

Barnes S.-J., Naldrett A.J., and Gorton M.P. (1985) The origin of the fractionation of platinum-group elements in terrestrial magmas. *Chem. Geol.* **53**, 302–323.

Becker H., Morgan J.W., Walker R.J., MacPherson G.L. and Grossman J.N. (2001) Rhenium–osmium systematics of calcium–aluminum-rich inclusions in carbonaceous chondrites. *Geochim. Cosmochim. Acta* **65**, 3379–3390.

Birck J.L. and Allégre C.L. (1994) Contrasting Re/Os magmatic fractionation in planetary basalts. *Earth Planet. Sci. Lett.* **124**, 139–148.

Birck J.L., Barman M.R., and Capmas, F. (1997) Re–Os isotopic measurements at the femtomole level in natural samples. *Geostand. Newsl.* **21**, 19–27.

Borisov A., Palme H., and Spettel B. (1994) Solubility of palladium in silicate melts: Implications for core formation in the Earth. *Geochim. Cosmochim. Acta* **58**, 705–716.

Borisov A. and Palme H. (1995) The solubility of iridium in silicate melts: new data from experiments with $Ir_{10}Pt_{90}$ alloys. *Geochim. Cosmochim. Acta* **59**, 481–485.

Borisov A. and Nachtweyh K. (1998) Ru solubility in silicate melts: experimental results in oxidizing region. *Lunar Planet. Sci. XXIX.* Lunar Planet. Inst., Houston. #1320 (abstr.).

Borisov A. and Palme H. (1998) Experimental determination of osmium metal-silicate partitioning coefficient. *Neues Jb. Miner. Abh.* **172**, 347–356.

Borisov A. (2006) Experimental study of the effect of $SiO_2$ on Ni solubility in silicate melts. *Petrologiya* **14**, 530–539.

Brandon A.D., Humayun M., and Puchtel I.S. (2005) Re–Os isotopic systematics and platinum group element concentration of the Tagish Lake carbonaceous chondrite. *Geochim Cosmochim Acta* **69**:1619–1631

Brandon A.D., Puchtel I.S., Walker R.J., Day J.M.D., Irving, A.J., and Taylor L.A. (2012) Evolution of the martian mantle inferred from the $^{187}$Re-$^{187}$Os isotope and highly siderophile element abundance systematics of shergottite meteorites. *Geochim. Cosmochim. Acta* **76**, 206-235.

Brown S. and L.T. Elkins-Tanton (2009) Composition of Mercury's oldest crust from magma ocean models. *Earth Planet. Sci. Lett.* **286**, 446-455.

Capobianco C.J., Jones J. H., and Drake M.J. (1993) Metal-silicate thermochemistry at high temperature: Magma oceans and the "excess siderophile element" problem of the Earth's Upper Mantle. *J. Geophys. Res.* **98**, 5433-5443.

Carlson R.W. and Hauri E.H. (2001) Extending the $^{107}$Pd–$^{107}$Ag chronometer to low Pd/Ag meteorites with multicollector plasma-ionization mass spectrometry. *Geochim. Cosmochim. Acta* **65**, 1839–1848.

Chou C.-L. (1978) Fractionation of siderophile elements in the Earth's upper mantle. *Proc. 9th Lunar Planet. Sci. Conf.*, 219–230.

Clayton R.N., Onuma N., and Mayeda T.K., (1976) Classification of Meteorites Based on Oxygen Isotopes. *Earth Planet. Sc. Lett.* **30**, 10-18.

Cohen A.S. and Waters F.G. (1996) Separation of osmium from geological materials by solvent extraction for analysis by thermal ionisation mass spectrometry. *Anal. Chim. Acta* **332**, 269–275.

Creaser R.A., Papanastassiou D.A., and Wasserburg G.J. (1991) Negative thermal ion mass spectrometry of osmium, rhenium and iridium. *Geochim. Cosmochim. Acta* **55**, 397–401.

Day J.M.D. (2013) Hotspot volcanism and highly siderophile elements. *Chem. Geol.* **341**, 50–74.

Day J.M.D., Pearson D.G., and Taylor L.A. (2007) Highly siderophile element constraints on accretion and differentiation of the Earth–Moon system. *Science* **315**, 217–219.

Day J.M.D., Ash R.D., Liu Y., Bellucci J.J., Rumble D. III., McDonough W.F., Walker R.J., and Taylor L.A. (2009) Early formation of evolved asteroidal crust. *Nature* **457**, 179–182.

Day J.M.D., Pearson D.G., Macpherson C.G., Lowry D. and Carracedo J.C. (2010a) Evidence for distinct proportions of subducted oceanic crust and lithosphere in HIMU-type mantle beneath El Hierro and La Palma, Canary Islands. *Geochim. Cosmochim. Acta* **74**, 6565–6589.

Day J.M.D., Walker R.J., James O.B., and Puchtel I.S. (2010b) Osmium isotope and highly siderophile element systematics of the lunar crust. *Earth Planet. Sci. Lett.* **289**, 595–605.

Day J.M.D., Walker R.J., Ash R.D., Liu Y., Rumble D. III., Irving A.J., Goodrich C.A., Tait K.,  McDonough W.F., and Taylor L.A. (2012a) Origin of felsic achondrites Graves Nunataks 06128 and 06129, and ultramafic brachinites and brachinite-like achondrites by partial melting of volatile-rich primitive parent bodies.  *Geochim. Cosmochim. Acta* **81**, 94-128.

Day J.M.D., Walker R.J., Qin L., and Rumble D. III. (2012b) Late accretion as a natural consequence of planetary growth. *Nat. Geosci.* **5**, 614–617.

Day J.M.D., Corder C.A., Rumble D., Assayag N., Cartigny P., Taylor L.A. (2015) Common differentiation processes in oxidised and reduced asteroids revealed by the achondrite Lewis Cliff 88763. *Meteor Planet Sci* (in press).

Day, J.M.D. (2016) Siderophile Elements. In *Encyclopedia of Geochemistry* (ed. W.M. White): Springer.

Elkins-Tanton L.T. (2012) Magma oceans in the inner solar system. *Annual Review of Earth and Planetary Sciences* **40**, 113-139.

Ertel W., O'Neill H.S.C., Sylvester P.J., and Dingwell D.B. (1999) Solubilities of Pt and Rh in a haplobasaltic melt at 1300°C. *Geochim. Cosmochim. Acta* **63**, 2439–2449.

Ertel W., O'Neill H.S.C., Sylvester P.J., Dingwell D.B., and Spettel B. (2001) The solubility of rhenium in silicate melts: Implications for the geochemical properties of rhenium at high temperature. *Geochim. Cosmochim. Acta* **65**, 2161–2170.

Fischer-Gödde M., Becker H., Wombacher F. (2010) Rhodium, gold and other highly siderophile element abundances in chondritic meteorites. *Geochim Cosmochim Acta* **74**:356–379.

Fortenfant S.S., Günther D., Dingwell D. B. and Rubie D. C. (2003) Temperature dependence of Pt and Rh solubilities in a haplobasaltic melt. *Geochim. Cosmochim. Acta* **67**, 123–131.

Goodrich C.A., Kita N.T., and Nakashima D. (2014) Petrology of the NWA 7325 ungrouped achondrite – meteorite from Mercury, the ureilite parent body, or a previously unsampled asteroid?. *Lunar Planet. Sci. XXXXV*. Lunar Planet. Inst., Houston. #1246 (abstr.).

Hibiya, Y. (2016) The origin of primitive achondrites inferred from a mineralogical and isotope cosmochemical study of NWA 6704. MS thesis. The University of Tokyo.

Hibiya Y., Archer G.J., Tanaka R., Iizuka T., Ozawa K., Walker R.J., and Yamaguchi A. The origin and formation process of the NWA 6704 primitive achondrite: Petrology, highly siderophile element chemistry, and O-Ti isotope systematics, in prep.

Horan M.F., Walker R.J., Morgan J.W., Grossman J.N., and Rubin A. (2003) Highly siderophile elements in chondrites. *Chem. Geol*. **196**, 5–20.

Iizuka T., Amelin Y., Puchtel I.S., Walker R.J., Irving A.J., Yamaguchi A., Takagi Y., Noguchi T., and Kimura M. (2013) U-Pb age, Re-Os isotopes, and HSE geochemistry of Northwest Africa 6704. *Lunar Planet. Sci. XLIV*. Lunar Planet. Inst., Houston. #1841 (abstr.).

Irving A.J., Tanaka R., Steele A., Kuehner S.M., Bunch T.E., Wittke J.H. and Hupe G.M. (2011) Northwest Africa 6704: a unique cumulate permafic achondrite containing sodic feldspar, awaruite and "fluid" inclusions, with an oxygen isotopic composition in the acapulcoite-lodranite field. *74th Annual Meteoritical Society Meeting* #5231 (abstr.).

Irving A. J., Kuehner S. M., Bunch T. E., Ziegler K., Chen G., Herd C. D. K., Conrey R. M., and Ralew S. (2013) Ungrouped mafic achondrite Northwest Africa 7325: a reduced, iron-poor cumulate olivine gabbro from a differentiated planetary parent body. *Lunar Planet. Sci. XLIV*. Lunar Planet. Inst., Houston. #2164 (abstr.)

Jambon A., Humayun M., Barrat J.-A., Greenwood R.C., and Franchi I. (2012) Northwest Africa 6693: a unique achondritic cumulate. *Lunar Planet. Sci. XLIII*. Lunar Planet. Inst., Houston. #2099 (abstr.).

Jones J.H. and Drake M.J. (1986) Geochemical constraints on core formation in the Earth. *Nature* **322**, 221–228.

Koefoed P., Amelin Y., Yin Q.-Z., Wimpenny J., Sanborn M.E., Iizuka T., and Irving A.J. (2016) U-Pb and Al-Mg systematics of the ungrouped achondrite Northwest Africa 7325. *Geochim. Cosmochim. Acta* **183**, 31-45.

Kimura, K., Lewis, R.S., and Anders, E. (1974) Distribution of gold and rhenium between nickel– iron and silicate melts: implications for the abundance of siderophile elements on the Earth and Moon. *Geochim. Cosmochim. Acta* **38**, 683–701.

Krot A.N., Keil K., Goodrich C.A., Scott E.R.D., and Weisberg M.K. (2004) Classification of Meteorites. In *Treatise on Geochemistry, Vol. 1: Meteorites, Comets, and Planets* (ed. A. M. Davis) Elsevier, Oxford. pp. 83–128.

Laurenz V., Fonseca R.O.C., Ballhaus C. and Sylvester P.J. (2010) Solubility of palladium in picritic melts: 1. The effect of iron. *Geochim. Cosmochim. Acta* **74**, 2989–2998.

Li J. and Agee C.B. (1996) Geochemistry of mantle-core formation at high pressure. *Nature* **381**, 686–689.

Ludwig K.R. 2001. Users Manual for Isoplot/Ex version 2.47. A geochronological toolkit for Microsoft Excel. Berkeley Geochronology Center Special Publication 1a, 55pp.

Mann U., Frost D.J., Rubie D.C., Becker H., and Audétat A. (2012) Partitioning of Ru, Rh, Pd, Re, Ir and Pt between liquid metal and silicate at high pressures and temperatures- Implications for the origin of highly siderophile element concentrations in the Earth's mantle. *Geochim. Cosmochim. Acta* **84**, 593–613.

Markowski A., Quitté G., Kleine T., Halliday A., Bizzarro M., and Irving A.J. (2007) Hf–W chronometry of angrites and the earliest evolution of planetary bodies. *Earth Planet. Sci. Lett.* **262**, 214–229.

McCord T.B., Adams J.B., and Johnson T.V. (1970) Asteroid Vesta: Spectral reflectivity and compositional implications. *Science* **168**, 1445–1447.

McSween H.Y. and 21 colleagues (2013) Composition of the Rheasilvia basin, a window into Vesta's interior. *J. Geophys. Res., Planets* **118** (2), 335–346.

Meisel T., Fellner N. and Moser J. (2003) A simple procedure for the determination of platinum group elements and rhenium (Ru, Rh, Pd, Re, Os, Ir, and Pt) using ID-ICP-MS with an inexpensive on-line matrix separation in geological and environmental materials. *J. Anal. Atomic Spectr.* **18**, 720–726.

Mikouchi T. and Miyamoto M. (2008) Mineralogy and pyroxene cooling rate of unique achondrite meteorite GRA 06129. *Lunar Planet. Sci. XXXIX.* Lunar Planet. Inst., Houston. #2297 (abstr.).

Mittlefehldt D.W. (2003) Achondrites. In *Meteorites, Planets, and Comets*, Vol. 1 (eds. H. D. Holland and K. K. Turekian). Elsevier-Pergamon, Oxford, pp. 291-324.

Newsom H.E. (1990) Accretion and core formation in the Earth: evidence from siderophile elements. In *Origin of the Earth* (eds. H.E. Newsom and J.H. Jones) Oxford Univ. Press, New York, pp. 273–288.

Nyquist L.E., Kleine T., Shih C. and Reese Y.D. (2009) The distribution of short-lived radioisotopes in the early solar system and the chronology of asteroid accretion, differentiation, and secondary mineralization. *Geochim. Cosmochim. Acta* **73**, 5115–5136.

O'Neill H.S.C., Dingwell D.B., Borisov A., Spettel B., and Palme H. (1995) Experimental petrochemistry of some highly siderophile elements at high temperatures, and some implications for core formation and the mantle's early history. *Chem. Geol.* **120**, 255–273.

Puchtel I.S., Humayun M., Campbell A.J., Sproule R.A. and Lesher C.M. (2004) Platinum group element geochemistry of komatiites from the Alexo and Pyke Hill areas, Ontario, Canada. *Geochim. Cosmochim. Acta* **68**, 1361–1383.

Puchtel I.S., Humayun M. and Walker R.J. (2007) Os–Pb–Nd isotope and highly siderophile and lithophile trace element systematics of komatiitic rocks from the Volotsk suite, SE Baltic Shield. *Precambrian Res.* **158**, 119–137.

Rankenburg K., Humayun M., Brandon A. D. and Herrin J. S. (2008) Highly siderophile elements in ureilites. *Geochim. Cosmochim. Acta* **72**, 4642–4659.

Rehkämper M., and Halliday, A.N. (1997) Development and application of new ion-exchange techniques for the separation of the platinum group and other siderophile elements from geological samples. *Talanta* **44**, 663-672.

Riches A.J.V., Day J.M.D., Walker R.J., Simonetti A., Liu Y., Neal C.R., and Taylor L.A. (2012) Rhenium-osmium isotope and highly-siderophile-element abundance systematics of angrites meteoerites. *Earth Planet. Sci. Lett.* **353-354**, 208-218.

Ringwood A.E. (1977) Composition of core and implications for origin of Earth. *Geochem. J.* **11**, 111–135.

Rubie D.C., Melosh H.J., Reid J.E., Liebske C., and Righter K. (2003) Mechanisms of metal-silicate equilibration in the terrestrial magma ocean. *Earth Planet. Sci. Lett.* **205**, 239–255.

Rudnick R.L. and Walker R.J. (2009) Interpreting ages from Re–Os isotopes in peridotites. *Lithos* **112S**, 1083–1095.

Ruzicka A., Snyder G.A., and Taylor L.A. (1997) Vesta as the howardite, eucrite and diogenite parent body: Implications for the size of a core and for large scale differentiation. *Meteoritics & Planetary Science* **32**, 825–840.

Shirey S.B. and Walker R.J. (1995) Carius tube digestion for low blank rhenium-osmium analysis. *Anal. Chem.* **67**, 2136-2141.

Sutton S.R., Wirick S., and Goodrich C.A. (2014) Ungrouped achondrite NWA 7325: Titanium, vanadium and chromium xanes of mafic silicates record highly-reduced origin. *Lunar Planet. Sci. XLV*. Lunar Planet. Inst., Houston. #1275 (abstr.)

Van Acken, D., Brandon, A.D., and Humayun, M. (2011) High-precision osmium isotopes in senstatite and Rumuruti chondrites. *Geochim. Cosmochim. Acta.* **75**, 4020-4036.

Walker R.J. (2009) Highly siderophile elements in the Earth, Moon and Mars: update and implications for planetary accretion and differentiation. *Chemie der Erde* **69**, 101–125.

Walker R.J., Storey M., Kerr A.C., Tarney J. and Arndt N.T. (1999) Implication of [187]Os isotopic heterogeneities in a mantle plume: evidence from Gorgona Island and Curacao. *Geochim. Cosmochim. Acta* **63**, 713–728.

Walker R.J., Horan M.F., Morgan J.W., Becker H., Grossman J.N., and Rubin A. (2002) Comparative [187]Re–[187]Os systematics of chondrites: Implications regarding early solar system processes. *Geochim. Cosmochim. Acta.* **66**:4187–4201.

Walker R.J., Bermingham K., Liu J., Puchtel I.S., Touboul M., and Worsham E.A. (2015) In search of late-stage planetary building blocks. *Chem. Geol*. **411**, 125–142.

Walter M.J., Newsom H.E., Ertel W., and Holzheid A. (2000) Siderophile elements in the Earth and Moon. Metal/Silicate partitioning and implication for core formation. In: *Origin of the Earth and Moon* (eds. Canup R.M. and Righter K.). University of Arizona Press, Tucson, pp. 265–289.

Warren P.H., Ulff-Møller F., Huber H. and Kallemeyn G.W. (2006) Siderophile geochemistry of ureilites: a record of early stages of planetesimal core formation. *Geochim. Cosmochim. Acta* **70**, 2104–2126.

Warren P.H., Rubin A.E., Isa J., Brittenham S., Ahn I., and Choi B.-G. (2013) Northwest Africa 6693: A new type of FeO-rich, low-$\Delta^{17}$O, poikilitic cumulate achondrite. *Geochim. Cosmochim. Acta* **107**, 135-154.

Weisberg M.K., McCoy T.J., and Krot A.N. (2006). Systematics and evaluation of meteorite classification. In *Meteorites and the Early Solar System II, Part I: Meteoritics Overview*: (eds. Lauretta, D.S. and McSween Jr., H.Y.). University of Arizona Press, Tucson, pp. 19–52.

Yin Q.-Z., Wimpenny J.B., and Amelin Y. (2013) Al-Mg systematics of the ungrouped achondrite NWA 6704. *76th Annual Meteoritical Society Meeting* #5160 (abstr.).

# Chapter 3: High-precision analysis of $^{182}$W/$^{184}$W and $^{183}$W/$^{184}$W by negative thermal ionization mass spectrometry: Per-integration oxide corrections using measured $^{18}$O/$^{16}$O

## 3.1. Abstract

Here we describe a new analytical technique for the high-precision measurement of $^{182}$W/$^{184}$W and $^{183}$W/$^{184}$W using negative thermal ionization mass spectrometry (N-TIMS). We improve on the recently reported method of Trinquier et al. (2016), which described using Faraday cup collectors coupled with amplifiers utilizing $10^{13}\,\Omega$ resistors to continuously monitor the $^{18}$O/$^{16}$O of WO$_3^-$ and make per-integration oxide corrections. In our study, we report and utilize a newly measured oxygen mass fractionation line, as well as average $^{17}$O/$^{16}$O and $^{18}$O/$^{16}$O, which allow for more accurate per-integration oxide interference corrections. We also report a Faraday cup and amplifier configuration that allows $^{18}$O/$^{16}$O to be continuously monitored for WO$_3^-$ and ReO$_3^-$, both of which are ionized during analyses of W using Re ribbon. The long-term external precision of $^{182}$W/$^{184}$W is 5.7 ppm and 3.7 ppm (2SD) when mass bias corrected using $^{186}$W/$^{184}$W and $^{186}$W/$^{183}$W, respectively. For $^{183}$W/$^{184}$W mass bias is corrected using $^{186}$W/$^{184}$W, yielding a long-term external precision of 6.6 ppm. An observed, correlated variation in $^{182}$W/$^{184}$W and $^{183}$W/$^{184}$W, when mass bias corrected using $^{186}$W/$^{184}$W, is most likely the result of Faraday cup degradation over months-long intervals.

The $^{182}$Hf-$^{182}$W isotopic system ($t_{1/2}$=8.9 Myr; Vockenhuber et al., 2004) is useful for constraining the timing of early Solar System metal-silicate equilibration because W is moderately siderophile and largely partitions into Fe-rich metal, whereas Hf is lithophile and partitions entirely into silicate. The most widely used application for this system has been dating core formation of planetary bodies (e.g., Lee and Halliday, 1995; Harper and Jacobsen, 1996; Kruijer et al., 2014a). This system has also been used to assess the thermal histories of chondrite parent bodies (Kleine et al., 2008), and to investigate mantle evolution (e.g., Willbold et al., 2011; 2015; Touboul et al., 2012; 2014; Liu et al., 2016). In some instances, isotopic variations in $^{182}$W/$^{184}$W are <20 ppm.

During the analysis of W by N-TIMS when using Re filaments as the ionizing substrate, the different species of ReO$_3^-$ and WO$_3^-$ that incorporate $^{17}$O and/or $^{18}$O (e.g., $^{182}$W$^{16}$O$_2$$^{18}$O$^-$ and $^{185}$Re$^{16}$O$_2$$^{17}$O$^-$) form isobaric interferences on the signals of some of the primary W$^{16}$O$_3^-$ beams measured. The O isotopic compositions of ReO$_3^-$ and WO$_3^-$ must, therefore, be accurately determined for isobaric interference corrections, and the in-run fractionation of O isotopes during analyses must also be monitored.

Touboul and Walker (2012) reported an N-TIMS method capable of measuring $^{182}$W/$^{184}$W with a long-term external reproducibility of <5 ppm (2SD). That study used the O isotopic composition of the atmosphere reported by Nier (1950) to make a first-order correction for oxide interferences on primary $^x$W$^{16}$O$_3^-$ signals. Then, a second-order correction utilized the coevolution of $^{183}$W/$^{184}$W and $^{182}$W/$^{184}$W to correct for in-run fractionations of O isotopes. Because it used an assumed $^{183}$W/$^{184}$W in the

correction process, this method did not allow a corresponding measurement of $^{183}W/^{184}W$, which varies among some meteorites (e.g., Kruijer et al., 2014b).

A more recent analytical technique (Trinquier et al., 2016) reported measurements of both $^{182}W/^{184}W$ and $^{183}W/^{184}W$ with long term external reproducibilities of ~10-11 ppm (2SD) and ~17-18 ppm (2SD), respectively. As in Touboul and Walker (2012), they corrected minor oxide interferences assuming the atmospheric composition reported by Nier (1950). They corrected in-run fractionations of O isotopes using per-integration measured $^{186}W^{16}O_2^{18}O/^{186}W^{16}O_3$ to calculate $^{18}O/^{16}O$ and infer $^{17}O/^{16}O$, using a terrestrial fractionation slope passed through the $^{17}O/^{16}O$ and $^{18}O/^{16}O$ reported by Nier (1950).

The methods reported by these two prior studies bear some additional scrutiny. The use of the $^{17}O/^{16}O$ and $^{18}O/^{16}O$ ratios reported by Nier (1950) may not be appropriate for measurements of $ReO_3^-$ and $WO_3^-$ via N-TIMS. Further, Trinquier et al. (2016) measured only the $^{18}O/^{16}O$ of $WO_3^-$ for each integration. The O isotopic composition of $ReO_3^-$ was assumed to uniformly follow the same evolution trend, which may not be the case. Trinquier et al. (2016) reported that the method was limited to analyses with Re/W < 0.3, as a systematic bias to higher values was observed for analyses with high Re/W. Some sample and standard analyses, especially those with low W abundances, sometimes have Re/W >0.3.

Here we present a new analytical technique, refining the methods of Touboul and Walker (2012) and Trinquier et al. (2016), for making measurements of $^{182}W/^{184}W$ and $^{183}W/^{184}W$ to external precisions ~5 ppm, even for analyses with Re/W > 0.3. This analytical technique uses a new average $^{17}O/^{16}O$ and $^{18}O/^{16}O$, appropriate for measuring

ReO$_3^-$ and WO$_3^-$ by N-TIMS, and a new O mass fractionation line for oxide corrections. Per-integration fractionations of oxygen isotopes are corrected for both ReO$_3^-$ and WO$_3^-$ by measuring both $^{186}$W$^{16}$O$_2$$^{18}$O/$^{186}$W$^{16}$O$_3$ and $^{187}$Re$^{16}$O$_2$$^{18}$O/$^{187}$Re$^{16}$O$_3$.

### *3.3. Experimental Section*

#### *3.3.1. Filament Preparation and Loading*

A filament loading technique slightly modified from Touboul and Walker (2012) was used. Either 300 ng, 500 ng, or 1000 ng of *Alfa Aesar* W standard solution were loaded onto single Re filaments, which were outgassed ~48 hours in advance. Throughout this study, both thick (0.76 mm wide x 0.030 mm thick) and thin (0.51 mm wide x 0.025 mm thick) Re filaments were used. After loading W, Re filaments were briefly (~1s) heated to a dull glow to remove trace organics, and then left to sit for at least 24 hours before loading activator. To enhance ionization, 1 µL of activator solution containing 5 µg each of La and Gd in 5% Teflon distilled HNO$_3$ was then added in 2-3 aliquots to the standard and sample deposits, and then dried until a white crust formed.

#### *3.3.2. Instrumental Setup*

Analyses were performed on the UMd *Thermo-Fisher Triton* thermal ionization mass spectrometer. Oxide production was enhanced by bleeding O (P$_{O2}$=1.0x10$^{-7}$ mbar) into the source can using a *Varian* leak valve. Similar to the method of Touboul and Walker (2012), all analyses by this study used a multi-static analytical protocol with two lines of acquisition, which allowed Faraday cup biases to be monitored. Each line of acquisition utilized 9 Faraday cups (Table 3.1). Seven Faraday cups (L4-H2)

were electronically connected to amplifiers with $10^{11}$ Ω resistors, which were electronically rotated during analyses to mitigate amplifier biases. Faraday cups H3 and H4 were connected to amplifiers with $10^{12}$ Ω resistors to measure the low signals generated by the minor $^{186}W^{16}O_2{}^{18}O^-$ and $^{187}Re^{16}O_2{}^{18}O^-$ species, which were used to calculate per-integration oxide corrections. These amplifiers were not rotated during analyses. The center Faraday cup was centered on masses 232 ($^{184}W^{16}O_3{}^-$) and 234 ($^{186}W^{16}O_3{}^-$) for acquisition lines 1 and 2, respectively.

Table 3.1. Faraday cup-amplifier-resistor configuration for measurement of W using N-TIMS utilizing 9 Faraday cups.

| | L4 | L3 | L2 | L1 | C | H1 | H2 | H3 | H4 |
|---|---|---|---|---|---|---|---|---|---|
| Line 1 | $^{180}W^{16}O_3$ | $^{181}Ta^{16}O_3$ | $^{182}W^{16}O_3$ | $^{183}W^{16}O_3$ | $^{184}W^{16}O_3$ | $^{185}Re^{16}O_3$ | $^{186}W^{16}O_3$ | $^{186}W^{16}O_2{}^{18}O$ | $^{187}Re^{16}O_2{}^{18}O$ |
| Line 2 | $^{182}W^{16}O_3$ | $^{183}W^{16}O_3$ | $^{184}W^{16}O_3$ | $^{185}Re^{16}O_3$ | $^{186}W^{16}O_3$ | $^{187}Re^{16}O_3$ | $^{186}W^{16}O_2{}^{18}O$ | $^{190}Os^{16}O_3$ | |
| Resistor | $10^{11}$ Ω | $10^{11}$ Ω | $10^{11}$ Ω | $10^{11}$ Ω | $10^{11}$ Ω | $10^{11}$ Ω | $10^{11}$ Ω | $10^{12}$ Ω | $10^{12}$ Ω |

With this analytical protocol, all $W^{16}O_3{}^-$ and $Re^{16}O_3{}^-$ species were measured, and inter-collector biases were corrected for all major W species ($^{182}W^{16}O_3{}^-$, $^{183}W^{16}O_3{}^-$, $^{184}W^{16}O_3{}^-$, and $^{186}W^{16}O_3{}^-$). The $^{186}W^{16}O_2{}^{18}O^-$ and $^{187}Re^{16}O_2{}^{18}O^-$ species were also measured, from which the $^{18}O/^{16}O$ could be calculated, and the $^{17}O/^{16}O$ could be inferred using an O mass fractionation line. One isotope each of Ta and Os ($^{181}Ta$ and $^{190}Os$) were also monitored so that isobaric interference corrections for species of these elements could be made (e.g., $^{180}Ta^{16}O_3{}^-$ or $^{186}Os^{16}O_3{}^-$). However, these signals were below detection limits for all analyses.

Typically, 600 integrations were measured over 770 minutes, although some analyses were cut short because of rapidly decreasing signals. A 1260 s baseline (background signal) was measured at the beginning of each analysis and then re-measured every 100 integrations. Each integration consisted of 33.6 s and 8.4 s of

integration time for acquisition lines 1 and 2, respectively. The idle times before integrations were 10 s and 4 s for acquisition lines 1 and 2, respectively.

### 3.3.3. Data Reduction

In the first data reduction step, single estimated values (see section 3.4.1) for $^{17}O/^{16}O$ (0.0003913) and $^{18}O/^{16}O$ (0.002096) were used to make first-order oxide interference corrections to all $^{x}W^{16}O_3^{-}$ and $^{x}Re^{16}O_3$ signals. Relative abundances of trioxide species for each W and Re isotope (e.g., $^{184}W^{17}O^{16}O_2^{-}$, $^{184}W^{18}O^{16}O_2^{-}$, $^{184}W^{18}O_2^{16}O^{-}$, etc.) were calculated following the calculations of Harper and Jacobsen (1996), using the estimated $^{17}O/^{16}O$ and $^{18}O/^{16}O$. In the next step, first-order oxide-corrected $^{186}W^{16}O_2^{18}O^{-}/^{186}W^{16}O_3^{-}$ and $^{187}Re^{16}O_2^{18}O^{-}/^{187}Re^{16}O_3^{-}$ from each integration were used to calculate per-integration $^{18}O/^{16}O$ for $WO_3^{-}$ and $ReO_3^{-}$. A linear trend with a terrestrial fractionation slope (0.0954) that passed through the estimated values for $^{17}O/^{16}O$ (0.0003913) and $^{18}O/^{16}O$ (0.002096) was then used to calculate per-integration $^{17}O/^{16}O$ from each per-integration $^{18}O/^{16}O$.

Per-integration $^{17}O/^{16}O$ and $^{18}O/^{16}O$ were then used to make line-by-line oxide corrections to all $^{x}W^{16}O_3^{-}$ and $^{x}Re^{16}O_3^{-}$ signals. All isobaric interferences on $^{x}W^{16}O_3^{-}$ and $^{x}Re^{16}O_3^{-}$ for which corrections were made are listed in Table 3.2. No corrections were made for low abundance trioxide species (e.g., $^{x}W^{18}O_3^{-}$) that do not significantly interfere with primary $^{x}W^{16}O_3^{-}$ and $^{x}Re^{16}O_3^{-}$ signals (Yin, 1995).

Finally, the per-integration oxide-corrected $^{182}W^{16}O_3^{-}/^{184}W^{16}O_3^{-}$ were corrected for instrumental mass bias by normalizing to $^{186}W/^{183}W= 0.92767$ or $^{186}W/^{184}W=1.98594$ (Völkening et al., 1991), using the exponential law (Russell et al., 1978). Per-integration oxide corrected $^{183}W^{16}O_3^{-}/^{184}W^{16}O_3^{-}$ were only corrected for

mass bias using $^{186}W/^{184}W=1.98594$. Mass bias corrections were calculated using molecular masses (e.g., 232 for $^{184}W$).

Table 3.2. Interferences on primary $x^{16}O_3^-$ species that require corrections. Oxygen isotopic compositions represent total oxygen masses (e.g., $^{184}W^{50}O_3^- = {}^{184}W^{16}O_2^{18}O^- + {}^{184}W^{16}O^{17}O_2^-$).

| Species | $^{180}W^{16}O_3^-$ | $^{182}W^{16}O_3^-$ | $^{183}W^{16}O_3^-$ | $^{184}W^{16}O_3^-$ | $^{185}Re^{16}O_3^-$ | $^{186}W^{16}O_3^-$ | $^{187}Re^{16}O_3^-$ | $^{186}W^{16}O_2^{18}O^-$ | $^{187}Re^{16}O_2^{18}O^-$ |
|---|---|---|---|---|---|---|---|---|---|
| Mass | 228 | 230 | 231 | 232 | 233 | 234 | 235 | 236 | 237 |
| | $^{180}Ta^{48}O_3^-$ | $^{180}W^{50}O_3^-$ | $^{180}W^{51}O_3^-$ | $^{180}W^{52}O_3^-$ | $^{181}Ta^{52}O_3^-$ | $^{182}W^{52}O_3^-$ | $^{183}W^{52}O_3^-$ | $^{184}W^{52}O_3^-$ | $^{185}Re^{52}O_3^-$ |
| Interfering | | $^{180}Ta^{50}O_3^-$ | $^{180}Ta^{51}O_3^-$ | $^{180}Ta^{52}O_3^-$ | $^{182}W^{51}O_3^-$ | $^{183}W^{51}O_3^-$ | $^{184}W^{51}O_3^-$ | $^{185}Re^{51}O_3^-$ | $^{186}W^{51}O_3^-$ |
| Species | | $^{181}Ta^{49}O_3^-$ | $^{181}Ta^{50}O_3^-$ | $^{181}Ta^{51}O_3^-$ | $^{183}W^{50}O_3^-$ | $^{184}W^{50}O_3^-$ | $^{185}Re^{50}O_3^-$ | $^{187}Re^{49}O_3^-$ | |
| | | | $^{182}W^{49}O_3^-$ | $^{182}W^{50}O_3^-$ | $^{184}W^{49}O_3^-$ | $^{185}Re^{49}O_3^-$ | $^{186}W^{49}O_3^-$ | | |
| | | | | $^{183}W^{49}O_3^-$ | | | | | |

## 3.4. Results and Discussion

In order to determine the isotopic composition of O associated with Re trioxide formation, we measured the isotopic compositions of Re beams generated by loading activator onto Re filaments with no W. The results of 8 analyses of Re ribbon are summarized in Table 3.3, and shown in Figure 3.1. Using these results, data for 30 analyses of standard solutions (300 ng – 1000 ng Alfa Aesar W) are summarized in Table 3.4, and shown in Figures 3.2, 3.3, and 3.4. A natural sample (group IVB iron meteorite Skookum) analyzed using this method, and compared to previously published results, is shown in Fig. 3.8.

### 3.4.1 First-order and Per-Integration Oxide Corrections

High-precision W analyses at the ~5 ppm level require either second-order (Touboul and Walker, 2012) or per-integration (Trinquier et al., 2016) oxide corrections because of in-run mass-dependent O fractionation. This study utilized per-

integration oxide corrections because $^{183}W/^{184}W$, which varies in nature, can be measured using this method.

Before per-integration oxide corrections could be performed, the signals used to calculate per-integration $^{17}O/^{16}O$ and $^{18}O/^{16}O$ for $WO_3^-$ and $ReO_3^-$ ($^{186}W^{16}O_2^{18}O^-$, $^{186}W^{16}O_3^-$, $^{187}Re^{16}O_2^{18}O^-$, and $^{187}Re^{16}O_3^-$) had to be first-order oxide-corrected, using an estimated $^{17}O/^{16}O$ and $^{18}O/^{16}O$. For this estimate, the means of $^{17}O/^{16}O$ and $^{18}O/^{16}O$ calculated from $^{187}Re^{16}O_2^{17}O^-/^{187}Re^{16}O_3^-$ and $^{187}Re^{16}O_2^{18}O^-/^{187}Re^{16}O_3^-$ measured on Re filaments (n=8) loaded with only 5 µg each of La and Gd were used (Table 3.3). The means of $^{17}O/^{16}O$ and $^{18}O/^{16}O$ determined by this study were 0.0003913 and 0.002096, respectively (Fig. 3.1). These values are significantly higher than the values used by previous studies, e.g., $^{17}O/^{16}O$=0.0003749 and $^{18}O/^{16}O$=0.002044 (Nier, 1950). Because $^{187}Re^{16}O_3^-$ is an isobar with $^{186}W^{16}O_2^{17}O^-$, measured $^{186}W^{16}O_2^{17}O^-/^{186}W^{16}O_3^-$ and $^{186}W^{16}O_2^{18}O^-/^{186}W^{16}O_3^-$ could not be used to make this estimate.

Table 3.3. Data for 8 analyses of Re ribbon with only activator (5 µg each La and Gd loaded). Errors are 2SD internal precisions and reflect in-run evolution of oxygen isotopic compositions.

| Analysis # | $^{18}O/^{16}O$ | 2SD (‰) | $^{17}O/^{16}O$ | 2SD (‰) |
|---|---|---|---|---|
| 1 | 0.002085 | 5.4 | 0.0003894 | 6.2 |
| 2 | 0.002090 | 7.6 | 0.0003905 | 7.1 |
| 3 | 0.002100 | 2.6 | 0.0003917 | 3.8 |
| 4 | 0.002110 | 2.9 | 0.0003926 | 3.9 |
| 5 | 0.002125 | 2.3 | 0.0003940 | 4.7 |
| 6 | 0.002098 | 4.1 | 0.0003919 | 3.8 |
| 7 | 0.002088 | 8.1 | 0.0003906 | 9.1 |
| 8 | 0.002074 | 8.1 | 0.0003896 | 5.7 |
| Mean | 0.002096 | 7.7‰ | 0.0003913 | 4.1‰ |
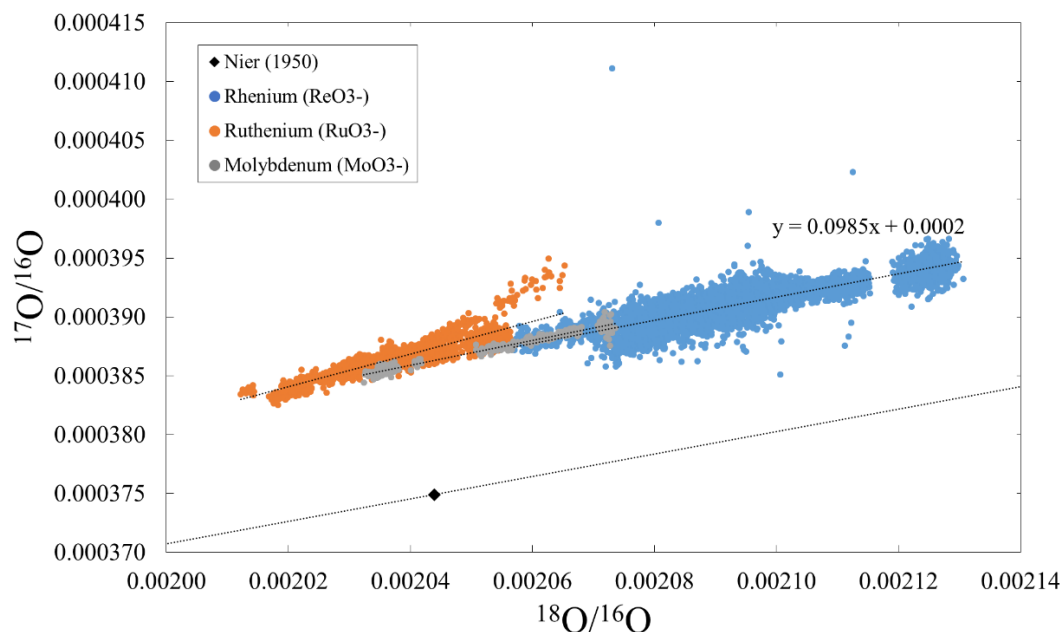
Figure 3.1. Measured O isotopic compositions for $ReO_3^-$ (this study), $RuO_3^-$ (Bermingham et al., 2016), and $MoO_3^-$ (Worsham et al., in press). The O isotopic composition of atmosphere reported by Nier (1950) and a terrestrial fractionation line, which were used by previous studies (Touboul and Walker, 2012; Trinquier et al., 2016) are shown for reference.

The repeated measurements of $^{187}Re^{16}O_2^{17}O^-/^{187}Re^{16}O_3^-$ and $^{187}Re^{16}O_2^{18}O^-/^{187}Re^{16}O_3^-$ from Re filaments also provides an O mass fractionation line that is consistent with recently reported O mass fractionation lines for $OsO_3^-$, $RuO_3^-$, and $MoO_3^-$ (Fig. 3.1) measured by N-TIMS (Chu et al., 2015; Nagai et al., 2016; Bermingham et al., 2016; Worsham et al., in press). These lines are all offset from the oxygen fractionation line used by previous W studies utilizing N-TIMS. The cause of the offset is unknown (e.g., analytical artifact or mass-independent effect), but the offset is reproducible for all of the oxide systems measured so far via N-TIMS.

The slope of a linear regression through the $ReO_3^-$ O mass fractionation line (0.0985±0.0018 2SD) is similar to the slope of the terrestrial fractionation line (0.0954), so the terrestrial fractionation slope was used to infer $^{17}O/^{16}O$ from measured $^{18}O/^{16}O$.

### 3.4.2 External and Internal Precision

The external precision (n=6) of 300 ng-1000 ng *Alfa Aesar* W standards analyzed in February 2016 was 4.0 ppm and 3.6 ppm for $^{182}W/^{184}W$ normalized to $^{186}W/^{184}W$ ($^{182}W/^{184}W_{N6/4}$) and $^{186}W/^{183}W$ ($^{182}W/^{184}W_{N6/3}$), respectively (Table 3.4; Fig. 3.2 and 3.3). After Faraday cup maintenance was performed in April 2016, the mean $^{182}W/^{184}W_{N6/4}$ shifted downwards by ~3 ppm (Fig. 3.2), whereas the $^{182}W/^{184}W_{N6/3}$ only shifted by ~1 ppm (Fig. 3.3). Faraday cup condition, therefore, appears to have a ~3x larger influence on $^{182}W/^{184}W_{N6/4}$ than $^{182}W/^{184}W_{N6/3}$.

Table 3.4.  Standards data for 30 analyses of 300 ng-1000 ng of *Alfa Aesar* W. Errors are 2SE absolute internal precisions. $^{185}$Re/$^{184}$W are the average signal intensity ratios for entire analyses.

| Standard # | Session ID # | W Abundance | Date | $^{185}$Re/$^{184}$W | $^{182}$W/$^{184}$W$_{N6/4}$ | 2SE | $^{183}$W/$^{184}$W$_{N6/4}$ | 2SE | $^{182}$W/$^{184}$W$_{N6/3}$ | 2SE |
|---|---|---|---|---|---|---|---|---|---|---|
| 1 | 381 | 1 µg | Feb 18 2016 | 0.126 | 0.864893 | 0.000004 | 0.467148 | 0.000002 | 0.864869 | 0.000003 |
| 2 | 381 | 300 ng | Feb 19 2016 | 0.196 | 0.864890 | 0.000005 | 0.467146 | 0.000002 | 0.864866 | 0.000004 |
| 3 | 382 | 1 µg | Feb 24 2016 | 0.115 | 0.864893 | 0.000004 | 0.467149 | 0.000002 | 0.864867 | 0.000003 |
| 4 | 382 | 1 µg | Feb 25 2016 | 0.125 | 0.864893 | 0.000004 | 0.467147 | 0.000002 | 0.864870 | 0.000003 |
| 5 | 382 | 1 µg | Feb 29 2016 | 0.052 | 0.864890 | 0.000004 | 0.467146 | 0.000002 | 0.864869 | 0.000003 |
| 6 | 382 | 1 µg | March 3 2016 | 0.039 | 0.864893 | 0.000004 | 0.467147 | 0.000002 | 0.864870 | 0.000003 |
| Cup Maintenance Performed | | | April 1st 2016 | Mean | 0.864892 | | 0.467147 | | 0.864869 | |
| | | | | 2SD (ppm) | 4.0 | | 4.3 | | 3.6 | |
| 7 | 385 | 1 µg | April 5 2016 | 0.048 | 0.864889 | 0.000005 | 0.467144 | 0.000002 | 0.864870 | 0.000004 |
| 8 | 385 | 1 µg | April 6 2016 | 0.066 | 0.864889 | 0.000004 | 0.467146 | 0.000002 | 0.864866 | 0.000003 |
| 9 | 385 | 300 ng | April 7 2016 | 0.118 | 0.864890 | 0.000004 | 0.467145 | 0.000002 | 0.864867 | 0.000003 |
| 10 | 386 | 1 µg | April 11 2016 | 0.162 | 0.864889 | 0.000004 | 0.467145 | 0.000002 | 0.864867 | 0.000003 |
| 11 | 386 | 1 µg | April 12 2016 | 0.176 | 0.864889 | 0.000004 | 0.467148 | 0.000002 | 0.864866 | 0.000003 |
| 12 | 386 | 1 µg | April 13 2016 | 0.057 | 0.864887 | 0.000004 | 0.467146 | 0.000002 | 0.864866 | 0.000003 |
| 13 | 386 | 1 µg | April 13 2016 | 0.088 | 0.864891 | 0.000004 | 0.467146 | 0.000002 | 0.864868 | 0.000003 |
| 14 | 386 | 500 ng | April 14 2016 | 0.061 | 0.864892 | 0.000004 | 0.467145 | 0.000002 | 0.864870 | 0.000003 |
| 15 | 386 | 1 µg | April 18 2016 | 0.050 | 0.864890 | 0.000004 | 0.467144 | 0.000002 | 0.864870 | 0.000003 |
| 16 | 386 | 500 ng | April 19 2016 | 0.096 | 0.864890 | 0.000004 | 0.467145 | 0.000002 | 0.864868 | 0.000003 |
| 17 | 386 | 1 µg | April 19 2016 | 0.170 | 0.864891 | 0.000004 | 0.467146 | 0.000002 | 0.864869 | 0.000003 |
| 18 | 386 | 500 ng | April 20 2016 | 0.102 | 0.864884 | 0.000004 | 0.467143 | 0.000002 | 0.864865 | 0.000003 |
| 19 | 386 | 500 ng | April 21 2016 | 0.164 | 0.864887 | 0.000005 | 0.467146 | 0.000002 | 0.864868 | 0.000004 |
| 20 | 387 | 1 µg | April 25 2016 | 0.081 | 0.864893 | 0.000004 | 0.467146 | 0.000002 | 0.864871 | 0.000003 |
| 21 | 387 | 1 µg | May 1 2016 | 0.026 | 0.864893 | 0.000004 | 0.467145 | 0.000002 | 0.864872 | 0.000003 |
| 22 | 387 | 500 ng | May 2 2016 | 0.312 | 0.864886 | 0.000006 | 0.467143 | 0.000003 | 0.864867 | 0.000004 |
| 23 | 389 | 500 ng | May 16 2016 | 0.042 | 0.864885 | 0.000004 | 0.467141 | 0.000002 | 0.864868 | 0.000003 |
| 24 | 389 | 1 µg | May 17 2016 | 0.038 | 0.864888 | 0.000004 | 0.467145 | 0.000002 | 0.864868 | 0.000003 |
| 25 | 389 | 1 µg | May 20 2016 | 0.022 | 0.864892 | 0.000004 | 0.467147 | 0.000002 | 0.864869 | 0.000003 |
| 26 | 389 | 1 µg | May 22 2016 | 0.031 | 0.864886 | 0.000004 | 0.467143 | 0.000002 | 0.864866 | 0.000003 |
| 27 | 390 | 1 µg | May 26 2016 | 0.051 | 0.864888 | 0.000003 | 0.467144 | 0.000001 | 0.864868 | 0.000002 |
| 28 | 390 | 1 µg | May 27 2016 | 0.031 | 0.864887 | 0.000003 | 0.467143 | 0.000002 | 0.864868 | 0.000002 |
| 29 | 390 | 1 µg | May 30 2016 | 0.034 | 0.864888 | 0.000004 | 0.467145 | 0.000002 | 0.864867 | 0.000003 |
| 30 | 390 | 500 ng | June 2 2016 | 0.081 | 0.864887 | 0.000004 | 0.467142 | 0.000002 | 0.864868 | 0.000003 |
| | | | | Mean | 0.864889 | | 0.467145 | | 0.864868 | |
| | | | | 2SD (ppm) | 5.7 | | 6.6 | | 3.7 | |

71
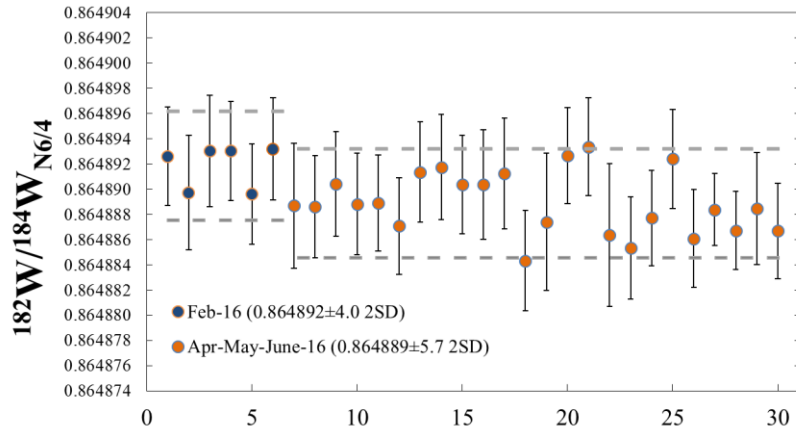
Figure 3.2. $^{182}W/^{184}W$ normalized to $^{186}W/^{184}W$ for 30 analyses of 300ng-1000 ng *Alfa Aesar* W standards. Mean $^{182}W/^{184}W$ and 2SD for each period shown in legend. Grey dashed lines mark 5 ppm from the mean. Error bars represent 2SE internal precisions.
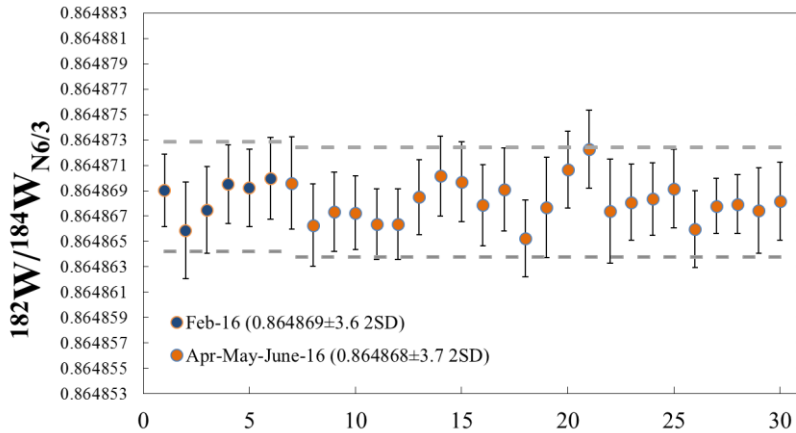


Figure 3.3. $^{182}W/^{184}W$ normalized to $^{186}W/^{183}W$ for 30 analyses of 300ng-1000 ng *Alfa Aesar* W standards. Mean $^{182}W/^{184}W$ and 2SD for each period shown in legend. Grey dashed lines mark 5 ppm from the mean. Error bars represent 2SE internal precisions.

The long-term external precision (n=24) of 300 ng-1000 ng *Alfa Aesar* W standards analyzed from April-June 2016 was 5.7 ppm and 3.7 ppm for $^{182}W/^{184}W_{N6/4}$ and $^{182}W/^{184}W_{N6/3}$, respectively (Table 3.4; Fig. 3.2 and 3.3), which is 2-3x more precise for $^{182}W/^{184}W_{N6/4}$ and $^{182}W/^{184}W_{N6/3}$ than the most recently reported method for measuring W via N-TIMS (Trinquier et al., 2016). These improvements in precision

are likely the result of the more accurate oxide corrections for both $WO_3^-$ and $ReO_3^-$.

Consistent with prior studies (Touboul and Walker, 2012; Trinquier et al., 2016), the long-term external precision of $^{182}W/^{184}W$ is better when normalizing to $^{186}W/^{183}W$ than $^{186}W/^{184}W$ because of the closer proximity of the normalizing isotopes ($^{183}W$ vs. $^{184}W$). However, normalization to $^{186}W/^{183}W$ is only appropriate for samples with $^{183}W/^{184}W$ identical to terrestrial standards, as $^{183}W$ varies among some meteorites.

The external precision of $^{183}W/^{184}W_{N6/4}$ for February 2016 was 4.3 ppm (Table 3.4; Fig. 3.4). $^{183}W/^{184}W_{N6/4}$ is also sensitive to Faraday cup condition and shifted by ~5 ppm after cup maintenance was performed in April 2016. The long-term external precision (n=24) of 300 ng-1000 ng *Alfa Aesar* W standards analyzed from April-June 2016 was 6.6 ppm for $^{183}W/^{184}W_{N6/4}$ (Table 3.4; Fig. 3.4).
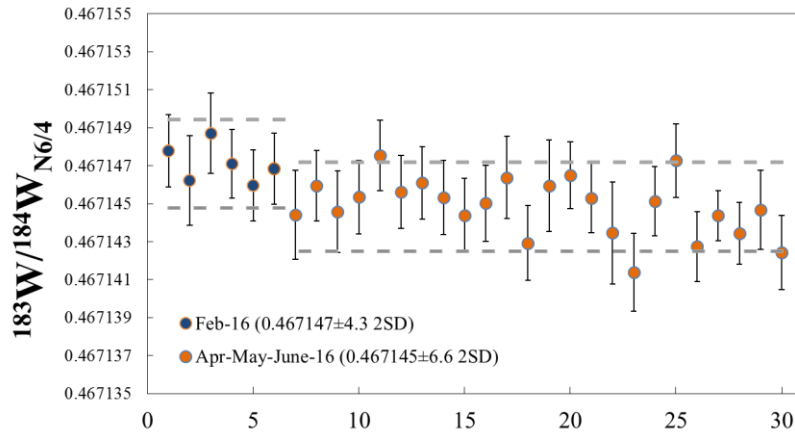


Figure 3.4. $^{183}W/^{184}W$ normalized to $^{186}W/^{184}W$ for 30 analyses of 300ng-1000 ng *Alfa Aesar* W standards. Mean $^{183}W/^{184}W$ and 2SD for each period shown in legend. Grey dashed lines mark 5 ppm from the mean. Error bars represent 2SE internal precisions.

The internal precisions of interspersed 300 ng, 500 ng, and 1000 ng *Alfa Aesar* W standards were similar (~4 to 5 ppm 2SE for $^{182}W/^{184}W_{N6/4}$) when the same signal size (~1V on $^{184}W$) was achieved for 600 integrations (Fig. 3.5). However, only 1000 ng W standards measured on thin Re ribbon achieved much greater than ~1V on $^{184}W$,

and correspondingly better internal precision (~3 ppm 2SE for $^{182}W/^{184}W_{N6/4}$). The best internal precisions (average 2SE of 3.6 ppm) for $^{182}W/^{184}W$ were achieved by using $^{186}W/^{183}W$ for mass bias corrections. By contrast, the average of internal precisions of $^{182}W/^{184}W$ mass bias corrected using $^{186}W/^{184}W$ was 4.7 ppm 2SE. For $^{183}W/^{184}W$ mass bias corrected using $^{186}W/^{184}W$, the average internal precision was 4.2 ppm 2SE.
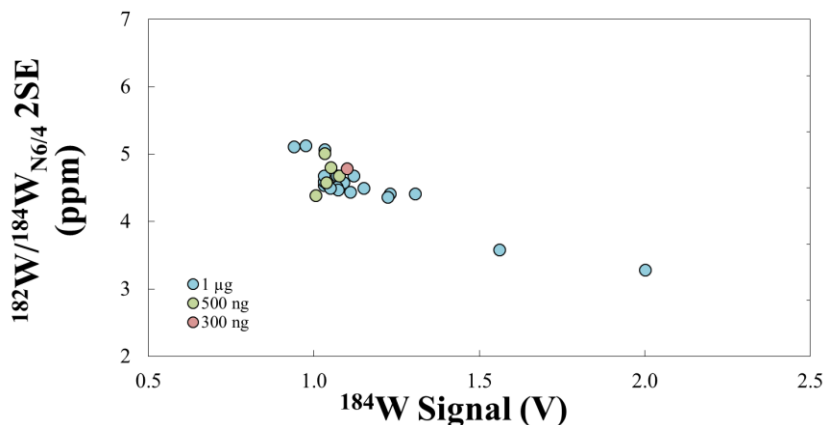


Figure 3.5. Mean $^{184}W$ signal (volts) vs. $^{182}W/^{184}W$ (normalized to $^{186}W/^{184}W$) absolute 2SE for 26 analyses of 300ng-1000 ng *Alfa Aesar* W standards that were measured for 600 integrations.

### 3.4.3. Measurements with high Re Signals

Trinquier et al. (2016) reported correlations between Re/W signals, $^{182}W/^{184}W$, and oxygen isotopic compositions. Because that study used the O isotopic composition of atmosphere reported by Nier (1950) to calculate $^{17}O/^{16}O$ from measured $^{18}O/^{16}O$, corrections for species incorporating $^{17}O$ were too low, as the Nier (1950) isotopic composition deviates negatively in $^{17}O/^{16}O$ from the O isotopic compositions measured during N-TIMS analyses and reported here (Fig. 3.1). Thus, the interference corrections for $^{187}Re^{17}O^{16}O_2$ on $^{186}W^{18}O^{16}O_2$ (which that study used to measure $^{18}O/^{16}O$ and then calculate $^{17}O/^{16}O$) were too low. In this study, the use of more accurate

$^{17}O/^{16}O$ removes this bias, and a correlation between Re/W signals and $^{182}W/^{184}W$ is not observed (Fig. 3.6).
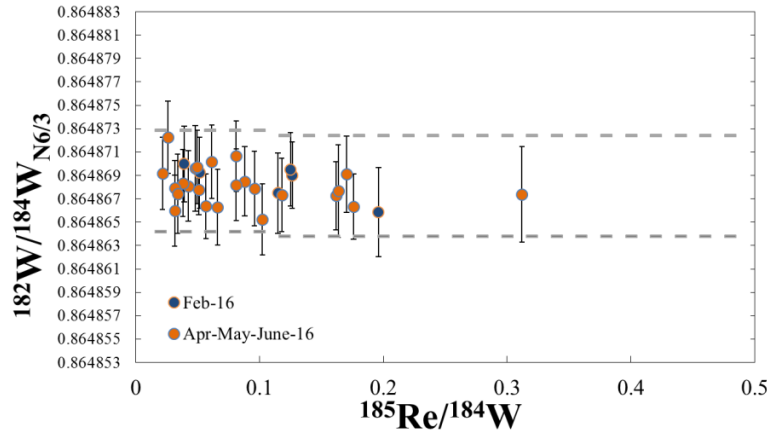


Figure 3.6. Mean $^{185}Re/^{184}W$ (for each measurement) vs. $^{182}W/^{184}W$ (normalized to $^{186}W/^{183}W$) for 30 analyses of 300ng-1000 ng Alfa Aesar W standards. Grey dashed lines mark 5 ppm from the mean. Error bars represent 2SE internal precisions.

### 3.4.4. Correlation of Mass Bias Corrected Ratios

Within the standards data reported by this study, a correlation exists between $^{182}W/^{184}W_{N6/4}$ and $^{183}W/^{184}W_{N6/4}$ (Fig. 3.7). A linear regression through the 30 measured standards using ISOPLOT (Ludwig, 2001) has a slope of 1.41±0.53 (2σ) and a mean square weighted deviation (MSWD) of 0.5. Trinquier et al., (2016) also observed a correlated drift in $^{182}W/^{184}W_{N6/4}$ and $^{183}W/^{184}W_{N6/4}$ over a 9 month period. Among other possibilities, they stated that this could be the result of Faraday cup degradation over time. Because of the correlated, pronounced shift in $^{182}W/^{184}W_{N6/4}$ and $^{183}W/^{184}W_{N6/4}$ after cup maintenance, we conclude that the most likely cause of the correlated shift is Faraday cup degradation.
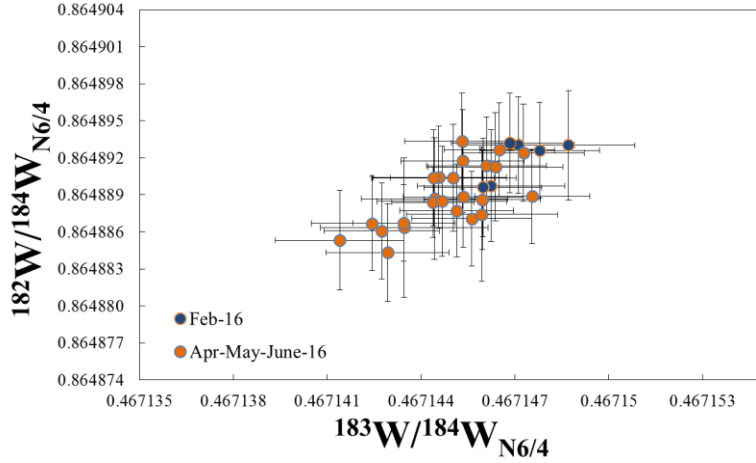
Figure 3.7. $^{183}W/^{184}W_{N6/4}$ vs. $^{182}W/^{184}W_{N6/4}$ for 30 analyses of 300ng-1000 ng Alfa Aesar W standards. Error bars represent 2SE internal precisions.

### 3.4.5. Measurement of Natural Samples

The measurement of natural samples with previously reported $^{182}W/^{184}W$ and $^{183}W/^{184}W$ provides a means to assess the accuracy of this analytical method. Kruijer et al. (2014a) reported that the $^{182}W/^{184}W$ and $^{183}W/^{184}W$ of group IVB iron meteorite Skookum, measured via multi collector-inductively coupled plasma mass spectrometer (MC-ICP-MS), were well resolved from terrestrial standards (Fig. 3.8). Isotopic deviations of samples from standards here are described in μ units, where $μ^xW$ is the isotopic deviation in parts per million of $^xW/^{184}W$ from a terrestrial standard. The $μ^{182}W_{6/4}$ (-334.8±5.7 2SD) and $μ^{183}W_{6/4}$ (12.7±6.6 2SD) of Skookum reported here is identical, within uncertainty, to one of two W isotopic compositions for the sample ($μ^{182}W_{6/4}$=-330±4 2SE, and $μ^{183}W_{6/4}$=13±4 2SE) reported by Kruijer et al., (2014a). Further, the precision reported here is for a single measurement and is defined as the 2SD long-term external precision of standards analyzed during this study. By contrast, the precision reported by Kruijer et al. (2014a) represents the 2SE (n=5) of repeated measurements. The calculated 2SD of the measurements from Kruijer et al. (2014a)

76

are $\pm 9$ $\mu$ units for both $\mu^{182}W_{6/4}$ and $\mu^{183}W_{6/4}$. Thus, the datum reported here illustrates the accuracy and precision of single measurements using this new analytical method.
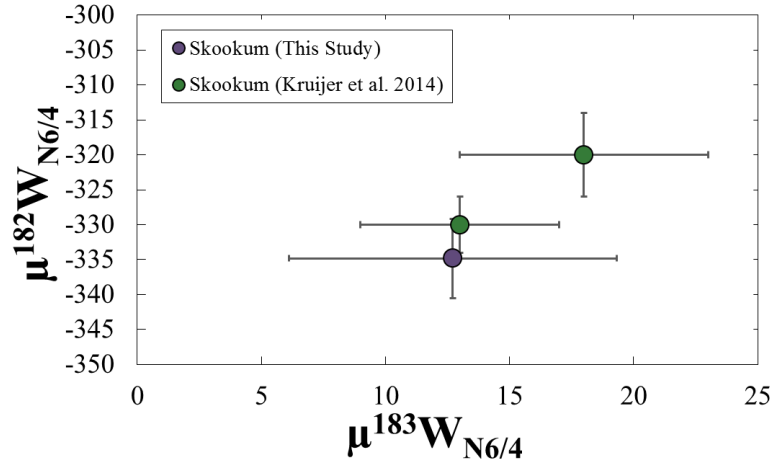


Figure 3.8. $\mu^{183}W_{N6/4}$ vs. $\mu^{182}W_{N6/4}$ for the group IVB iron meteorite Skookum. One analysis is from this study, and two analyses were taken from Kruijer et al. (2014a). The error bars for the datum from this study are 2SD, and the error bars for the data from Kruijer et al. (2014a) are 2SE (n=5) of repeated measurements.

## *3.5. Conclusions*

We have refined recently reported N-TIMS techniques (Touboul and Walker, 2012; Trinquier et al., 2016) to measure $WO_3^-$ and determine $^{182}W/^{184}W$ and $^{183}W/^{184}W$ to high-precision. Most significantly, this technique makes more accurate first-order and per-integration oxide corrections to primary $^xWO_3^-$ signals by (i) utilizing updated values for $^{17}O/^{16}O$ and $^{18}O/^{16}O$ for first-order corrections, (ii) measuring $^{18}O/^{16}O$ for both $WO_3^-$ and $ReO_3^-$, and (iii) using a new oxide mass fractionation line to calculate per-integration $^{17}O/^{16}O$ from measured $^{18}O/^{16}O$. The long-term external precisions for $^{182}W/^{184}W_{N6/4}$, $^{182}W/^{184}W_{N6/3}$, and $^{183}W/^{184}W_{N6/4}$ are 5.7 ppm, 3.7 ppm, and 6.6 ppm, respectively. This level of precision is ~2-3x better for single measurements than the most recently reported N-TIMS method for measuring both $^{182}W/^{184}W$ and $^{183}W/^{184}W$ (Trinquier et al., 2016). We have demonstrated that this method is capable of producing

77

accurate and precise data for natural samples by using this method to measure a group

IVB iron meteorite, and comparing the datum to previously reported data for this

sample (Kruijer et al., 2014a).

*References for Chapter 3*

Bermingham K.R., Walker R.J., and Worsham E.A., 2016. Refinement of high precision Ru isotope analysis using negative thermal ionization mass spectrometry. *Int. J. Mass Spec.* **403**, 15-26.

Chu Z.-Y., Li C.-F., Chen Z., Xu J.-J., Di Y.-K., and Guo J.-H., 2015. High-precision measurement of $^{186}Os/^{188}Os$ and $^{187}Os/^{188}Os$: Isobaric oxide corrections with in-run measured oxygen isotope ratios. *Anal. Chem.* **87**, 8765-8771.

Harper C.L. and Jacobsen S.B., 1996. Evidence for $^{182}Hf$ in the early Solar System and constraints on the timescale of terrestrial accretion and core formation, *Geochim. Cosmochim. Acta* **60**, 1131–1153.

Kleine T., Touboul M., Van Orman J.A., Bourdon B., Maden C., Mezger K. and Halliday A., 2008. Hf–W thermochronometry: closure temperature and constraints on the accretion and cooling history of the H chondrite parent body. *Earth Planet. Sci. Lett.* **270**, 106–118.

Kruijer T.S., Touboul M., Fischer-Godde M., Bermingham K.R., Walker R.J. and Kleine T., 2014a. Protracted core formation and rapid accretion of protoplanets. *Science* **344**, 1150–1154.

Kruijer T.S., Kleine T., Fischer-Gödde M., Burkhardt C. and Wieler R., 2014b. Nucleosynthetic W isotope anomalies and the Hf-W chronometry of Ca-Al-rich inclusions. *Earth Planet. Sci. Lett.* **403**, 317–327.

Lee D.C. and Halliday A.N., 1995. Hafnium–tungsten chronometry and the timing of terrestrial core formation. *Nature* **378**, 771–774.

Liu J., Touboul M., Ishikawa A., Walker R.J., and Pearson D.G., 2016. Widespread tungsten isotope anomalies and W mobility in crustal and mantle rocks of the Eoarchean Saglek Block, northern Labrador, Canada: Implications for early Earth processes and W recycling. *Earth Planet. Sci. Lett.* **448**, 12-23.

Ludwig K.R. 2001. Users Manual for Isoplot/Ex version 2.47. A geochronological toolkit for Microsoft Excel. Berkeley Geochronology Center Special Publication 1a, 55pp.

Nagai Y. and Yokoyama T., 2016. Molybdenum isotopic analysis by negative thermal ionization mass spectrometry (N-TIMS): Effects on oxygen isotopic composition. *J. Anal. At. Spectrom.* **29**, 1090-1096.

Nier A.O., 1950. A redetermination of the relative abundances of the isotopes of carbon, nitrogen, oxygen, argon, and potassium, *Phys. Rev.* **77**, 789–793.

Russell W.A., Papanastassiou D.A., and Tombrello T.A., 1978. Ca isotope fractionation in the Earth and other solar system materials. *Geochim. Cosmochim. Acta* **42**, 1075–1090.

Touboul M., Puchtel I.S., and Walker R.J., 2012. [182]W evidence for long-term preservation of early mantle differentiation products. *Science* **335**, 1065–1069.

Touboul M., and Walker R.J., 2012. High precision measurement of tungsten isotopes by thermal ionization mass spectrometry. *Int. J. Mass Spectrom.* **309**, 109–117.

Touboul M., Liu J., O'Neil J., Puchtel I.S., and Walker R.J., 2014. New insights into the Hadean mantle revealed by [182]Wand highly siderophile element abundances of supracrustal rocks from the Nuvvuagittuq Greenstone Belt, Quebec, Canada. *Chem. Geol.* **383**, 63–75.

Trinquier A., Touboul M., and Walker R.J., 2016. High-precision tungsten isotopic analysis by multicollection negative thermal ionization mass spectrometry based on simultaneous measurement of W and $^{18}O/^{16}O$ isotope ratios for accurate fractionation correction. *Anal.Chem.* **88**, 1542-1546.

Vockenhuber C., Oberli F., Bichler M., Ahmad I., Quitté G., Meier M., Halliday A.N., Lee D.C., Kutschera W., Steier P., Gehrke R.J., and Helmer R.G., 2004. New half-life measurement of [182]Hf: improved chronometer for the early solar system. *Phys. Rev. Lett.* **93**, 172501.

Völkening J., Köppe M., and Heumann K.G., 1991. Tungsten isotope ratio determinations by negative thermal ionization mass spectrometry, *Int. J. Mass Spectrom. Ion Processes* **107**, 361–368.

Willbold M., Elliott T., and Moorbath S., 2011. The tungsten isotopic composition of the Earth's mantle before the terminal bombardment. *Nature* **477**, 195–198.

Willbold M., Mojzsis S.J., Chen H.-W., and Elliott T., 2015. Tungsten isotope composition of the Acasta Gneiss Complex. *Earth Planet. Sci. Lett.* **419**, 168-177.

Worsham E.A., Walker R.J., and Bermingham K.R., 2016. High-precision molybdenum isotope analysis by negative thermal ionization mass spectrometry *Int. J. Mass Spec.*, in press.

Yin Q.Z., 1995. N-TIMS technique for the Re-Os and Ru isotopic systems and its application to selected geochemical and cosmochemical problems. PhD thesis, University of Mainz and Max Planck Institute for Chemistry.

# Chapter 4: $^{182}$Hf-$^{182}$W and $^{187}$Re-$^{187}$Os Isotopic Systematics, and Highly Siderophile Elements of H Chondrites: Constraining the Thermal History of the H Chondrite Parent Body

## *4.1 Abstract*

The abundances of highly siderophile elements (HSE: Re, Os, Ir, Ru, Pt, Pd), as well as $^{187}$Re-$^{187}$Os and $^{182}$Hf-$^{182}$W isotopic systematics were determined for separated metal, slightly magnetic, and nonmagnetic fractions from H4-6 chondrites. The $^{182}$Hf-$^{182}$W isotopic systematics of a separated CR2 chondrite metal fraction were also determined.

The abundances of HSE in the nonmagnetic fractions of H4-6 chondrites are too high to reflect complete equilibration with the metal fractions. Further, there is no correlation between metamorphic grade and apparent degree of HSE equilibration. Linear regressions of $^{182}$Hf-$^{182}$W data for metal, slightly magnetic, and nonmagnetic fractions do not form precise isochrons for most H chondrites, except Richardton (H5), further indicating that silicates and oxides were not in equilibrium with metal when diffusive transport of W among components ceased. Tungsten disequilibrium appears to be greatest for the least metamorphosed sample, Avanhandava (H4). By contrast, slightly magnetic and nonmagnetic fractions from H4-6 chondrites form precise isochrons with minimal scatter, indicating that silicates and oxides were in equilibrium when diffusive transport ceased below the Hf-W closure temperature. For all H chondrites, model ages calculated from metal grains (1.0±0.6 to 7.2±2.1 Ma after CAI formation) are older than the slope-derived isochron ages for their respective slightly magnetic and nonmagnetic fractions (5.2±1.6 to 15.2±0.7 Ma after CAI formation),

consistent with disequilibrium between metal and silicate-rich fractions. The slightly magnetic and nonmagnetic fractions from the H6 chondrite Oakley give the youngest isochron age ($\Delta t_{CAI}$=15.2±0.7 Ma), whereas the isochron ages for all H4 and H5 chondrites are older (ranging from $\Delta t_{CAI}$=5.2±1.6 Ma to 8.6±1.6 Ma). The isochron ages of most H4 and H5 chondrites are within uncertainties of each other ($\Delta t_{CAI}$ =8.0±1.7 Ma), except Richardton ($\Delta t_{CAI}$=5.2±1.6 Ma), which has a resolvably older isochron age than Avanhandava ($\Delta t_{CAI}$=8.6±1.6 Ma).

The $^{182}$Hf-$^{182}$W systematics for H4-6 chondrites examined here are inconsistent with the undisturbed onion shell thermal model, as previously proposed by some for an H chondrite parent body (e.g., Pellas and Storzer, 1981; Trieloff et al., 2003; Kleine et al., 2008; Henke et al., 2012; Monnereau et al., 2013). Instead, the data are consistent with a major disruption, possibly by impact, of the H chondrite parent body within 8.6±1.6 Ma after CAI formation, before it cooled below ~800±50ºC, the Hf-W closure temperature of H4 chondrites.

The older metal age for Richardton suggests that it may have experienced earlier thermal metamorphism on a separate parent body from the other H chondrites examined here, and therefore H chondrites probably originated from multiple parent bodies. It is also possible that early cosmic ray exposure modified the W isotopic compositions of Richardton, and that the $^{182}$W metal age is not comparable to the other H chondrites.

A metal fraction from CR2 chondrite Acfer 395 has a $^{183}$W isotopic composition that is consistent with nucleosynthetic s- process depletion. The nucleosynthetic-corrected $^{182}$W model age of Acfer 395 is similar to the model ages of most metal

fractions from H chondrites. Therefore, the metal could not have formed by condensation in the solar nebula around the formation time of CAIs, and must have formed by a later process.

## *4.2 Introduction*

Chondrites are unmelted aggregates of primitive components that formed in different early Solar System environments. They are composed of refractory inclusions (e.g., calcium-aluminum-rich inclusions), chondrules, matrix, and FeNi metal. Chondritic materials coalesced into planetesimals with diameters of up to hundreds of km, within a few million years of Solar System formation (Dauphas and Chaussidon, 2011). Chondrites are classified into three major classes: carbonaceous, enstatite, and ordinary, as well as several minor groups (Rumuruti, etc.). Members of each ordinary chondrite group (H, L, or LL) have petrologic, geochemical, and isotopic similarities, suggesting that they originated from the same or similar parent bodies. The ordinary H chondrites have similar O isotopic compositions (Clayton et al., 1976), bulk chemical compositions (Wasson and Kallemeyn, 1988), and oxidation states (Rubin et al., 1988). They are characterized by high Fe contents and contain abundant FeNi metal grains (15-19%), compared to other ordinary chondrites.

Since aggregation, chondritic parent bodies have undergone varying degrees of processing, including thermal and aqueous alteration. The H chondrites have experienced a wide range of thermal-metamorphic conditions, ranging from petrologic types H3 (peak temperatures of 400-600 ℃; Keil, 2000) through petrologic types H4-H6 (peak temperatures of 500-1000 ℃; Keil, 2000). The H4-H6 chondrites show increasing degrees of chemical equilibration of some elements (e.g., Fe and Mg in

olivine) and textural integration of chondritic components (e.g., decrease in abundance of identifiable chondrules; Rubin, 2000; Rubin et al., 2001) with increasing petrologic type (e.g., Huss et al., 2006; Weisberg et al., 2006). However, metal grains in H4-H6 chondrites retain evidence for disequilibrium, with heterogeneous Ni abundances (e.g., Wood, 1967).

Some prior studies have proposed an onion-shell thermal model for the parent body of H chondrites to explain an apparent correlation between H chondrite petrologic type and closure ages (e.g., Pellas and Storzer, 1981; Trieloff et al., 2003). In this model, the parent body was internally heated by the decay of now-extinct $^{26}$Al ($t_{1/2}$=0.7 Ma; Norris et al., 1983). Those H chondrites that were located deepest within the parent body reached the highest temperatures, cooled slowest, and therefore experienced the highest degrees of thermal metamorphism. Those chondrites that were closer to the surface cooled more rapidly and experienced lower degrees of thermal metamorphism. Thus, according to this model, H chondrites of higher petrologic type (deeper in the H chondrite parent body) should record the youngest closure ages for each radiogenic isotope system applied.

The short-lived $^{182}$Hf-$^{182}$W radiogenic isotopic system ($t_{1/2}$=8.9 Ma; Vockenhuber et al., 2004) is useful for constraining processes that occurred during the first ~50 million years of Solar System history. It is especially useful for constraining the timing of metal-silicate equilibration, because W is moderately siderophile (metal/silicate D value ≤871; Schmitt et al., 1989) and strongly partitions into planetary metals, whereas Hf is lithophile and is retained exclusively in silicates. The system has been used widely to constrain the timing of core formation on planetary bodies (e.g.,

84

Lee and Halliday, 1995; Harper and Jacobsen, 1996; Kruijer et al., 2014a), and may also be used as a thermochronometer, with closure temperatures of 800-875°C for H4-6 chondrites, mathematically estimated by Kleine et al., (2008) using the diffusion model of Van Orman et al. (2001).

Kleine et al. (2008) applied the $^{182}$Hf-$^{182}$W isotopic system to H chondrite metals and silicates in order to constrain the cooling history of H chondrites after metamorphic heating. They reported older closure ages for lower petrologic type H chondrites. Further, they combined Hf-W data with the closure ages of multiple isotopic systems characterized by different closure temperatures (Pb-Pb, Ar-Ar, and $^{244}$Pu fission tracks), and calculated cooling rate curves for the H chondrite parent body. They estimated cooling rates of 55° C/Ma, 30° C/Ma, and 10° C/Ma for H4, H5, and H6 chondrites, respectively. The consistent relations among closure ages, cooling rates, and petrologic types were interpreted as strong evidence for the onion shell thermal model.

Kleine et al. (2008), however, also reported that some metal fractions from the H5 chondrite Richardton appeared to have W isotopic compositions that were too low to be readily explained by the decay of $^{182}$Hf in a body with an onion shell thermal structure. They speculated that the anomalous isotopic compositions could reflect an early irradiation of the metal, which led to a modification of its W isotopic composition. Recently, correlated $^{182}$W and $^{183}$W anomalies have been reported for some meteorites (Kruijer et al., 2014b), which are interpreted to be the result of nucleosynthetic heterogeneities in the early Solar System. If present in Richardton, nucleosynthetic anomalies might also account for a low $^{182}$W isotopic composition.

In this study, the $^{182}$Hf-$^{182}$W systematics of H chondrite metals and oxide-silicate mixtures are revisited using a new analytical technique that achieves higher precision than prior studies (~5 ppm 2SD external precision for $^{182}$W/$^{184}$W and $^{183}$W/$^{184}$W). We also examine the highly siderophile element (HSE) abundances and $^{187}$Re-$^{187}$Os isotopic systematics of H chondrite metal and oxide-silicate fractions. The primary goals of this study are: (1) to reassess the thermal history of the H chondrite parent body, using Hf-W measured to higher precision than previous studies, (2) to explore diffusive exchange of HSE among silicates, oxides, and metals during thermal metamorphism, and (3) to investigate processes other than $^{182}$Hf decay that may have led to $^{182}$W isotopic variations among some H chondrite metal fractions.

The $^{182}$Hf-$^{182}$W isotopic system can also potentially be used to constrain the initial formation process(es) of chondrite metal, if the W isotopic systematics of the metal was not overprinted by thermal metamorphism. Renazzo-like carbonaceous chondrites (CR chondrites) commonly occur as petrologic type 2, and are characterized by reduced silicates, high abundances of Fe,Ni metal, volatile element depletions, and low degrees of thermal metamorphism (Weisberg et al., 1995; Krot et al., 2002). Some prior studies have proposed that CR chondrite metal formed by condensation directly from nebular gas (Campbell and Humayan, 2004). Consequently, the $^{182}$Hf-$^{182}$W isotopic systematics of a CR2 chondrite metal fraction is investigated in order to constrain the timing and formation mechanisms of another type of chondrite metal.

## 4.3 Samples

Seven H chondrites and one CR chondrite were investigated by this study. The H chondrites range from petrologic type H4 to H6, and the CR chondrite is petrologic type 2. Two samples were provided by the University of California Los Angeles Meteorite Collection, including the H5 chondrite Faucett and the CR2 chondrite Acfer 395 (UCLA 2701). The H5 chondrite Richardton was provided by the Carnegie Institution for Science (CIS). All other samples were provided by the Smithsonian National Museum of Natural History (SI), including H4 chondrite Avanhandava (USNM 6882), H5 chondrites Allegan (USNM 215) and Forest City (USNM 2774 2), and H6 chondrites Oakley (USNM 3350) and ALHA 78115 (USNM 7318 78115,1). Avanhandava, Richardton, Forest City, and Allegan were observed falls, and the other chondrites were finds.

## 4.4 Methods

### 4.4.1. $^{182}$Hf-$^{182}$W Systematics of H Chondrites

All samples were magnetically separated at the University of Maryland Isotope Geochemistry Lab (IGL). The W isotopic compositions, and Hf and W abundances of metal fractions were determined at the IGL. For slightly magnetic and nonmagnetic fractions, the W isotopic compositions, and Hf and W abundances were determined at the Unversity of Münster, Institut für Planetologie.

### 4.4.1.1. Sample Preparation

All samples from the SI and the CIS were previously processed as part of a complementary study on Pb-Pb dating of separated phosphates from H chondrites (Blackburn et al., 2016). Before being transferred to the University of Maryland for this study, the chondrites from that study were gently crushed using an agate mortar and pestle and then separated by magnetic susceptibility using an S.G. Frantz® magnetic separator. Detailed methods are provided in Blackburn et al. (2016). Two samples (Faucett, and Acfer 395) were processed from bulk chondritic fragments at IGL. They were gently crushed, and then a hand magnet was used to separate material into highly magnetic (primarily metal), slightly magnetic (NM-2), and nonmagnetic (NM-1) fractions. Nonmagnetic and slightly magnetic fractions that were separated at different times are denoted by A and B.

Fractions from all samples were purified by repeated crushing using a mortar and pestle while immersed in ultrapure $H_2O$ from a MilliQ® water purification system, followed by further magnetic separation using a hand magnet. This process was repeated until no further separation of metal from silicate was possible. All metal fractions retained small fractions of adhering nonmagnetic dust that could not be removed. Metal grains were separated into >150 µm and <150 µm fractions using a nylon sieve.

### 4.4.1.2. Separation and Purification of W for Isotopic Compositions

Metal fractions were combined with ~40 mL of 8M HCl in 60 mL Teflon vials and heated to 130°C for 48 hours. The 8M HCl did not efficiently digest silicates, so

88

W from Hf-rich silicate phases was not efficiently accessed during digestion. After digestion, sample solutions were centrifuged, and the higher density undigested nonmagnetic phases were separated. Then, a ~0.5% aliquot by volume was removed and spiked with $^{178}$Hf and $^{182}$W. The remaining sample solution was auto-oxidized in an open beaker by exposure to atmosphere for at least one week, in order to convert $Fe^{2+}$ to $Fe^{3+}$. The $Fe^{3+}$ was then removed by solvent extraction into diisopropyl ether (Myers and Metzler, 1950). Tungsten was separated and purified using the cation and anion exchange chromatography method reported by Touboul and Walker (2012). After separation and purification of W, all fractions were dried down with either concentrated Teflon-distilled $HNO_3$ + quartz-distilled HCl, or with Teflon-distilled $HNO_3$ + $H_2O_2$ (30%) several times to destroy organics. Total analytical blanks for W were ~1 ng, and blank corrections were insignificant.

Slightly magnetic and nonmagnetic separates were combined with ~15 mL 2:1 concentrated, Teflon-distilled HF-$HNO_3$ and heated to 120°C for ~30 hours. After digestion, samples were dried and then redissolved in concentrated $HNO_3$ to remove organics. The samples were then redissolved in 6M HCl-0.06M HF, and a 10% aliquot was removed and spiked with a mixed $^{180}$Hf-$^{183}$W spike.

Tungsten was separated and purified using a modified version of the two-stage anion exchange chromatography method reported by prior studies (e.g., Kleine et al., 2004, Kleine et al., 2012; Kruijer et al., 2012; Kruijer et al. 2015). For the first column stage, samples were dissolved in 75 mL 0.5M HCl-0.5M HF and then loaded onto pre-cleaned anion exchange columns (4 mL BioRad AG1 x 8, 200-400 mesh). After rinsing the sample matrix with 10 mL 0.5M HCl-0.5M HF, W (along with high field strength

elements) was eluted with 15 mL 6M HCl-1M HF.  The samples were dried, and then repeatedly redissolved in a few drops each of $HNO_3$ and $H_2O_2$ (30%), and dried at 80°C to remove organics.  High field strength elements were removed in a second anion exchange column using the method reported by Kruijer et al., (2015).  Samples were further purified of organics using $HNO_3$ and $H_2O_2$.  Total procedural blanks ranged from 29 to 123 pg, with a mean of 71 pg (n=7).  Uncertainties for blank corrections are reflected in the reported uncertainties for W isotopic compositions.

### 4.4.1.3. Mass Spectrometry for W Isotopic Compositions

Purified W from each metal fraction was loaded onto a previously outgassed (48 hours before) Re filament using a method slightly modified from Touboul and Walker (2012).  Twenty-four hours after loading W, a mixed activator containing 5 µg each of La and Gd was added (Touboul and Walker, 2012).

The W isotopic compositions of the metal fractions were measured by negative thermal ionization (N-TIMS) on the UMd *Thermo-Fisher Triton 1* using Faraday cup collection.  Tungsten was measured as $WO_3^-$, and oxide production was enhanced by bleeding $O_2$ ($P_{O2}=1.0\times10^{-7}$) into the source.  The N-TIMS method of Touboul and Walker (2012), which allows the measurement of $^{182}W/^{184}W$ to an external precision of ~5 ppm, was used for two Faucett, one Richardton, and one Avanhandava metal fractions.  For these analyses, $^{183}W/^{184}W$ could not be measured, as it is used in a second order fractionation correction.  A new N-TIMS method, which allows measurement of both $^{182}W/^{184}W$ and $^{183}W/^{184}W$ to external precisions of ~5 ppm by measuring in-run O isotopic compositions using $10^{12}$ Ω resistors on two Faraday cups (H3 and H4), was

developed during the course of this study, and was used for all other fractions (Archer et al., in review; Chapter 3). For both N-TIMS methods, instrumental mass bias was corrected using normalizing ratios $^{186}W/^{184}W=0.92767$ and $^{186}W/^{183}W=1.9859$ (Kleine et al., 2004) and the exponential law. Measured signal intensities evolved during analyses, and typically ranged from 700mV to 1.2V.

The W isotopic compositions of slightly magnetic and nonmagnetic separates were measured on the *Thermo-Fisher Neptune Plus* multi collector-inductively coupled plasma mass spectrometer (MC-ICPMS) in the Institut fur Planetologie at the University of Münster, with a setup similar to Kruijer et al. (2014) and Kruijer et al. (2015), using Faraday cup collection. Samples were introduced using an ESI self-aspirating nebulizer and a *Cetac Aridus II* desolvating nebulizer system. A Jet sampler and an X-skimmer cone were used for optimal sensitivity. Instrumental mass bias corrections were made using $^{186}W/^{184}W=0.92767$ and $^{186}W/^{183}W=1.9859$ (Kleine et al., 2004) using the exponential law. Signal intensities varied from 440mV to 10.9V among analyses.

### 4.4.1.4. Hf and W Concentrations by Isotope Dilution

Spiked-sample mixtures from metal fractions were equilibrated in closed 15 mL vials on a hotplate at 120 ºC for 24 hours. After drying, spike-sample mixtures were redissolved in 2 mL of 0.5M HCl-0.5M HF. Hafnium and W were then separated and purified using a single-stage anion exchange chromatographic technique (Touboul et al., 2007; Touboul et al., 2009; Touboul et al., 2015). Purified W and Hf from metal fractions were measured on the UMd *Nu Plasma* MC-ICPMS using Faraday cup

collection.  Tungsten and Hf standards were analyzed during each analytical session to correct for instrumental bias.  Blanks for W ranged from 10 pg to 84 pg, with a mean of 51 pg (n=4).  Hafnium blanks ranged from 15 pg to 122 pg, with a mean of 47 pg (n=4).  Because metal fractions have low Hf concentrations, Hf blank corrections exceeded 50% for some samples.  Uncertainties for blank corrections are reflected in the reported uncertainties for $^{180}$Hf/$^{182}$W.

Unlike metal fractions, the $^{180}$Hf/$^{182}$W of slightly magnetic and nonmagnetic fractions were highly variable, and precise determinations of $^{180}$Hf/$^{182}$W were critical for applications.  Therefore, care was taken to increase the abundance ratio of sample to blank.  Larger (~10% by volume) aliquots were removed and spiked with appropriate amounts of $^{180}$Hf and $^{183}$W.  The sample-spike mixtures were equilibrated on a hotplate in closed 15 mL vials at 120 ℃ overnight.  Hafnium and W were separated and purified using a modified version of the method described in Kleine et al., (2004).  In order to remove organics, samples were dried and then redissolved in several drops of $HNO_3$ and $H_2O_2$.  They were then re-dried at 80°C.  After redissolving in loading acid (0.56M HNO3-0.24M HF), spiked Hf and W from slightly magnetic and nonmagnetic fractions were measured on the *Thermo-Fisher Neptune Plus* using Faraday cup collection. Mass bias corrections were made using $^{179}$Hf/$^{177}$Hf = 0.73250 and $^{186}$W/$^{184}$W = 0.92768.  Blanks for W ranged from 1 pg to 20 pg, with a mean of 8 pg (n=3).  Blanks for Hf ranged from 5 pg to 24 pg, with a mean of 11 pg (n=3).

*4.4.2. $^{187}Re$-$^{187}Os$ Isotopic Systematics and Highly Siderophile Element Abundances of H Chondrite Metal and Nonmagnetic Fractions*

Metal fractions (>150 µm and <150 µm) and nonmagnetic (NM1) fractions from Avanhandava (H4), Richardton (H5), and ALHA 78115 (H6) were combined with a 2:1 mixture of Teflon distilled, concentrated $HNO_3$ + HCl, and two isotopic spikes, one enriched in $^{185}Re$ and $^{190}Os$, the other enriched in $^{191}Ir$, $^{99}Ru$, $^{194}Pt$, and $^{105}Pd$. Sample-spike mixtures were sealed in 8 mL Pyrex™ Carius tubes (Shirey and Walker, 1995) and heated to 260 °C for 72 hours. After digestion, Os was removed via solvent extraction using $CCl_4$, and back extraction into Teflon distilled concentrated HBr (Cohen and Waters, 1996). Separated Os was purified by microdistillation from dichromate into concentrated HBr (Birck et al., 1997). Ruthenium, Pd, Re, Ir, and Pt were separated and purified using an anion exchange chromatography technique (Rehkämper and Halliday, 1997). Blanks contributions using this method were <<1%, and blank corrections were insignificant.

Osmium was measured by N-TIMS on a UMd *Thermo-Fisher Triton* using Faraday cup collection. Osmium was loaded onto previously outgassed Pt filaments, and a $Ba(OH)_2$ activator was added (Creaser et al., 1991). All other HSE were measured as solutions on the UMd *Nu Plasma* MC-ICPMS using Faraday cup collection. The reported data were corrected for instrumental bias by measuring standards within each analytical session.

*4.4.3. High-precision Osmium Isotopic Compositions of H Chondrite Metal Fractions*

Metal fractions from Richardton (H5), Allegan (H5), and Oakley (H6) were combined with ~3 mL 8N HCl in 15 mL Savillex® Teflon vials and digested on a hotplate at 130 °C for 48 hours. As with the fractions measured for W isotopic compositions, a residue of nonmagnetic (silicate and oxide) material remained after digestion, so samples were centrifuged and the nonmagnetic material was removed. Samples and 3 mL of a 2:1 mixture of Teflon distilled, concentrated $HNO_3$ + HCl were then sealed in 8 mL Pyrex™ Carius tubes (Shirey and Walker, 1995) and heated to 260 °C for 24 hours. Osmium separation and purification followed the procedure described in section 4.4.2. Osmium was measured in a method similar to the method described in section 4.4.2. Mass bias corrections were made using $^{192}Os/^{188}Os = 3.08271$ (Allègre and Luck, 1980), which is optimal for investigating neutron capture reactions (Walker, 2012). Signal intensities ranged from ~1V to ~1.5V for $^{192}Os$ during each analysis. External precisions for these measurements were ~5 ppm.

*4.5 Results*

*4.5.1 Highly Siderophile Element Abundances, $^{187}Re$-$^{187}Os$ Isotopic Systematics, and High Precision Os*

In order to investigate the diffusive exchange of HSE during thermal metamorphism, a metal fraction and a nonmagnetic (NM1) fraction from one H chondrite of each petrologic type (H4, H5, and H6) were analyzed for HSE abundances and Re-Os isotopic systematics (Table 4.1; Figs. 4.1 and 4.2).

Table 4.1. Highly siderophile element abundances (ppb) and $^{187}$Re-$^{187}$Os systematics of H chondrite metal and nonmagnetic (NM1) fragments. $\Delta_{Os}$ is the deviation in parts per 10,000, from a primordial 4568 Ma reference isochron. Uncertainties for $^{187}$Re/$^{188}$Os, $^{187}$Os/$^{188}$Os, and $\Delta_{Os}$ are 2σ.

| | Mass (g) | Re | Os | Ir | Ru | Pt | Pd | $^{187}$Re/$^{188}$Os | 2σ | $^{187}$Os/$^{188}$Os | 2σ | ΔOs | 2σ |
|---|---|---|---|---|---|---|---|---|---|---|---|---|---|
| **Avanhandava (H4)** | | | | | | | | | | | | | |
| >150 µm metal | 0.00761 | 162.3 | 1490 | 1422 | 2256 | 3197 | 2642 | 0.5273 | 0.0009 | 0.13654 | 0.00041 | -3.3 | 0.7 |
| <150 µm metal | 0.01123 | 302.5 | 3652 | 3083 | 4687 | 6568 | 3621 | 0.4003 | 0.0007 | 0.12889 | 0.00022 | 21 | 0.6 |
| NM1 | 0.16794 | 5.747 | 88.92 | 83.03 | 125.8 | 70.74 | 57.61 | 0.3121 | 0.0009 | 0.12446 | 0.00012 | 46 | 0.7 |
| | | | | | | | | | | | | | |
| **Richardton (H5)** | | | | | | | | | | | | | |
| >150 µm metal | 0.00575 | 190.2 | 1871 | 1740 | 2916 | 4036 | 2784 | 0.4920 | 0.0010 | 0.13401 | 0.00029 | -0.6 | 0.8 |
| <150 µm metal | 0.00907 | 607.9 | 6663 | 5785 | 8492 | 12910 | 6489 | 0.4410 | 0.0009 | 0.13091 | 0.00016 | 8.7 | 0.7 |
| NM1 | 0.32782 | 0.504 | 8.868 | 10.31 | 13.72 | 8.723 | 2.107 | 0.2739 | 0.0010 | 0.11294 | 0.00012 | -39 | 0.8 |
| | | | | | | | | | | | | | |
| **ALHA 78115 (H6)** | | | | | | | | | | | | | |
| >150 µm metal | 0.00717 | 266.2 | 2743 | 2464 | 4003 | 5803 | 3118 | 0.4696 | 0.0008 | 0.13249 | 0.00025 | 1.8 | 0.7 |
| <150 µm metal | 0.00998 | 396.7 | 4626 | 3761 | 6214 | 8701 | 5250 | 0.4144 | 0.0009 | 0.12995 | 0.00026 | 20 | 0.7 |
| NM1 | 0.15281 | 10.02 | 149.8 | 146.5 | 187.8 | 213.6 | 86.05 | 0.3231 | 0.0007 | 0.12255 | 0.00007 | 18 | 0.5 |
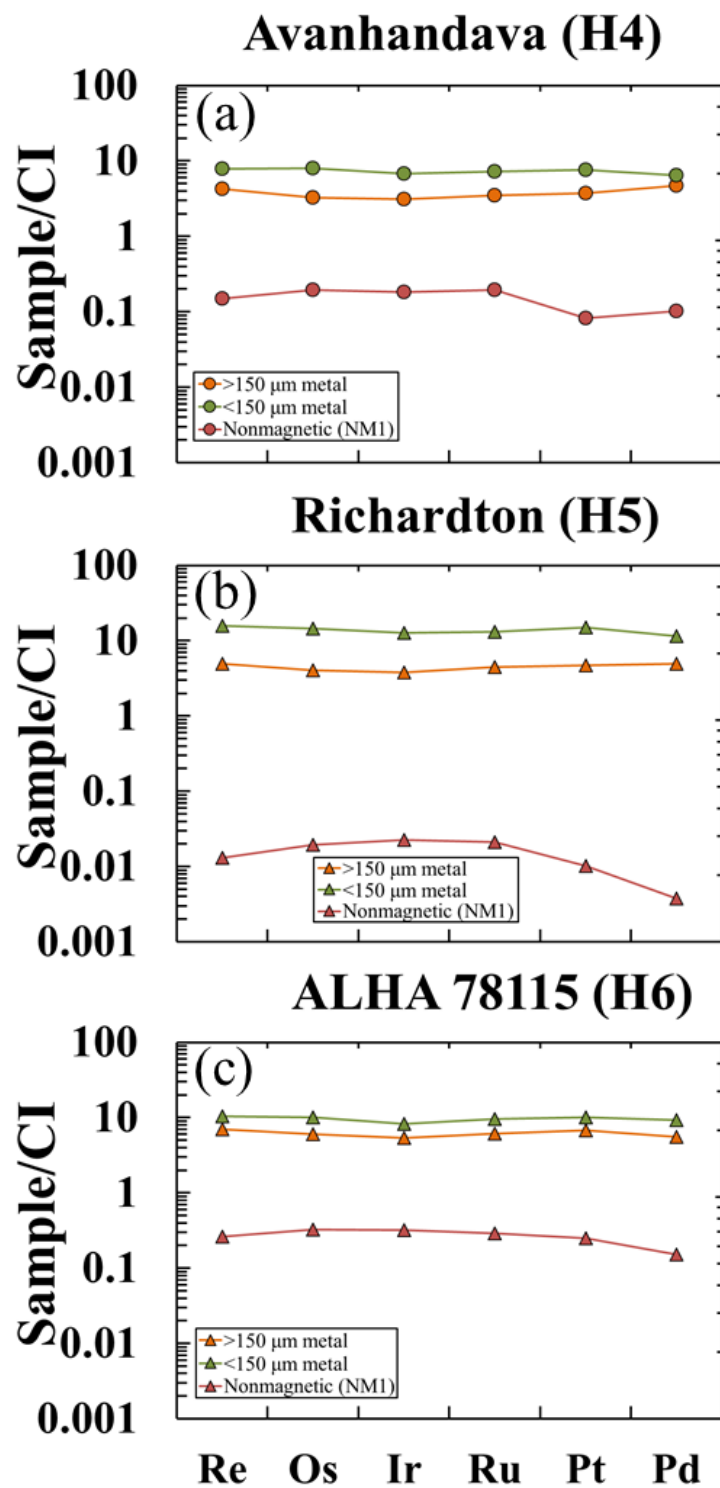
Figure 4.1. CI normalized (Horan et al., 2003) HSE abundances of (a) Avanhandava, (b) Richardton, and (c) ALHA 78115 metal and nongmagnetic fractions. Uncertainties are smaller than symbol size.

The HSE characteristics of metal and nonmagnetic fractions from 3 H chondrites investigated here are broadly similar to previously reported data for an H3.8 and an H4 chondrite (Horan et al., 2009). However, Pd/Os for the Avanhandava and ALHA 78115 nonmagnetic fractions are higher than the Pd/Os of Richardton and the previously reported H3.8 and H4 chondrites. Re/Os varies systematically among the three components, with >150 µm metal having the highest Re/Os, and nonmagnetic fractions having the lowest.

Fine- and coarse-grained metals have suprachondritic HSE abundances that range from ~3x to ~15x CI for Os, and the relative abundances of HSE (e.g., Pt/Os) are similar to those of bulk chondrites. For the three H chondrites, fine-grained metal fractions have higher HSE abundances than coarse-grained metal fractions, as was observed by Horan et al. (2009) for H chondrites. The abundances of HSE in the >150 µm metal fractions increase with petrologic type. By contrast, the HSE abundances of the <150 µm metal do not correlate with petrologic type. The <150 µm metal fraction from Richardton (H5) has the highest HSE abundances, and the <150 µm metal fraction from Avanhandava (H4) has the lowest.

Nonmagnetic fractions have subchondritic HSE abundances, ranging from ~0.02-0.3x CI for Os. Relative HSE abundances are moderately fractionated relative to bulk chondrites, with subchondritic Re/Os and Pd/Os that range from 0.057 to 0.067 and 0.24 to 0.65, respectively (CI chondrite Orguiel has Re/Os and Pd/Os of 0.084 and 1.2, respectively; Horan et al., 2003). Avanhandava and Richardton nonmagnetic fractions are also Pt depleted, with Pt/Os of 0.80 and 0.98, respectively (CI chondrite Orguiel has Pt/Os of 1.9; Horan et al., 2003). The abundances of HSE in nonmagnetic

fractions do not have a systematic relationship with petrologic type. The nonmagnetic fraction from Richardton (H5) has the lowest HSE abundances of the three chondrites examined, and the nonmagnetic fraction from ALHA 78115 (H6) has the highest.

The deviation of samples from a primordial 4568 Ma $^{187}$Re-$^{187}$Os isochron (Fig. 4.2a) can be expressed using $\Delta_{Os}$ notation (e.g., Becker et al., 2001; Archer et al., 2014):

$$\Delta_{Os} = 10^4[^{187}Os/^{188}Os_{sample} - (0.09517 + 0.07908 \text{ x } ^{187}Re/^{188}Os_{sample})]$$

Eqn. 4.1

where $^{187}$Os/$^{188}$Os$_{sample}$ and $^{187}$Re/$^{188}$Os$_{sample}$ are the measured $^{187}$Os/$^{188}$Os and $^{187}$Re/$^{188}$Os of a sample, and 0.09517 and 0.07908 are the initial $^{187}$Os/$^{188}$Os of the Solar System, and slope of a 4568 Ma primordial isochron, respectively (Archer et al., 2014). The $^{187}$Re-$^{187}$Os systematics of coarse-grained metal show little deviation from a primordial isochron (<3.3±0.7 $\Delta_{Os}$ units, Fig. 4.2b). By contrast, the $\Delta_{Os}$ values of fine-grained metal and nonmagnetic fractions deviate by as much as 21±0.6 and 46±0.7, respectively.
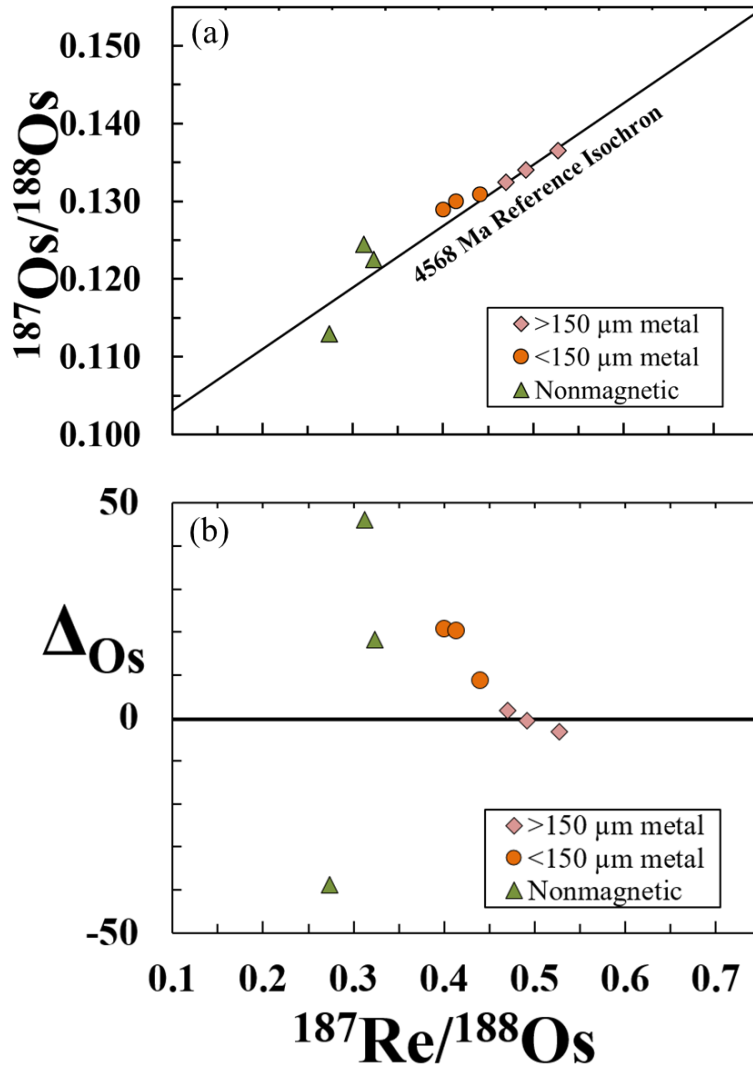
Figure 4.2. $^{187}$Re-$^{187}$Os systematics for H chondrite metal and nonmagnetic fractions. Uncertainties are smaller than symbols unless shown. (a) Re-Os isotopic systematics compared to 4568 Ma reference isochron, using parameters from Archer et al. (2014). (b) $^{187}$Re-$^{187}$Os vs. $\Delta_{Os}$. $\Delta_{Os}$ is the deviation in parts per 10,000, from a primordial 4568 Ma reference isochron.

The high-precision Os isotopic compositions of 3 H chondrite metal fractions, mass bias corrected using $^{192}$Os/$^{188}$Os to investigate neutron capture effects, are reported in Table 4.2, and shown in Fig. 4.3.

Table 4.2. Osmium isotopic data for H chondrite metal fractions normalized using $^{192}Os/^{188}Os = 3.08271$

| Sample | $\mu^{189}Os$ | $2\sigma$ | $\mu^{190}Os$ | $2\sigma$ |
|---|---|---|---|---|
| Richardton (H5) | -7.2 | 4.6 | 0.3 | 6.4 |
| Allegan (H5) | -1.2 | 4.6 | 1.6 | 6.4 |
| Oakley (H6) | -0.9 | 4.6 | -4.7 | 6.4 |

The isotopic compositions are reported in $\mu^x Os$ units, which is the deviation in parts per million of the measured isotopic composition of a sample from a terrestrial standard. Allegan and Oakley have $\mu^{189}Os$ and $\mu^{190}Os$ values that are within uncertainties of terrestrial standards. By contrast, Richardton metal has a $\mu^{189}Os$ value of -7.2±4.6, compared to the terrestrial standards.
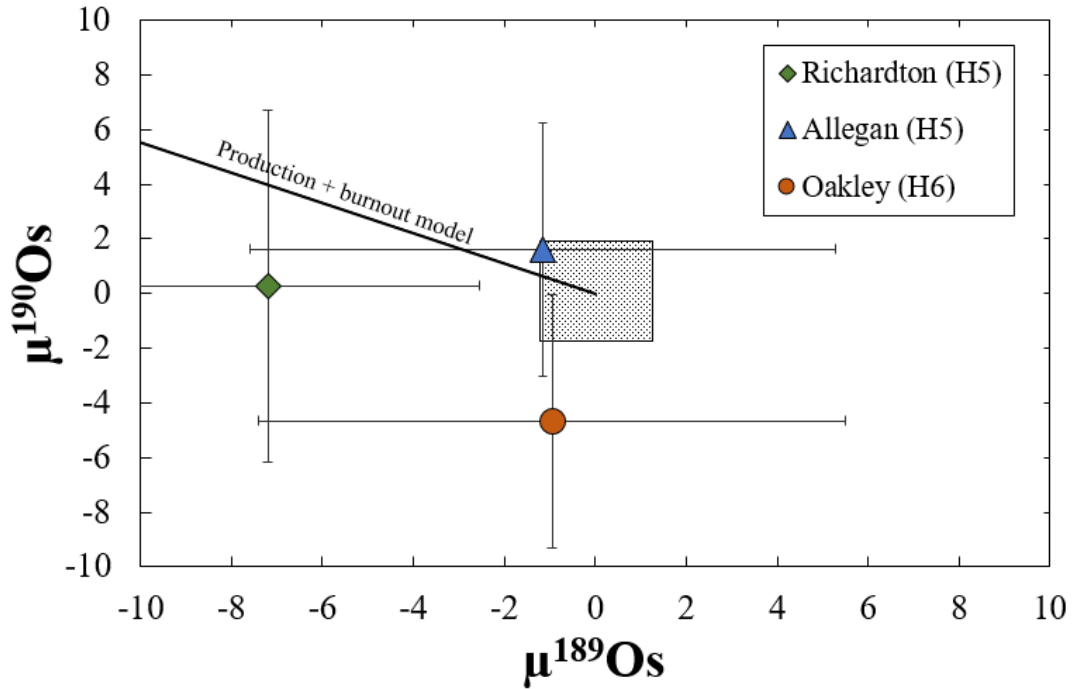


Figure 4.3. Osmium isotopic compositions of H chondrite metal fractions. Production and burnout model line from Walker (2012). Error bars represent $2\sigma$ external reproducibility of standard analyses. Grey box represents the 2SE of standard analyses.

*4.5.2 Hf and W abundances, $^{182}$Hf-$^{182}$W Isotopic Systematics, and $^{183}$W*

The results of Hf and W abundances, and the $^{182}$Hf-$^{182}$W isotopic systematics of H chondrite metal, slightly magnetic, and nonmagnetic fractions from H4-6 chondrites and the one CR chondrite are presented in Table 4.3.

Table 4.3. Hafnium and W abundances (ppb), $^{182}$Hf-$^{182}$W systematics, and $\varepsilon^{183}$W of H chondrite metal, slightly magnetic (NM2) and nonmagnetic (NM1) fractions.

| | Hf | W | $^{180}$Hf/$^{184}$W | ± | $\varepsilon^{182}$W$_{6/3}$ | ± | $\varepsilon^{182}$W$_{6/4}$ | ± | $\varepsilon^{183}$W$_{6/4}$ | ± |
|---|---|---|---|---|---|---|---|---|---|---|
| **Avanhandava (H4)** | | | | | | | | | | |
| Metal >150 μm | 2 | 834 | 0.003 | 0.001 | -3.14 | 0.06 | -3.13 | 0.09 | n.d. | n.d. |
| | | | | | -3.10 | 0.06 | -3.14 | 0.09 | -0.09 | 0.07 |
| NM-1A | 165.3 | 262.0 | 0.744 | 0.004 | | | 0.50 | 0.18 | | |
| NM-2A | 165.3 | 337.5 | 0.578 | 0.003 | | | 0.33 | 0.18 | | |
| NM-1B | 169.1 | 332.8 | 0.599 | 0.003 | | | 0.33 | 0.07 | | |
| NM-2B | 193.7 | 107.8 | 2.12 | 0.01 | | | 1.26 | 0.18 | | |
| | | | | | | | | | | |
| **Faucett (H5)** | | | | | | | | | | |
| Metal >150 μm | 7 | 782 | 0.011 | 0.003 | -3.08 | 0.05 | -3.09 | 0.06 | n.d. | n.d. |
| Metal <150 μm | 10 | 642 | 0.02 | 0.02 | -3.09 | 0.05 | -3.10 | 0.05 | n.d. | n.d. |
| | | | | | | | | | | |
| **Allegan (H5)** | | | | | | | | | | |
| Metal >150 μm | 12 | 960 | 0.015 | 0.004 | -3.12 | 0.04 | -3.13 | 0.06 | -0.03 | 0.07 |
| Metal <150 μm | 12 | 608 | 0.023 | 0.006 | -3.02 | 0.08 | -3.10 | 0.11 | -0.13 | 0.09 |
| NM-1A | 160.9 | 3.10 | 61.3 | 0.4 | | | 38.37 | 2.03 | | |
| NM-2A | 179.0 | 25.7 | 8.22 | 0.04 | | | 3.31 | 0.27 | | |
| NM-1B | 125.0 | 2.62 | 56.3 | 0.4 | | | 36.37 | 0.79 | | |
| | | | | | | | | | | |
| **Richardton (H5)** | | | | | | | | | | |
| Metal >150 μm | 9 | 759 | 0.013 | 0.002 | -3.35 | 0.05 | -3.37 | 0.05 | n.d. | n.d. |
| | | | | | -3.37 | 0.07 | -3.42 | 0.09 | -0.04 | 0.08 |
| NM1 | 168.4 | 19.1 | 10.4 | 0.1 | | | 5.28 | 0.27 | | |
| NM2 | 179.1 | 30.9 | 6.84 | 0.07 | | | 2.49 | 0.18 | | |
| | | | | | | | | | | |
| **Forest City (H5)** | | | | | | | | | | |
| NM1 | 164.4 | 24.1 | 8.04 | 0.08 | | | 2.79 | 0.26 | | |
| NM2 | 186.0 | 43.4 | 5.06 | 0.03 | | | 0.97 | 0.19 | | |
| | | | | | | | | | | |
| **Oakley (H6)** | | | | | | | | | | |
| Metal <150 μm | 4 | 737 | 0.007 | 0.002 | -2.81 | 0.07 | -2.86 | 0.09 | -0.08 | 0.08 |
| Oakley NM1 | 207.9 | 1.8 | 140 | 20 | | | 47.47 | 2.68 | | |
| Oakley NM2 | 177.8 | 11.9 | 17.6 | 0.3 | | | 5.32 | 0.40 | | |
| Oakley NM1.5 | 203 | 3.8 | 63 | 3 | | | 21.76 | 0.91 | | |
| | | | | | | | | | | |
| **ALHA 78115 (H6)** | | | | | | | | | | |
| Metal >150 μm | 8 | 876 | 0.011 | 0.004 | -2.89 | 0.05 | -2.97 | 0.07 | -0.08 | 0.06 |
| Metal <150 μm | 18 | 846 | 0.025 | 0.006 | -2.58 | 0.10 | -2.80 | 0.15 | -0.30 | 0.12 |
| NM1 | 140.6 | 52.8 | 3.14 | 0.02 | | | 0.60 | 0.10 | | |
| NM2 | 136.6 | 53.9 | 2.99 | 0.02 | | | -0.52 | 0.12 | | |
| | | | | | | | | | | |
| **Acfer 395 (CR2)** | | | | | | | | | | |
| Metal (unsorted) | 45 | 581 | 0.09 | 0.01 | -2.46 | 0.13 | -2.11 | 0.16 | 0.57 | 0.15 |

n.d.- not determined. $\varepsilon^x$W$_{x/x}$ – subscript denotes normalizing isotopes.

The W abundances for the H chondrite metal fractions range from 642 ppb to 834 ppb, and average 751 ppb. Those abundances are consistent with prior studies (Rambaldi, 1976; Kong and Ebihara, 1996; Humayun and Campbell, 2002; Kleine et al., 2008). The W concentration of CR2 chondrite Acfer 395 metal is 581 ppb. Hafnium abundances for H chondrite metal fractions range from 2.46 ppb to 11.9 ppb and average 6.80 ppb. For Acfer 395, the Hf metal abundance is 45 ppb. Avanhandava nonmagnetic and slightly magnetic fractions have W abundances that range from 108 ppb to 338 ppb, with a mean of 260 ppb. By contrast, nonmagnetic and slightly magnetic fractions from the other H chondrites have lower W abundances that range from 1.8 ppb to 53.9 ppb, averaging 22.8 ppb. The Hf abundances are similar among all nonmagnetic and slightly magnetic fractions, and higher than those of metal fractions, and range from 125 ppb to 208 ppb, with a mean of 170 ppb.

The $\varepsilon^{182}W$ values (defined as the part in 10,000 deviation of $^{182}W/^{184}W$ from a terrestrial standard) of metal fractions are indistinguishable, within uncertainties, for most H4 and H5 chondrites (except Richardton), with a mean value of -3.11±0.03 (2SD). By contrast, Richardton (H5) metal fractions have lower $\varepsilon^{182}W$ values that average -3.36±0.01 (2SD). Kleine et al., (2008) reported similar $\varepsilon^{182}W$ values for Richardton coarse-metal fractions (-3.28±0.35 and -3.57±0.16 for >150 µm and >230 µm metal fractions, respectively). Metal fractions from the H6 chondrites Oakley and ALHA 78115 have resolvably higher $\varepsilon^{182}W$ values than H4 or H5 chondrites, with a mean of -2.83±0.05 (2SD). Metal fractions of different grain sizes (>150 µm and <150 µm) from all H chondrites examined here have indistinguishable $\varepsilon^{182}W$ values, within

uncertainties. The $\varepsilon^{182}W$ value (-2.11±0.16) of Acfer 395 is lower than $\varepsilon^{182}W$ values of metals for the H chondrites examined here.

Slightly magnetic and nonmagnetic fractions have variable $\varepsilon^{182}W$ that covary with $^{180}Hf/^{184}W$. The $\varepsilon^{182}W$ values of slightly magnetic and nonmagnetic fractions range from -0.52 to +47.47, and the $^{180}Hf/^{184}W$ vary from 0.578 to 140. The nonmagnetic (NM1) fractions from all samples, except Avanhandava, have the most radiogenic $\varepsilon^{182}W$, and highest $^{180}Hf/^{184}W$. Because of their relatively high W contents, compared to other H chondrites examined here, the possibility that the Avanhandava nonmagnetic and slightly magnetic fractions were contaminated with terrestrial W cannot be ruled out, although it is unlikely (see appendix).

The $\varepsilon^{183}W$ values of most H4 chondrite metal grains measured here are within the 2SD of terrestrial standards. Only one fraction, the <150 µm magnetic fraction from ALHA 78115, has a small negative $\varepsilon^{183}W$ anomaly of -0.29±0.12. However, this negative anomaly may be an analytical artifact, perhaps as a result of mass-independent isotopic fractionation of the odd $^{183}W$ isotope from the even isotopes because of differences in nuclear charge radii (e.g., Willbold et al., 2011; Kruijer et al., 2012). Negative mass-independent $^{183}W$ effects have been previously reported for various types of samples, including rock standards, iron meteorites, and silicate-rich samples (e.g., Willbold et al., 2011; Kruijer et al., 2012). Those studies argued the fractionation occurred during inefficient redissolutions of W in Savillex® Teflon vials. The $\varepsilon^{183}W$ of the separated metal fraction from CR chondrite Acfer 395 ($\varepsilon^{183}W$=+0.57±0.15) is resolvably higher than terrestrial standards and H chondrite metal fractions, and cannot

103

be an analytical artifact, as chemical separation and purification of W produces only negative effects for analytes (e.g., Willbold et al., 2011; Kruijer et al., 2012).

## *4.6 Discussion*

### *4.6.1. $^{187}$Re-$^{187}$Os Isotopic Systematics and Highly Siderophile Elements*

The $^{187}$Re-$^{187}$Os isotopic systematics of the >150 µm metal fractions are generally consistent with system closure since formation as they plot on or close to a primordial isochron (Fig. 4.2). By contrast, the <150 µm metal and nonmagnetic fractions plot well beyond uncertainties of a primordial isochron, deviating by as much as 46 $\Delta_{Os}$ units, most likely because of mobilization of a small fraction of Re during terrestrial alteration. Minor disturbances of the $^{187}$Re-$^{187}$Os system are common for chondrites, including some falls (e.g., Walker et al., 2002; Brandon et al., 2012, Archer et al., 2014; Kadlag et al., 2016). However, the open system behavior is minor (a few % gain or loss of Re). Consequently, the HSE abundances reported here for metal and nonmagnetic fractions likely closely reflect their HSE abundances present immediately following cessation of diffusive exchange.

Because chondrites are aggregates of materials that formed in different places and at different times, their components were probably not in chemical or isotopic equilibrium immediately following aggregation. Therefore, diffusive exchange of elements would have been required for these components to approach chemical and isotopic equilibrium. Experimentally derived, low-pressure metal-silicate distribution coefficients of the HSE are typically >10$^4$ (e.g., Kimura et al., 1974; Newsom, 1990; O'Neill et al., 1995; Borisov and Palme, 1995; Fortenfant et al., 2003; Brenan et al.,

2016).  When metal-silicate equilibrium is achieved, the difference in abundances between metal and silicate for each HSE should reflect these high metal-silicate distribution coefficients.  Further, at equilibrium, the HSE should be highly fractionated in the silicates because of the variable metal-silicate distribution coefficients among the HSE (Brenan et al., 2016).  Consistent with the H3.8 and H4 chondrite HSE data reported by Horan et al. (2009), the differences in HSE abundances between metal and nonmagnetic fractions for H4, H5, and H6 chondrites reported here are too small to reflect equilibrium between metals and silicates (Fig. 4.1).  Further, there is no correlation between metamorphic grade and HSE abundances of metals and nonmagnetic fractions.  It is possible that the lack of apparent equilibration between metal and nonmagnetic fractions reflects incomplete removal of metal from the nonmagnetic fractions (e.g., Chou et al., 1973).  However, the relative HSE abundances of the nonmagnetic fractions (especially Pd/Os) differ significantly from their respective metal fractions for the H chondrites investigated here, as well as for those investigated by Horan et al. (2009).  The comparatively high HSE abundances of H chondrite nonmagnetic fractions more likely reflect the presence of a nonmetallic refractory HSE carrier that never equilibrated with the metal, as argued by Horan et al. (2009).  The HSE data reported here indicate that at even high degrees of metamorphism (H5 and H6 chondrites), the HSE carrier in the nonmagnetic fraction did not fully equilibrate with the metal.

*4.6.2. H Chondrite Hf-W Isochrons and Metal Model Ages*

When plotted as $^{180}$Hf/$^{184}$W vs. $^{182}$W/$^{184}$W, the fractions of a sample with different Hf/W will form an isochron with minimal scatter (i.e., a mean square weighted deviations or MSWD <2) if the following conditions are met: (i) all components were initially in isotopic equilibrium, at the time of system closure, and (ii) the system was not subsequently disturbed.  The slope of an isochron corresponds to the $^{182}$Hf/$^{180}$Hf of the sample at the time of system closure.  This ratio can be related to the time of CAI formation using the following equation:

$$\Delta t_{\mathrm{CAI}} = -\frac{1}{\lambda} \text{ x } \ln\left[\frac{^{182}\mathrm{Hf}/^{180}\mathrm{Hf}_{\mathrm{Sample}}}{^{182}\mathrm{Hf}/^{180}\mathrm{Hf}_{\mathrm{CAI}}}\right]$$

Eqn. 4.2

where $\Delta t_{\mathrm{CAI}}$ is the time since formation of CAIs, $\lambda$ is the $^{182}$Hf decay constant of 0.078±0.002 Myr$^{-1}$ (Vockenhuber et al., 2004), $^{182}$Hf/$^{180}$Hf$_{\mathrm{Sample}}$ is the calculated $^{182}$Hf/$^{180}$Hf of the sample from the slope of the isochron, and $^{182}$Hf/$^{180}$Hf$_{\mathrm{CAI}}$ is the currently accepted $^{182}$Hf/$^{180}$Hf at the time of CAI formation of (1.018±0.043) x 10$^{-4}$ (Kruijer et al., 2014).

For most of the samples investigated here, Hf-W data for metal, slightly magnetic, and nonmagnetic fractions do not form isochrons when combined (i.e., MSWD>>2 when metal is included in regression).  Only the metal, slightly magnetic, and nonmagnetic fractions from Richardton are co-isochronous, with an MSWD of 1.4 (Fig. 4.4c).  By contrast, the slightly magnetic and nonmagnetic fractions of Avanhandava, Allegan, and Oakley only form precise isochrons (MSWD<2) when plotted without their respective metal fractions (Fig. 4.4a, b, and d).  In addition, slightly magnetic and nonmagnetic fractions from H5 chondrites Forest City and

106

Allegan are co-isochronous, but Richardton (H5) does not plot on the same isochron

(Fig. 4.4e).
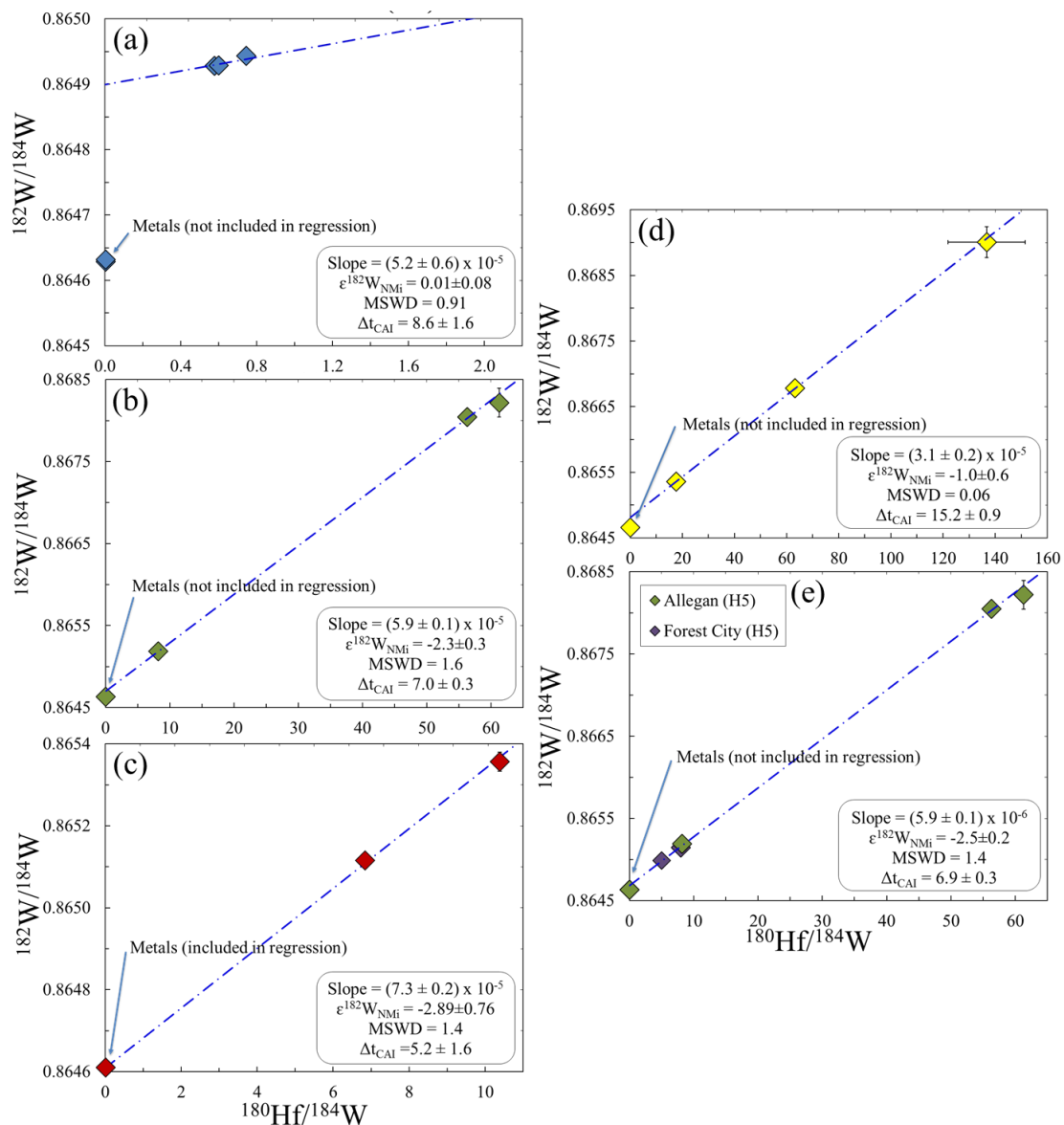


Figure 4.4. $^{182}$Hf-$^{182}$W linear regression for (a) Avanhandava, (b) Allegan, (c) Richardton, (d) Oakley, and (e) combined H5 plotted using ISOPLOT (Ludwig, 2001). Richardton (H5) is not included in combined H5. Metal fractions are not included in the linear regressions of a, b, d, and e.

The Hf-W closure ages calculated from the slopes of linear regressions of the slightly magnetic and nonmagnetic H chondrite fractions are provided in Table 4.4 and Fig. 4.5a. The Hf-W closure age of Oakley (H6) is the youngest (15.2±0.7 Ma after CAI formation). Avanhandava (H4) has a Hf-W closure age (8.6±1.6 Ma after CAI formation) that is identical, within uncertainties, to the Hf-W closure ages of the H5 chondrites reported here of 7.0±0.3 Ma (Allegan) and 8.4±3.2 Ma (Forest City) after CAI formation. Data for Allegan and Forest City are co-isochronous and have a combined age of 6.9±0.3 after CAI formation. Richardton (H5) appears to have the oldest closure age (5.2±1.6) after CAI formation, although it is within uncertainties of other H5 chondrites. This apparent age may be the result of nonradiogenic processes, as discussed later in section 4.6.

Table 4.4. Hf-W slope ages of H chondrites (in Ma since CAI formation) calculated from isochron regressions of silicate-rich fractions. Cooling rates from Willis and Goldstein (1981), Taylor et al. (1987), and Scott et al. (2014). The error for the cooling rates is a factor of 3-4 (Scott et al., 2014).

| H Chondrite | Slope Age $\Delta t_{CAI}$ | $2\sigma$ | $\varepsilon^{182}W_{NMi}$ | $2\sigma$ | Cooling Rate ($^0$C/Myr) |
|---|---|---|---|---|---|
| Avanhandava NM (H4) | 8.6 | 1.6 | 0.01 | 0.08 | 20 |
| Allegan NM (H5) | 7.0 | 0.3 | -2.3 | 0.3 | 15 |
| Forest City NM (H5) | 8.4 | 3.2 | -2.1 | 0.9 | 20 |
| Combined (H5) | 6.9 | 0.3 | -2.5 | 0.2 | |
| Richardton NM (H5) | 5.2 | 1.6 | -2.9 | 0.8 | 20 |
| Oakley NM (H6) | 15.2 | 0.7 | -1.0 | 0.6 | |

Because the H chondrite metal fractions have such low Hf/W ratios (≤0.025), their $\varepsilon^{182}W$ values should define the initial $\varepsilon^{182}W$ values of their respective isochrons. Two stage metal model ages, which are presumed to represent the time at which the metal fractions ceased to diffusively exchange W with surrounding silicates, are calculated using the following equation:

108

$$\Delta t_{CAI} = -\frac{1}{\lambda} \times \ln\left[1 - \frac{\varepsilon^{182}W_{Metal} - \varepsilon^{182}W_{Chondrite}}{\varepsilon^{182}W_{CAI} - \varepsilon^{182}W_{Chondrite}}\right]$$

Eqn. 4.3

where $\varepsilon^{182}W_{metal}$ is the measured $\varepsilon^{182}W$ of the metal, $\varepsilon^{182}W_{CAI}$ is the currently accepted $\varepsilon^{182}W_i$ of CAIs (-3.49±0.07), which represent the Solar System initial $\varepsilon^{182}W$ (Kruijer et al., 2014b), and $\varepsilon^{182}W_{Chondrite}$ is the value for chondrites today (-1.90; Kleine et al., 2002; Schönberg et al., 2002; Yin et al., 2002; Kleine et al., 2004). These model ages are based upon an assumption of a chondritic Hf/W for the parent body prior to equilibration. Metal model ages after CAI formation are presented in Table 4.5 and Fig. 4.5b, and range from 1.0±0.6 Ma, for one Richardton metal fraction, to 7.2±2.1 Ma for one ALHA 78115 metal fraction. The mean model age for most H4 and H5 chondrite metal fractions, excluding Richardton, is 3.5±0.4 Ma after CAI formation (2SD).

The H5 chondrite Richardton has a $\varepsilon^{182}W_{NMi}$ value (the initial $\varepsilon^{182}W$ value defined by linear regression of data combined for slightly magnetic and nonmagnetic fractions) of -2.89±0.76 (Table 4.4), which is within uncertainty of the $\varepsilon^{182}W$ values for their respective metal fractions. However, for all other samples, the metal fractions have resolvably lower $\varepsilon^{182}W$ values than the $\varepsilon^{182}W_{NMi}$ values. The $\varepsilon^{182}W_{NMi}$ values for these isochrons are -0.01±0.08 (Avanhandava), -2.3±0.3 (Allegan), and -1.0±0.6 (Oakley). The difference between the metal fraction $\varepsilon^{182}W$ and isochron $\varepsilon^{182}W_{NMi}$ values is largest for H4 chondrite Avanhandava (~3 $\varepsilon$ units).

Table 4.5. Model ages for H and CR chondrite metal fractions (in Ma since CAI formation). The model age for Acfer 395 metal has been corrected for nucleosynthetic effects.

| Metal Fraction | Model Age $\Delta t_{CAI}$ | $2\sigma$ |
|---|---|---|
| Avanhandava (H4)(>150 μm) | 3.2 | 0.6 |
| Avanhandava (H4)(>150 μm) | 3.6 | 0.7 |
| Faucett (H4)(>150 μm) | 3.8 | 0.5 |
| Faucett (H4)(<150 μm) | 3.7 | 0.5 |
| Allegan (H5)(>150 μm) | 3.4 | 0.5 |
| Allegan (H5)(<150 μm) | 3.4 | 1.2 |
| Richardton (H5)(>150 μm) | 1.2 | 0.4 |
| Richardton (H5)(>150 μm) | 1.0 | 0.6 |
| ALHA 78115 (H6)(>150 μm) | 6.1 | 0.6 |
| ALHA 78115 (H6)(<150 μm) | 7.2 | 2.1 |
| Oakley (H6)(<150 μm) | 7.1 | 0.9 |
| Acfer 395 (CR2)(Unsorted) | 7.0 | 3.6 |

If conditions (i) and (ii) were met, model ages for metals should be indistinguishable from isochron slope ages, and the $\varepsilon^{182}W$ values of the metal fractions should be indistinguishable from the $\varepsilon^{182}W_{NMi}$ values calculated from the isochrons. However, except for Richardton, the model ages of the metal determined here are older than the isochron ages in all cases, and $\varepsilon^{182}W$ values of metal fractions are lower than the $\varepsilon^{182}W_{NMi}$ values in all cases. Therefore, either the components were not initially in isotopic equilibrium at the time of system closure, or the systems were subsequently disturbed, or both. Despite this, H4-5 chondrites have metal model ages that are similar and isochron slope ages that are similar, whereas the H6 chondrites have both younger metal model ages and isochron slope ages. Therefore, the same general trends are observed for both metal model ages and isochron slope ages.
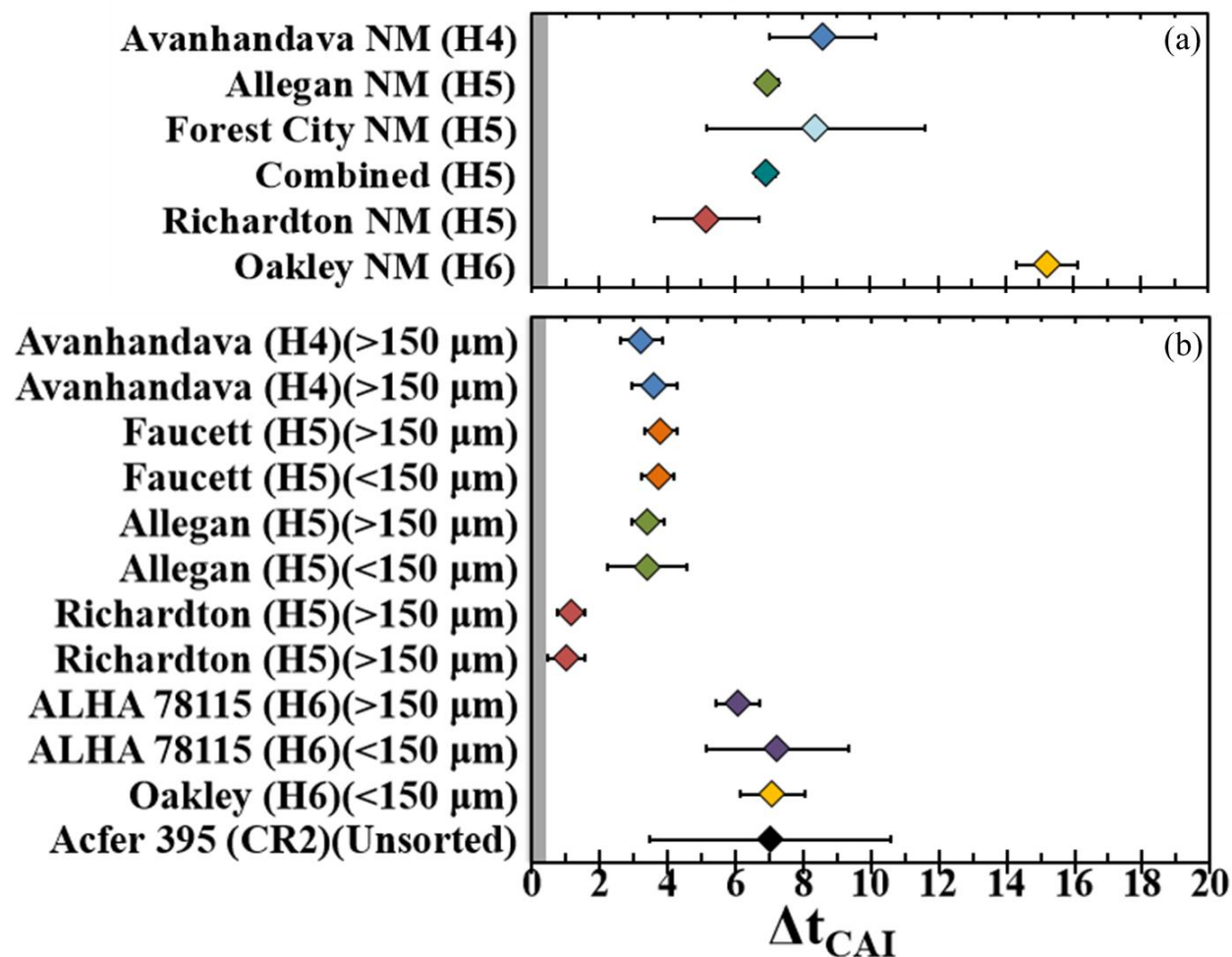
Figure 4.5. Hf-W ages for H and CR chondrites in Ma since CAI formation. Grey fields are the reported uncertainties for CAI formation. (a) Slope derived ages for linear regressions of H chondrite nonmagnetic and slightly magnetic fractions. (b) Model ages for H chondrite metal fractions. The model age for Acfer 395 metal has been corrected for nucleosynthetic effects.

*4.6.3. H Chondrite Metal-Silicate Disequilibrium*

The minimal scatter about the isochrons for the slightly magnetic and nonmagnetic fractions of individual H chondrites, coupled with their early Solar System closure ages (5-15 Ma after CAI formation), indicate that the Hf-W systematics of the nonmagnetic and slightly magnetic fractions were not significantly disturbed during late-stage open system behavior. Further, the high W concentrations and the absence of Hf in the metal mean that low-temperature alteration did not affect the Hf-W systematics of the metal fractions. Thus, disturbance of the Hf-W system by late-stage alteration is unlikely to be the cause of the non-isochronous behavior of metal versus oxide-silicate fractions. Instead, these characteristics must reflect differing rates of W diffusion between oxides and silicates, as compared to diffusion between oxides-silicates and metals.

Several studies have explored W diffusion in H chondrites and other materials that are geochemically relevant to H chondrites. For example, Humayun and Campbell (2002) measured W and other siderophile element abundances in H chondrite metal grains (H4-6) of different petrologic types, using laser ablation inductively-coupled plasma mass spectrometry. The *in situ* analytical technique allowed the authors to investigate siderophile element abundances of individual metal grains of varying size, major element composition, and petrographic context. Of greatest significance here, they reported that the W/Ir of H chondrite metal grains increases with increasing petrologic type, up to H5, so that H3<H4<H5=H6. They concluded that a large fraction of W entered the metal during metamorphism, but that diffusion only occurred during the earlier stages (H3-H4) of metamorphism, through the reduction of oxidized W in

nonmetallic phases. Once the reductant (carbonaceous material in the matrix) was exhausted during petrologic type 4 thermal conditions, W diffusion ceased, fixing the isotopic composition of the metal. Therefore, the low $\varepsilon^{182}$W of the metal fractions may solely reflect the early diffusive exchange of W between metal and silicate during metamorphism.

Cherniak and Van Orman (2014) reported experimental data for W diffusion in olivine over a range of temperatures and fO$_2$ conditions relevant to H chondrites. Using these data, they modeled diffusive loss of W from olivine into metal over a range of conditions. Of particular relevance to this study, they modeled the diffusive transport of W from olivine to metal following a model for multi-stage cooling during fragmentation and re-accreation of the H chondrite parent body, as proposed by Ganguly et al. (2013). In this three stage model, H chondrites are assumed to initially cool from peak temperatures (~750-~850 °C) at 50 °C/ka. Then in a second stage, the H5 and H6 chondrites cool more slowly at 15 °C/Ma. In the final stage, the H6 chondrites cool at 3 °C/Ma. Cherniak and Van Orman (2014) argued that during such a cooling history, H4 chondrite olivine grains would undergo less than 2% loss of W, even for the smallest grains (1-2 µm). Small olivine grains (2 µm radius) in the H5 and H6 chondrites would lose 17% and 18% of their W, respectively, while olivine grains that were 50 µm and larger would lose <1%.

There are currently no experimental data for W isotopic exchange between metal and silicates. Yokoyama et al. (2009) reported experimental data for chemical equilibration and isotopic exchange of Os, a HSE, between iron meteorites and basalts under high pressure and temperature conditions. They reported that despite the

apparently efficient diffusion of Os from silicates to metal nuggets, complete isotopic equilibration did not occur. They interpreted this to indicate that isotopic exchange occurred at a much slower rate than chemical equilibration under their experimental conditions. Osmium, however likely differs from W in metal-silicate diffusion rates. Consequently, similar experiments will be required to assess the absolute and relative nature of W chemical and isotopic equilibration.

The data presented here indicate that the W present in metals and silicates-oxides were likely not in isotopic equilibrium at the time of maximum thermal metamorphism (perhaps as high as ~1000 °C for H6 chondrites; Keil, 2000). Thus, metal-silicate isochrons do not record the time of peak metamorphism. By contrast, the precise isochrons for slightly magnetic and nonmagnetic fractions suggest that oxides and silicates were in equilibrium when W diffusion ceased, and therefore, may provide robust chronological information about the timing of peak thermal metamorphic conditions.

*4.6.4. Thermal Chronology of the H Chondrite Parent Body*

In the undisturbed onion shell thermal model (e.g., Pellas and Storzer, 1981; Trieloff et al., 2003), the H4 chondrites either reached the closure temperature for any given thermochronological system (e.g., Ar-Ar) earlier than H5 and H6 chondrites, as they were the fastest to cool, or they were never heated to temperatures above the closure temperature, in the case of the high temperature Hf-W thermochronometer (Kleine et al., 2008). In either case, the H4 chondrites should record the oldest closure ages. The H6 chondrites reached the highest peak temperatures, cooled the slowest,

114

and, therefore, should record the youngest closure ages.

The onion shell thermal model has largely been based upon evidence from members of a suite of nine H chondrites originally measured by Pellas and Storzer (1981) for $^{244}$Pu fission closure ages, and Trieloff et al. (2003) for both Ar-Ar and $^{244}$Pu fission track closure ages. Subsequent studies (e.g., Kleine et al., 2008; Harrison and Grimm, 2010; Henke et al., 2012; Monnereau et al., 2013) focused on the same suite of H chondrites in order to build a consistent, comprehensive thermochronometry dataset. Of the five H chondrites examined by Kleine et al. (2008) for Hf-W isotopic systematics, four were from the same suite of H chondrites examined by Trieloff et al. (2003). They reported that the H chondrite metal-silicate data produced precise Hf-W isochrons within the 0.3-0.4 ε unit external precision of their measurements, and that metals and silicates appeared to have been in equilibrium at the time of system closure. They also reported an inverse correlation between metamorphic grades and Hf-W closure ages, consistent with the onion shell thermal model. The least metamorphosed H chondrite examined by that study, Ste. Marguerite (H4), had the oldest Hf-W closure age (1.7±0.7 Ma after CAI formation), and the most metamorphosed H chondrites, H6 chondrites Estacado and Kernouvé, had the youngest (combined, 9.6±1.0 Ma after CAI formation). Kleine et al. (2008) combined the Hf-W data with previously reported closure ages for other systems with varying closure temperatures (Pb-Pb, Ar-Ar, $^{244}$Pu fission tracks) for the same samples to produce cooling rate curves for different portions of the H chondrite parent body. Consistent with the onion shell model, the H4 chondrites cooled the fastest (55 ºC/Ma), and the H6 chondrites cooled slowest (~10 ºC/Ma).

For this study, the observation that the Hf-W isochron age of H6 chondrite Oakley is youngest among the H chondrites examined is consistent with the onion shell thermal model. By contrast, the lack of substantial variation in Hf-W isochron ages for Avanhandava (H4) and the H5 chondrites reported here are inconsistent with the onion shell thermal model. Further, Avanhandava appears to have an even younger Hf-W isochron age (8.6±1.6) than the H5 chondrite Allegan (7.0±0.3), although they are not fully resolved. In support of these new Hf-W observations, Blackburn et al. (2016) reported [207]Pb-[206]Pb ages of Avanhandava phosphates (closure temperatures of ~500 and ~540ºC for apatite and merrillite, respectively) that are too young to be consistent with the onion shell thermal model, and they concluded that the H chondrite parent body must have been disrupted. Therefore, the Hf-W and Pb-Pb ages for H chondrites reported here and by Blackburn et al. (2016) are inconsistent with the undisturbed onion shell thermal model, as Hf-W and Pb-Pb closure ages are not inversely correlated with metamorphic grade, as required by the onion shell thermal model.

Prior studies have calculated metallographic cooling rates for H chondrites by measuring the grain sizes and central Ni concentrations of taenite grains. The Hf-W closure ages of H chondrites reported here are roughly correlated with available metallographic cooling rates (Fig. 4.6; Willis and Goldstein, 1981, Taylor et al., 1987; Scott et al., 2014). The H4 and H5 chondrites examined here have cooling rates that have previously been reported to be 15-20 ºC/Ma. Such cooling rates are indistinguishable within the reported precision (a factor of 2; Scott et al., 2014), which is consistent with the lack of variation in Hf-W closure ages of H4 and H5 chondrites reported here. Scott et al. (2014) argued that the cooling rates of H4-6 chondrites reflect

116

the combined effects of internal heating by [26]Al in a body that may have originally had an onion-shell structure, as well as impact disruption within a few Ma of accretion. They argued that impacts mixed materials of different metamorphic grades before they cooled through 500 °C (near the temperatures at which metallographic cooling rates are applicable). The Hf-W data reported here are consistent with disruption of the H chondrite parent body, because H4 and H5 chondrites appear to have cooled below their closure temperatures at similar times. Disruption must have occurred before H chondrites cooled below 800°C, the Hf-W closure temperature of H4 chondrites.
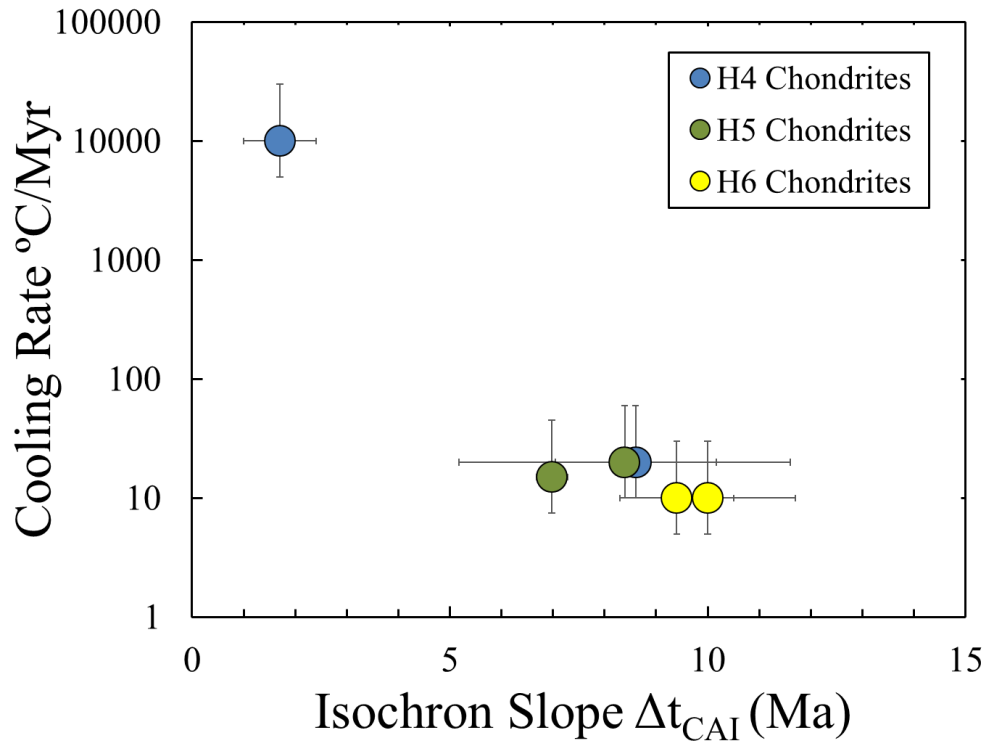


Figure 4.6. Isochron slope ages vs. cooling rates. Isochron slope ages include data from Kleine et al. (2008). Cooling rates are from Scott et al. (2014). Richardton has been omitted because its isochron age may reflect a nonradiogenic process (see section 4.6).

117

*4.6.5. Comparison with Previous Studies*

Kleine et al. (2008) argued that the Hf-W isotopic systematics of Ste. Marguerite (H4) were never reset by thermal metamorphism on the parent body. They argued that the Hf-W closure age of Ste. Marguerite (1.7±0.7 Ma after CAI formation) was too old to reflect parent body processes, and instead reflected the timing of chondrule formation. However, two-pyroxene peak metamorphic temperatures for H4 chondrites (757 ±50 2SD; Ganguly et al., 2013) are within uncertainties of the H4 chondrite closure temperature (800±50 ºC; Kleine et al., 2008). The Hf-W closure age of H4 chondrite Avanhandava (8.6±1.6 Ma after CAI formation) reported by this study is too young to be consistent with chondrule formation, and is instead consistent with resetting of the Hf-W isotopic system on the parent body. Therefore, it appears that the H4 chondrite examined here was likely heated to the Hf-W closure temperatures of H4 chondrites.

Scott et al. (2014) compared the metallographic cooling rates of the H chondrites from the suite of Trieloff et al. (2003) with a much larger (n=31) population of H chondrites. They reported that the suite of H chondrites examined by Trieloff et al. (2003) were characterized by an inverse correlation between metallographic cooling rates and metamorphic grade, as expected for a body with an onion shell thermal structure. The H4, H5, and H6 chondrites from Trieloff et al. (2003) had cooling rates that were ≥10,000 ºC/Ma, 15-20 ºC/Ma, and 10-15 ºC/Ma, respectively. However, Scott et al. (2014) argued that samples with cooling rates >1000 ºC/Ma could not have cooled anywhere within an onion shell thermal structure. Instead, cooling rates >1000 ºC/Ma are consistent with impact excavation of those samples followed by rapid

cooling. Scott et al. (2014) also reported that metallographic cooling rates for many H4 chondrites not included in the suite measured by Trieloff et al. (2003) were similar to those of H5 and H6 chondrites, which is inconsistent with the onion shell thermal model. Therefore, Scott et al. (2014) argued that the H chondrite meteorites, from which most evidence for an onion shell thermal model comes, are not representative of the general H chondrite population.

Three of the H chondrites examined here (Avanhandava, Forest City, and Oakley) were not included in the suite examined by Trieloff et al. (2003). In addition, Avanhandava (H4) records a metallographic cooling rate of 20 ℃/Ma, which is much slower than the ≥10,000 ℃/Ma cooling rates of the H4 chondrites of the Trieloff et al. (2003) suite, and is more typical of most H4 chondrite cooling rates (≤60 ℃/Ma; Scott et al., 2014). Therefore, the differences in observations and interpretations between this study and previous studies likely reflect a sampling difference. It is concluded that the suite of H chondrites examined here does not support an undisturbed onion shell thermal model, and that the H chondrite parent body was likely disrupted within a few Ma after accretion.

### 4.6.6. Low $^{182}W/^{184}W$ of Richardton Metal

The $\varepsilon^{182}W$ values of Richardton metal fractions reported here (with an average of -3.36±0.01; 2SD) and for two different-sized metal fractions (-3.28±0.35 and -3.18±0.19) by Kleine et al. (2008) are in good agreement. These metal fractions have the lowest $\varepsilon^{182}W$ values of any H chondrite metal fractions reported here, or by previous studies (Kleine et al., 2008). The $\varepsilon^{182}W$ values of the metal fractions are similar to

119

IIAB, IIIAB, and IVA iron meteorite groups (Kruijer et al., 2014a), and one metal fraction is within uncertainty of the initial $\varepsilon^{182}$W value of the Solar System defined by CAIs (Kruijer et al., 2014b). These metal data are, thus, inconsistent with the metal data from other H5 chondrites, as well as metal data for any other H chondrite.

The low $\varepsilon^{182}$W of Richardton metal fractions reflect either the timing of system closure or another process unrelated to the decay of $^{182}$Hf, such as cosmic ray exposure or nucleosynthetic effects. One possible explanation for the low $\varepsilon^{182}$W of Richardton metal fractions is that they record earlier thermal metamorphism, cooling, and then system closure than the metals of other H chondrites examined here. The average model age of Richardton metal is 1.1±0.3 Ma after CAI formation (2SD), compared to the average model age of metal from all other H4 and H5 chondrites (3.5±0.4 Ma after CAI formation; 2SD). However, the previously reported metallographic cooling rate of Richardton (20 °C/Ma; Scott et al., 2014) is indistinguishable, within uncertainties, from Avanhandava (H4) and the other H5 chondrites reported here. If all of these chondrites originated from the same parent body, they should have cooled below the Hf-W closure temperature at about the same time, as they share similar cooling rates. This appears to be the case for most of the H4 and H5 chondrites examined here, except Richardton. If Richardton originated from a parent body that accreted earlier than the parent body of the other H chondrites, Richardton could have cooled at a similar rate, but cooled below the Hf-W closure temperature earlier than the H4 and other H5 chondrites examined here. Therefore, it is important to reassess whether Richardton originated from the same body as the other H chondrites examined here.

Like O isotopic compositions, nucleosynthetic anomalies in some elements (e.g., Mo and Ru) can be used to assess genetic relationships among meteorites, and can provide stronger evidence that Richardton did not originate from the same parent body as other H chondrites. Worsham at el. (in review) reported that H5 chondrites Allegan and Richardton have nucleosynthetic anomalies in $\mu^{97}$Mo, corresponding to s-process depletions, but that Richardton has a larger s-process depletion than Allegan. This indicates that Richardton could not have originated from the same parent body as the other H chondrites.

Another possible interpretation of the low $^{182}$W for Richardton is that it reflects some other process unrelated to the decay of $^{182}$Hf. Prior studies have reported mass-independent $\varepsilon^{182}$W anomalies in some meteorites. Some anomalies were caused by the inheritance of W from carrier phases with presolar, mass-independent nucleosynthetic isotopic anomalies (Burkhardt et al., 2012a; Kruijer et al., 2014). Other anomalies have been attributed to the burnout of $^{182}$W by neutron capture reactions during cosmic ray exposure (e.g., Kleine et al., 2005). These two processes can affect the relative abundances of W isotopes in different ways, and can be distinguished by examining $\varepsilon^{182}$W vs. $\varepsilon^{183}$W (Fig. 4.7).
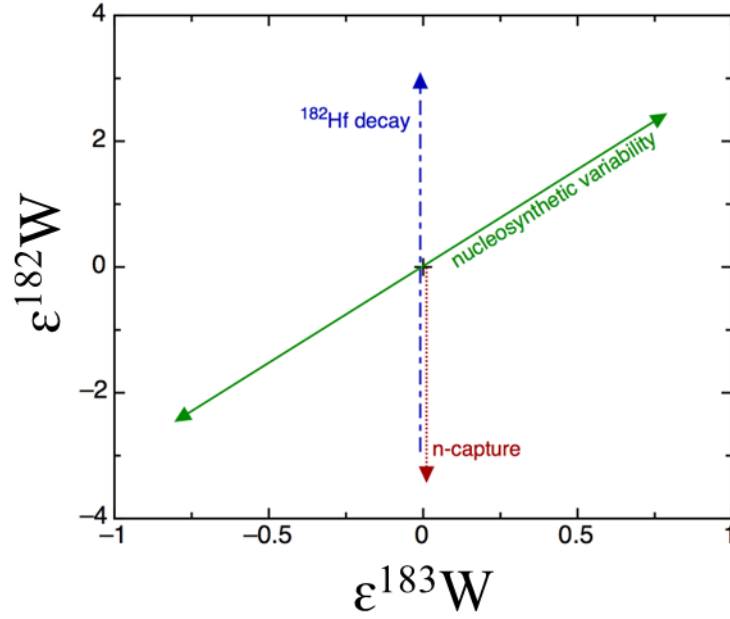
Figure 4.7. Direction of $\varepsilon^{182}$W and $^{183}$W effects for different processes including decay of $^{182}$Hf, neutron capture (cosmogenic effects), and nucleosynthetic effects. Modified from Kruijer (2013).

Nucleosynthetic W isotope anomalies have been reported for CAIs and chondrite leachates, and have been attributed to variable abundances of s- and r-process isotopes (Burkhardt et al., 2012a; 2015; Kruijer et al. 2014). Excesses of nucleosynthetic s-process carriers result in correlated deficits of $^{182}$W and $^{183}$W, with a slope of 1.41±0.06 (Kruijer et al., 2014; Burkhardt et al., 2015). If the anomalously low $\varepsilon^{182}$W of Richardton fractions were caused by s-process carrier excesses, a corresponding deficit in $^{183}$W would be expected. Assuming that the size of the $\varepsilon^{182}$W anomaly in Richardton metal is -0.23 $\varepsilon^{182}$W (the difference between the $\varepsilon^{182}$W of metals from H5 chondrites Richardton and Allegan), the metal should also have a corresponding $\varepsilon^{183}$W anomaly of -0.16, which would be resolved from the terrestrial standards, given the external precision of 0.07 for $\varepsilon^{183}$W. However, the measured $\varepsilon^{183}$W of -0.04±0.08 is indistinguishable from the standards within uncertainties. Therefore,

we conclude that nucleosynthetic effects have not affected the W isotopic composition of Richardton.

Kleine et al. (2008) argued that the low $\varepsilon\,^{182}$W of Richardton metal might be the result of cosmic irradiation-induced W isotope anomalies, which have been reported for iron meteorites (e.g., Kruijer et al., 2012). These anomalies occur because of the burnout (reduction) of certain nuclides with high epithermal neutron capture cross sections ($^{182}$W has a resonance integral of $604\pm90$ barns; Mughabghab, 2003). The reaction $^{182}$W + n $\rightarrow$ $^{183}$W + $\gamma$; or $^{182}$W(n,$\gamma$)$^{183}$W results in $^{182}$W burnout and $^{183}$W production. These effects result in some iron meteorites having measured $\varepsilon^{182}$W that is even lower than the initial $\varepsilon^{182}$W of the Solar System (Kleine et al., 2005). Although $^{183}$W is proportionally produced during burnout reactions involving $^{182}$W, corrections using $^{182}$W/$^{184}$W vs. $^{183}$W/$^{184}$W cannot be made because instrumental mass bias corrections applied to the measured data diminish the apparent effects in $^{183}$W (Fig. 4.7; Kruijer, 2013).

Cosmogenic $^{182}$W anomalies strongly correlate with the isotopic abundances of Os and Pt (Kruijer et al., 2013; Wittig et al., 2013) that are also susceptible to modification during irradiation by cosmic rays. Therefore, Pt or Os isotopes can be used as dosimeters to identify cosmogenic effects and make corrections to $\varepsilon^{182}$W to determine a 'pre-exposure' $\varepsilon^{182}$W. In this study, the $^{189}$Os-$^{190}$Os ($^{189}$Os + n $\rightarrow$ $^{190}$Os + $\gamma$) dosimeter is applied because of the high level of precision (4.5 ppm and 6 ppm for $^{189}$Os and $^{190}$Os, respectively) achievable by N-TIMS, and because no corrections for radiogenic ingrowth have to be made to these isotopes. Although no prior studies have reported cosmogenic Os, Pt, or W effects in bulk chondrites or their components, the

$\mu^{189}$Os value (Fig. 4.3) of Richardton metal is consistent with minor neutron capture and burnout effects, as reported by Walker, (2012) for iron meteorites. The relation between $\mu^{189}$Os values and $\varepsilon^{182}$W values allows cosmogenic $^{182}$W anomalies to be corrected using the slope (1.5±0.5) derived from IAB iron meteorites for $\mu^{189}$Os vs. $\varepsilon^{182}$W (main group, sLL, and sLM; Worsham et al., in review), and the magnitude of the measured $\mu^{189}$Os deficit. After correction for cosmogenic effects using this slope, the $\varepsilon^{182}$W values of the two Richardton >150 μm metal fractions (-3.25±0.09 and -3.3±0.1) are within uncertainties of some H4 and H5 chondrite metal fractions reported here. However, the $\mu^{189}$Os-$\varepsilon^{182}$W correlation appears to be specific to different meteorite groups and their parent bodies, probably because of differences in projectile neutron energy spectra, as parent bodies probably experienced different intensities of irradiation at different times, and the neutron energy spectra that any given sample experienced is highly dependent on its depth within the parent body. Therefore, this correction is not precise and can only serve to highlight the possibility of cosmic ray irradiation.

Although Os provides only tentative evidence for cosmic ray exposure (CRE), there are some other data suggestive of cosmogenic effects. Consistent with this interpretation, Goldmann et al. (2015) reported $^{238}$U/$^{235}$U of various achondrites and chondrites, including Richardton. Of note, Richardton has a $^{238}$U/$^{235}$U that is lower than all other measured meteorites, and ~600 ppm lower than the Solar System average. They argued that this variation was unlikely to be the result of $^{247}$Cm decay or nucleosynthetic effects. Instead, they argued that the effects could be the result of

124

condensation-evaporation processes in the solar nebula, or isotopic fractionation caused by U mobilization during parent body alteration.

Another possibility proposed here is that $^{238}U/^{235}U$ was modified by epithermal neutron capture. Uranium-238 has a large resonance integral of $277\pm3$ barns (Mughabghab, 2003), which is similar to that of $^{183}W$ ($337\pm50$), and almost half that of $^{182}W$ ($604\pm90$). Therefore, as with the low $^{182}W/^{184}W$ reported for Richardton here, the lower $^{238}U/^{235}U$ reported by Goldmann et al. (2015) could be the result of epithermal neutron capture. The difference in the magnitudes of the effects between $^{238}U$ and $^{182}W$ may reflect the energy spectra of epithermal neutrons that favorably overlaps with the capture resonances of $^{238}U$ with high neutron capture cross sections (some as high as $10^4$ barns; Chadwick et al., 2011), but only overlaps with capture resonances of $^{182}W$ with moderate neutron capture cross sections (possibly $\sim10^2$ barns). Neutron capture reactions for $^{238}U$ and $^{182}W$ are discussed further in the appendix.

Prior studies have typically reported cosmogenic effects in W and Os in iron meteorites, some of which have experienced high neutron fluences, consistent with their old exposure ages (hundreds of Ma), and Fe-rich bulk chemical compositions that are favorable for producing and moderating secondary neutrons. The possible W and Os cosmogenic effects suggested here for Richardton would be surprising, given that most CRE data indicate that chondrites experienced relatively low neutron fluences, compared to iron meteorites, and therefore should have negligible neutron capture effects. Compared to iron meteorites, chondrites have lower cosmic ray exposure ages (<100 Ma, and typically less than 50 Ma), and bulk chemical compositions that are less likely to produce secondary particles. Consistent with these general observations,

Richardton has a cosmic ray exposure age (23.4 Ma; Graf and Marti, 1995) that is considerably younger than iron meteorites with reported W cosmogenic effects (>60 Ma; Kruijer et al., 2012), and within the normal range of H chondrites. Some of the H chondrites reported here have higher cosmic ray exposure ages, but $\varepsilon^{182}$W within the normal range of the H4 and H5 chondrites. Therefore, it seems unlikely that this sample experienced a single-stage irradiation history similar to most iron meteorites. Instead, a more complicated irradiation history must be envisioned.

Kruijer et al., (2012) reported that one IIG iron meteorite, Tombigbee River, had a low exposure age, but significant W cosmogenic effects. They argued that this sample could have experienced a complex irradiation history. During an initial stage of irradiation, this sample was shielded at depth from primary cosmic rays (which determine the apparent exposure age), but not from thermal or epithermal neutrons, which result in $^{182}$W burnout. This same scenario could potentially explain the irradiation history of Richardton.

The W and Os isotopic compositions of Richardton reported here, the Mo isotopic composition reported by Worsham et al. (in review), and the U isotopic composition reported by Goldmann et al. (2015) are inconsistent with most H chondrites. Richardton appears to have formed on a separate parent body from other H chondrites. The Hf-W isotopic systematics indicate that Richardton experienced either earlier thermal metamorphism, cooling, and system closure than the other H chondrites examined here, or a higher epithermal neutron fluence. A future investigation of Pt isotopic compositions of H chondrite metal fractions may provide further evidence for which of the two explanations can account for the low $\varepsilon^{182}$W of

Richardton metal, as some isotopes of Pt are more sensitive dosimeter than Os isotopes, and have resonance integrals of $3500\pm100$ and $1350\pm100$ barns for target nuclides $^{191}$Ir and $^{193}$Ir ($^{191}$Ir(n,$\gamma$)$^{192}$Ir($\beta$-)$^{192}$Pt and $^{193}$Ir(n,$\gamma$)$^{194}$Ir($\beta$-)$^{194}$Pt).

### 4.6.7. Formation of CR2 Chondrite Metal

The measured $\varepsilon^{182}$W of Acfer 395 metal is $-2.11\pm0.16$, which is much more radiogenic than the H chondrite metal fractions. Also unlike the H chondrite metal fractions, the CR chondrite metal fraction has a $\varepsilon^{183}$W nucleosynthetic anomaly. This complicates determining a precise formation age from $\varepsilon^{182}$W, because $\varepsilon^{182}$W is likely also abnormal as a result of a nucleosynthetic effect. The resolvably higher $\varepsilon^{183}$W of the CR2 chondrite metal fraction is consistent with a nucleosynthetic s-process deficit. Nucleosynthetic $^{183}$W anomalies have also been previously reported for Allende (CV3) chondrules and matrix (Budde et al., 2016), and were argued to be the result of different proportions of presolar material distributed among the components. The nucleosynthetic s-process deficit of CR2 chondrite metal reported here could also be the result of disproportionate amounts of presolar material among CR chondrite components. Using the measured $\varepsilon^{183}$W and the slope of the $\varepsilon^{182}$W-$\varepsilon^{183}$W correlation reported by Budde et al. (2016) for Allende components leads to a decrease in $\varepsilon^{182}$W. The nucleosynthetic-corrected $\varepsilon^{182}$W of Acfer 395 metal is $-2.8\pm0.2$, which overlaps within uncertainties of most H chondrites measured here. The calculated metal model age using the corrected $\varepsilon^{182}$W is reported in Table 4.5 and shown in Fig. 4.5b. Even after a large correction for a nucleosynthetic effect, the age does not overlap with CAI formation, indicating that CR chondrite metal did not form by direct condensation from

nebular gas, which was proposed by some previous studies (e.g., Campbell and Humayun, 2004). Instead, the metal must have formed by a later process, such as reduction of FeO in silicates, or localized evaporation followed by condensation during chondrule formation (e.g., Connolly et al., 2001).

### 4.7. Conclusions

The Hf-W systematics and HSE abundances of metal and silicate fractions indicate that diffusion of siderophile elements from silicates-oxides to metals was limited. There is no clear correlation between metamorphic grade and extent of HSE equilibration. Combined metal-silicate Hf-W data do not form precise linear regressions. Instead, metal fractions plot below linear regressions of nonmagnetic and slightly magnetic fractions for all but one H chondrite examined, indicating that equilibration was incomplete. Combined metal-silicate Hf-W data therefore do not have clear chronological meaning. By contrast, the slightly magnetic and nonmagnetic fractions form precise isochrons (MSWD<2), and therefore provide chronological evidence for the thermal history of the H chondrite parent body or bodies.

In contrast to the Hf-W data for H chondrites reported by Kleine et al. (2008), the Hf-W data for H chondrites reported here are inconsistent with the onion shell thermal model. Instead, the new data are more consistent with major disruption, possibly by impact, of the H chondrite parent body before cooling below the Hf-W closure temperature of ~800ºC. The discrepancy between our study and the previous study reflects sampling, as Kleine et al. (2008) investigated meteorites that were from

a well-studied H chondrite suite that was probably not representative of the H chondrite population (Scott et al., 2014).

Metal from Richardton (H5) has the lowest $\varepsilon^{182}W$ of any H chondrite measured here. Richardton metal also has different Os and Mo (Worsham et al., in review) isotopic compositions from other H chondrite metal fractions. One possible explanation for this is that Richardton experienced earlier thermal metamorphism on a parent body that was separate from the parent body of the other H chondrites and formed earlier. Alternatively, Richardton metal experienced a large neutron fluence, modifying the W and Os isotopic compositions. Regardless of the true nature of the processes that established the $^{182}W$ isotopic compositions of the metal, the Mo isotopic compositions (Worsham et al., in review) indicate that Richardton samples a parent body that is different from other H chondrites.

The W isotopic composition of metal from CR chondrite Acfer 395 is consistent with a nucleosynthetic s-process depletion. The nucleosynethic-corrected model age for Acfer 395 does not overlap with CAI formation, and therefore the metal does not appear to have formed by condensation from nebular gas. Instead, CR chondrite metal must have formed by a later process.


## 4.A. Appendix

*Richardton (H5): Neutron Capture on $^{182}W$ and $^{238}U$*

Unless shielded, meteorites are exposed to solar and galactic cosmic rays on their parent bodies and during their transit to Earth as smaller meteoroids. During spallation reactions on the surface, primary cosmic rays, which are typically high

energy (0.1-10 GeV) α particles and protons produce a variety of secondary particles near the surface, including secondary protons, isotopes of noble gases, and secondary neutrons. Secondary neutrons can be slowed by elastic scattering to thermal (<0.1 eV) and epithermal (0.1-300 eV) energies as they pass through the parent body or meteoroid.

Nuclides can capture free neutrons and form a compound nucleus. After capturing a neutron, nuclides reach ground state by gamma ray emission, ejection of nucleons, or fission. Isotopes of W and Os typically reach ground state through gamma ray emission (e.g., $^{189}Os(n,\gamma)^{190}Os$. The probability that a nuclide will accept a free neutron is described by its neutron capture cross section in barns ($10^{-24}$ $cm^2$). Neutron capture cross sections are primarily a function of the energy of the projectile neutron. In the thermal energy region, the cross section is directly proportional to the energy of the projectile neutron ($1/v$). By contrast, in the epithermal energy region, oscillating capture resonances (peaks in Fig. 4.A1a and 4.A1b) exist with enhanced cross sections (Fig. 4.A1a and b). Because of the capture resonances of the epithermal region, two different nuclides (e.g., $^{182}W$ and $^{238}U$) could experience the same energy spectra of epithermal neutrons and have very different probabilities for neutron capture reactions, if the energy spectra overlaps with more resonances of one nuclide than the other.
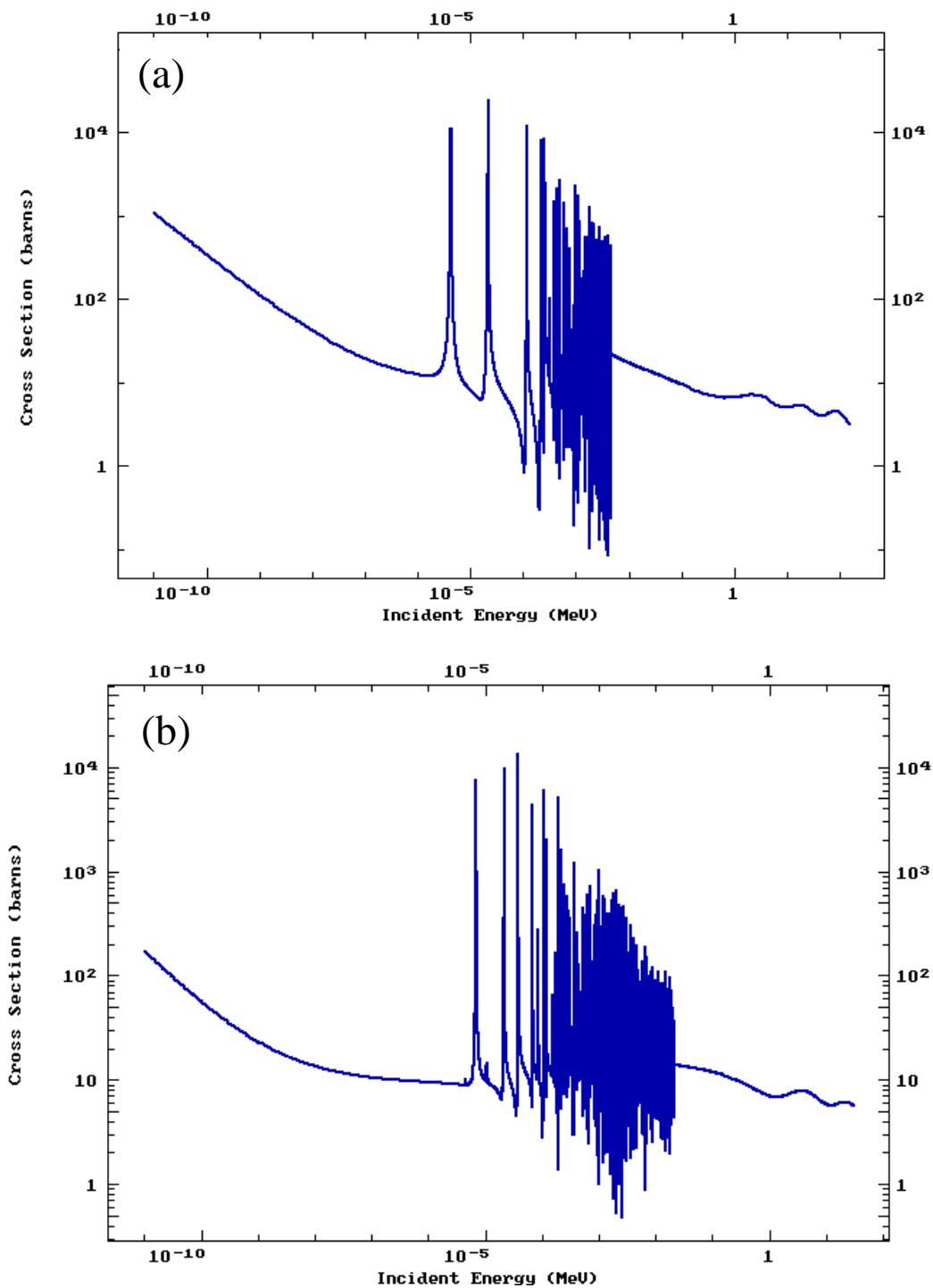
Figure 4.A.1. Cross section (in barns) vs incident energy for all neutron capture reactions on (a) [182]W and (b) [238]U. Taken from ENDF database (Chadwick et al., 2011). Thermal and epithermal cross sections discussed in text.

*Avanhandava (H4): Extreme Disequilibrium or Contamination*

Linear regressions of the Avanhandava (H4) nonmagnetic fractions define a $^{182}W/^{184}W_i$ that is ~300 ppm higher than the $^{182}W/^{184}W$ of the magnetic fractions, which should define the $^{182}W/^{184}W_i$ of this sample if it reached equilibrium during diffusive exchange of W between silicates and metal fractions. The difference for this sample is considerably larger than the difference for all other H chondrites. Further, the $^{182}W/^{184}W_i$ from linear regression of the nonmagnetic fractions is 0.8648995 or $\varepsilon^{182}W$ = -0.01, well within uncertainty of terrestrial W ($\varepsilon^{182}W$ = 0). Therefore, it is possible that the linear regression for Avanhandava nonmagnetic fractions is a mixing line between terrestrial W and a radiogenic-rich Avanhandava endmember, and that the linear regression has no chronological significance.

To test this, typically 1/W vs. $\varepsilon^{182}W$ would be plotted and a mixing line would be revealed in the case of two component mixing. However, this test is inappropriate for these fractions because 3 of the 4 fractions have nearly the same Hf concentrations (within 2.3%) and the other fraction has only 17% higher Hf abundance. Therefore, a linear correlation of 1/W vs. $\varepsilon^{182}W$ is meaningless because $\varepsilon^{182}W$ must correlate with W abundance with a fixed Hf abundance.

Kleine et al. (2008) argued that that phases of H chondrites can be binned into at least 3 components (Fig. 4.A2) for Hf and W, and that the linear regressions they reported in that study could therefore not be mixing lines. If we consider the addition of a 4th component (a terrestrial contaminant), a two component mixture is even less likely.

The larger difference in metal $^{182}W/^{184}W$ and $^{182}W/^{184}W_i$ calculated from nonmagnetic fractions of Avanhandava, compared to the other H chondrites, could be the result of less equilibration, and a smaller fraction of radiogenic W diffusing from the silicates into the metal. This would be consistent with the H4 chondrite having experienced the lowest degrees of thermal metamorphic heating, and therefore lowest degree of equilibration. Prior studies have argued that the H4 chondrites may have never been heated to the closure temperature of Ca-rich pyroxene (Kleine et al., 2008), which is the most significant carrier of Hf and radiogenic W in H chondrites. Therefore, the W of nonmagnetic fractions and metal may have never reached even partial equilibrium, and silicates and metals therefore have very different $^{182}W/^{184}W_i$.

Because of the lack of equilibration, the Hf-W isotopic systematics of Avanhandava nonmagnetic fractions may reflect an essentially metal-free system. The high initial is therefore the result of radiogenic ingrowth of $^{182}W$ in a system with a higher Hf/W than chondritic, because W is primarily hosted in the metal. In order to reach the initial $^{182}W/^{184}W$ by 8.9 Ma after CAI formation, the $^{180}Hf/^{184}W$ ratio of the nonmagnetic fractions (bulk-metal) must have been ~3, whereas chondritic $^{180}Hf/^{184}W$ for carbonaceous chondrites is ~1.23 (Kleine et al., 2004).
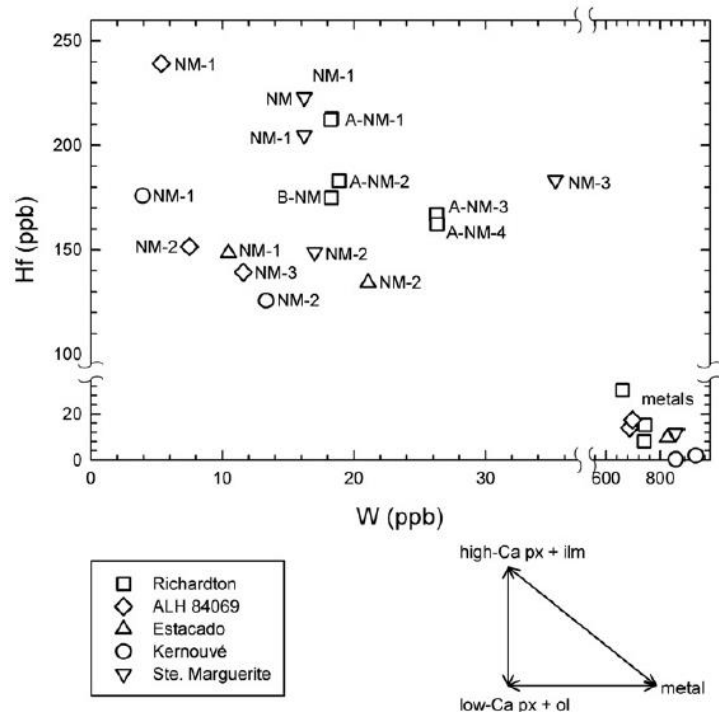
Figure 4.A.2. Components of H chondrites for Hf and W. Figure taken from Kleine et al. (2008).

*References for Chapter 4*

Allègre, C.M., Luck, J.-M., (1980) Osmium isotopes as petrogenetic and geological tracers. *Earth Planet. Sci. Lett.* **48**, 148–154.

Archer G.J., Ash R.D., Bullock E.S., and Walker R.J. (2014) Highly siderophile elements and [187]Re-[187]Os isotopic systematics of the Allende meteorite: Evidence for primary nebular processes and late-stage alteration. *Geochim. Cosmochim. Acta* **131**, 402-414.

Archer G.J., Mundl A., Walker R.J., Worsham E.A., and Bermingham K. (2016) High-precision analysis of [182]W/[184]W and [183]W/[184]W by negative thermal ionization mass spectrometry: Per-integration oxide corrections using measured ^{18}O/[16]O. *Int. J. Mass Spec.*, in review.

Becker H., Morgan J. W., Walker R. J., MacPherson G. L., and Grossman J. N. (2001) Rhenium–osmium systematics of calcium–aluminum-rich inclusions in carbonaceous chondrites. *Geochim. Cosmochim. Acta* **65**, 3379–3390.

Birck J.L., Barman M.R., and Capmas, F. (1997) Re–Os isotopic measurements at the femtomole level in natural samples. *Geostand. Newsl.* **21**, 19–27.

Blackburn T., Alexander C., Carlson R.C., and Elkins-Tanton L., The accretion and impact history of the ordinary chondrite parent bodies. *Geochim. Cosmochim. Acta.* In review.

Borisov A. and Palme H. (1995) The solubility of iridium in silicate melts: new data from experiments with $Ir_{10}Pt_{90}$ alloys. *Geochim. Cosmochim. Acta* **59**, 481–485.

Brandon A.D., Puchtel I.S., Walker R.J., Day J.M.D., Irving, A.J., and Taylor L.A. (2012) Evolution of the martian mantle inferred from the $^{187}Re$-$^{187}Os$ isotope and highly siderophile element abundance systematics of shergottite meteorites. *Geochim. Cosmochim. Acta* **76**, 206-235.

Brenan J.M., Bennett N.R., and Zajacz Z. (2016) Experimental results on fractionation of the highly siderophile elements (HSE) at variable pressures and temperatures during planetary and magmatic differentiation. *Rev. Mineral. Geochem.* **81**, 1–87.

Burkhardt C., Kleine T., Dauphas N., and Wieler R. (2012a) Nucleosynthetic tungsten isotope anomalies in acid leachates of the Murchison chondrite: implications for hafnium-tungsten chronometry. *Astrophys. J. Lett.* **753**, L6.

Burkhardt C., Kleine T., Dauphas N. and Wieler R. (2012b) Origin of isotopic heterogeneity in the solar nebula by thermal processing and mixing of nebular dust. *Earth Planet. Sci. Lett.* **357–358**, 298–307.

Burkhardt C., Schönbächler M. (2015) Intrinsic W nucleosynthetic isotope variations in carbonaceous chondrites: Implications for W nucleosynthesis and nebular vs. parent body processing of presolar materials. *Geochim. Cosmochim. Acta* **165**, 361-375.

Budde G., Kleine T., Kruijer T.S., Burkhardt C., Metzler K. (2016) Tungsten isotopic constraints on the age and origin of chondrules. *Proceedings of the National Academy of Sciences* **113**, 2886-2891

Campbell A. J. and Humayun M. (2004) Formation of metal in the CH chondrites ALH 85085 and PCA 91467. *Geochim. Cosmochim. Acta* **68**, 3409–3422.

Chadwick M.B., Herman M., Oblozinsky P., Dunn M.E., Danon Y., Kahler A.C., Smith D.L., Pritychenko B., Arbanas G., Arcilla R., Brewer R., Brown D.A., Capote R., Carlson A.D., Cho Y.S., Derrien H., Guber K., Hale G.M., Hoblit S., Holloway S., Johnson T.D., Kawano T., Kiedrowski B.C., Kim H., Kunieda S., Larson N.M., Leal L., Lestone J.P., Little R.C., McCutchan E.A., MacFarlane R.E., MacInnes M., Mattoon C.M., McKnight R.D., Mughabghab S.F., Nobre G.P.A., Palmiotti G., Palumbo A., Pigni M.T.,

Pronyaev V.G., Sayer R.O., Sonzogni A.A., Summers N.C., Talou P., Thompson I.J., Trkov A., Vogt R.L., van der Marck S.C., Wallner A., White M.C., Wiarda D., Young P.G. (2011) ENDF/B-VII.1 Nuclear data for science and technology: cross sections, covariances, fission product yields and decay data. *Nucl Data Sheets* **112**(12):2887–2996

Cherniak D. J. and Van Orman J. A. (2014) Tungsten diffusion in olivine. *Geochim. Cosmochim. Acta* **129**, 1–12.

Chou C.-L., Baedecker P.A. and Wasson J.T. (1973) Distribution of Ni, Ga, Ge and Ir between metal and silicate portions of H group chondrites. *Geochim. Cosmochim. Acta* **37**, 2159–2171.

Clayton R.N., Onuma N., and Mayeda T.K., (1976) A classification of meteorites based on oxygen isotopes. *Earth Planet. Sc. Lett.* **30**, 10-18.

Cohen A.S. and Waters F.G. (1996) Separation of osmium from geological materials by solvent extraction for analysis by thermal ionisation mass spectrometry. *Anal. Chim. Acta* **332**, 269–275.

Connolly H.C., Huss G.R., and Wasserburg G.J. (2001) On the formation of Fe-Ni metal in Renazzo-like carbonaceous chondrites. *Geochim. Cosmochim. Acta* **65**, 4567–4588.

Creaser R.A., Papanastassiou D.A., and Wasserburg G.J. (1991) Negative thermal ion mass spectrometry of osmium, rhenium and iridium. *Geochim. Cosmochim. Acta* **55**, 397–401.

Dauphas N. and Chaussidon M. (2011) A Perspective from Extinct Radionuclides on a Young Stellar Object: The Sun and Its Accretion Disk. *Annual Review of Earth and Planetary Sciences* **39**, 351-386.

Fortenfant S.S., Günther D., Dingwell D. B. and Rubie D. C. (2003) Temperature dependence of Pt and Rh solubilities in a haplobasaltic melt. *Geochim. Cosmochim. Acta* **67**, 123–131.

Ganguly J., Tirone M., Chakraborty S., and Domanik K. (2013) H chondrite parent asteroid: A multistage cooling, fragmentation and re-accretion history constrained by thermometric studies, diffusion kinetic modeling and geochronological data. *Geochim. Cosmochim. Acta* **105**, 206–220.

Goldmann A., Brennecka G., Noordmann J., Weyer S., and Wadhwa M. (2015) The uranium isotopic composition of the Earth and the Solar System. *Geochim. Cosmochim. Acta* **148**, 145–158.

Graf T. and Marti K. (1995) Collisional history of H chondrites. *J. Ceophys. Res.* **100**, 21-247.

Harrison K. P. and Grimm R. E. (2010) Thermal constraints on the early history of the H-chondrite parent body reconsidered. *Geochim. Cosmochim. Acta* **74**, 5410–5423.

Harper C.L. and Jacobsen S.B. (1996) Evidence for $^{182}$Hf in the early Solar System and constraints on the timescale of terrestrial accretion and core formation, *Geochim. Cosmochim. Acta* **60**, 1131–1153.

Henke S., Gail H.-P., Trieloff M., Schwarz W. H. and Kleine T. (2012) Thermal history modeling of the H chondrite parent body. *Astron. Astrophys*. **545**, A135.

Horan M.F., Walker R.J., Morgan J.W., Grossman J.N., and Rubin A. E. (2003) Highly siderophile elements in chondrites. *Chem. Geol*. **196**, 5-20.

Horan M. F., Alexander C. M. O'D., and Walker R. J. (2009) Highly siderophile element evidence for early Solar System processes in components from ordinary chondrites. *Geochim. Cosmochim. Acta* **73**, 6984-6997.

Humayun M. and Campbell A.J. (2002) The duration of ordinary chondrite metamorphism inferred from tungsten microdistribution in metal. *Earth Planet. Sci. Lett.* **198**, 225–243.

Huss G.R., Rubin A.E. and Grossman J.N. (2006) Thermal metamorphism in chondrites. In *Meteorites and the Early Solar System II* (eds. D. S. Lauretta and H. Y. McSween). The University of Arizona Press, Tucson, pp. 567–586.

Kadlag Y. and Becker H. (2016) $^{187}$Re-$^{187}$Os systematics, highly siderophile and chalcogen element abundances in the components of unequilibrated L chondrites. *Geochim. Cosmochim. Acta* **172**, 225-246.

Keil K (2000) Thermal alteration of asteroids: Evidence from meteorites. *Planet. Space Sci.* **48**: 887–903.

Kimura, K., Lewis, R.S., and Anders, E. (1974) Distribution of gold and rhenium between nickel– iron and silicate melts: implications for the abundance of siderophile elements on the Earth and Moon. *Geochim. Cosmochim. Acta* **38**, 683–701.

Kleine T., Münker C., Mezger K., and Palme H. (2002) Rapid accretion and early core formation on asteroids and the terrestrial planets from Hf–W chronometry. *Nature* **418**, 952–955.

Kleine, T., Mezger K., Münker C., Palme H. and Bischoff, A. (2004) $^{182}$Hf-$^{182}$W isotope systematics of chondrites, eucrites, and martian meteorites: chronology of core formation and early mantle differentiation in Vesta and Mars. *Geochim. Cosmochim. Acta* **68**, 2935–2946.

Kleine T., Mezger K., Palme H., Scherer E., Münker C., (2005) Early core formation in asteroids and late accretion of chondrite parent bodies: evidence from $^{182}$Hf–$^{182}$W in CAIs, metal-rich chondrites and iron meteorites. *Geochim. Cosmochim. Acta* **69**, 5805–5818.

Kleine T., Touboul M., Van Orman J.A., Bourdon B., Maden C., Mezger K. and Halliday A., (2008) Hf–W thermochronometry: closure temperature and constraints on the accretion and cooling history of the H chondrite parent body. *Earth Planet. Sci. Lett.* **270**, 106–118.

Kleine T., Hans U., Irving A.J. and Bourdon B. (2012) Chronology of the angrite parent body and implications for core formation in protoplanets. *Geochim. Cosmochim. Acta* **84**, 186–203.

Kong P. and Ebihara M. (1996) Distribution of W and Mo in ordinary chondrites and implications for nebular and parent body thermal processes. *Earth Planet. Sci. Lett.* **137**, 83–93.

Krot A. N., Meibom A., Weisberg M. K. and Keil K. (2002) The CR chondrite clan: Implications for early solar system processes. *Meteorit. Planet. Sci.* **37**, 1451–1490.

Kruijer T.S., Sprung P., Kleine T., Leya I., Burkhardt C., Wieler R. (2012) Hf–W chronometry of core formation in planetesimals inferred from weakly irradiated iron meteorites. *Geochim. Cosmochim. Acta* **99**, 287–304.

Kruijer T.S. (2013) Hf-W chronology of planetary accretion and differentiation at the dawn of solar system history. PhD thesis. ETH.

Kruijer T.S., Fischer-Gödde M., Kleine T., Sprung P., Leya I., and Wieler R. (2013) Neutron capture on Pt isotopes in iron meteorites and the Hf–W chronology of core formation in planetesimals. *Earth Planet. Sci. Lett.* **361**, 162–172.

Kruijer T.S., Touboul M., Fischer-Godde M., Bermingham K.R., Walker R.J. and Kleine T. (2014a) Protracted core formation and rapid accretion of protoplanets. *Science* **344**, 1150–1154.

Kruijer T.S., Kleine T., Fischer-Gödde M., Burkhardt C. and Wieler R. (2014b) Nucleosynthetic W isotope anomalies and the Hf-W chronometry of Ca-Al-rich inclusions. *Earth Planet. Sci. Lett.* **403**, 317–327.

Kruijer T.S., Kleine T., Fischer-Gödde M., Sprung P. (2015) Lunar tungsten isotopic evidence for the late veneer. *Nature* **520**: 534-537.

Lee D.C. and Halliday A.N. (1995) Hafnium–tungsten chronometry and the timing of terrestrial core formation. *Nature* **378**, 771–774.

Ludwig K.R. 2001. Users Manual for Isoplot/Ex version 2.47. A geochronological toolkit for Microsoft Excel. Berkeley Geochronology Center Special Publication 1a, 55pp.

Monnereau M., Toplis M.J., Baratoux D. and Guignard J. (2013) Thermal history of the H- chondrite parent body: implications for metamorphic grade and accretionary time-scales. *Geochim. Cosmochim. Acta* **119**, 302–321.

Mughabghab, S. F. (2003). Thermal neutron capture cross sections resonance integrals and g-factors. *Report, INDC (NDS)-440, IAEA NDS*.

Myers R.J. and Metzler D.E. (1950) The distribution of ferric iron between hydrochloric acid and isopropyl ether solutions. II. Polymerization of the iron in the ether phase, the effect of the acid concentration on the distribution, and two ether-phase region. *J. Amer. Chem. Soc.* **72**, 3772–3776.

Newsom H.E. (1990) Accretion and core formation in the Earth: evidence from siderophile elements. In *Origin of the Earth* (eds. H.E. Newsom and J.H. Jones) Oxford Univ. Press, New York, pp. 273–288.

Norris T.L., Gancarz A.J., Rokop D.J. and Thomas K.W. (1983) Half-life of $^{26}$Al. *J. Geophys. Res.* **88**, B331–B333.

O'Neill H.S.C., Dingwell D.B., Borisov A., Spettel B., and Palme H. (1995) Experimental petrochemistry of some highly siderophile elements at high temperatures, and some implications for core formation and the mantle's early history. *Chem. Geol.* **120**, 255–273.

Pellas R. and Storzer D. (1981) $^{244}$Pu fission track thermometry and its application to stony meteorites. *Proceedings of the Royal Society of London A: Mathematical, Physical and Engineering Sciences* **374**, 253–270.

Rambaldi E.R. (1976) Trace element of metals from L-group chondrites. *Earth Planet. Sci. Lett.* **31**, 224–238.

Rehkämper M., and Halliday, A. N. (1997) Development and application of new ion-exchange techniques for the separation of the platinum group and other siderophile elements from geological samples. *Talanta* **44**, 663-672.

Rubin A. E., Fegley B., and Brett R. (1988) Oxidation state in chondrites. In *Meteorites and the Early Solar System* (JF Kerridge, MS Matthews eds) The University of Arizona Press, Tucson, 488–511.

Rubin A.E. (2000) Petrologic, geochemical and experimental constraints on models of chondrule formation. *Earth Sci. Rev.* **50**, 3–27.

Rubin A.E., Ulff-Møller F., Wasson J.T., and Carlson W.D. (2001) The Portales Valley meteorite breccia: Evidence for impact-induced melting and metamorphism of an ordinary chondrite. *Geochim. Cosmochim. Acta* **65**, 323–342.

Scott E.R., Krot T.V., Goldstein J.I., and Wakita S. (2014). Thermal and impact history of the H chondrite parent asteroid during metamorphism: Constraints from metallic Fe–Ni. *Geochim. Cosmochim. Acta* **136**, 13-37.

Schönberg R., Kamber B.S., Collerson K.D., and Eugster O. (2002) New W-isotope evidence for rapid terrestrial accretion and very early core formation. *Geochim. Cosmochim. Acta* **66**, 3151–3160.

Shirey S. B. and Walker R. J. (1995) Carius tube digestion for low blank rhenium-osmium analysis. *Anal. Chem.* **67**, 2136-2141.

Taylor G. J., Maggiore P., Scott E. R. D., Rubin A. E. and Keil K. (1987) Original structures, and fragmentation and reassembly histories of asteroids: evidence from meteorites. *Icarus* **69**, 1–13.

Touboul M., Kleine T., Bourdon B., Palme H., and Wieler R. (2007) Late formation and prolonged differentiation of the Moon inferred from W isotopes in lunar metals *Nature* **450**, 1206-1209.

Touboul M., Kleine T., Bourdon B., Van Orman J. A., Maden C. and Zipfel J. (2009) Hf-W thermochronometry: II. Accretion and thermal history of the acapulcoite-lodranite parent body. *Earth Planet. Sci. Lett.* **284**, 168-178.

Touboul M., Walker R.J. (2012) High precision measurement of tungsten isotopes by thermal ionization mass spectrometry. *Int. J. Mass Spectrom.* **309**, 109–117.

Trieloff M., Jessberger E. K., Herrwerth I., Hopp J., Fiéni C., Ghélis M., Bourot-Denise M. and Pellas P. (2003) Structure and thermal history of the H-chondrite parent asteroid revealed by thermochronometry. *Nature* **422**, 502–506.

Van Orman J.A., Grove T.L. and Shimizu N. (2001) Rare earth element diffusion in diopside: influence of temperature, pressure, and ionic radius, and an elastic model for diffusion in silicates. *Contrib. Mineral. Petrol*. **141**, 687–703.

Walker R.J. (2012) Evidence for homogenous distribution of osmium in the protosolar nebula. *Earth Planet. Sci. Lett.* **351-352**, 36-44.

Walker R.J., Horan M.F., Morgan J.W., Becker H., Grossman J.N., and Rubin A. (2002) Comparative $^{187}$Re–$^{187}$Os systematics of chondrites: Implications regarding early solar system processes. *Geochim. Cosmochim. Acta.* **66**:4187–4201.

Wasson, J.T. and Kallemeyn, G.W. (1988) Compositions of Chondrites. *Philosophical Transactions of the Royal Society of London* **325**, 535-544.

Weisberg M. K., Prinz M., Clayton R. N., Mayeda T. K., Grady M. M. and Pillinger C. T. (1995) The CR chondrite clan. *Proc. NIPR Symp. Antarct. Meteorit*. **8**, 11–32.

Weisberg M.K., McCoy T.J., and Krot A.N. (2006) Systematics and evaluation of meteorite classification. In *Meteorites and the Early Solar System II* (eds. D. S. Lauretta and H. Y. McSween). The University of Arizona Press, Tucson, pp. 19-52.

Willbold M., Elliott T., and Moorbath S. (2011) The tungsten isotopic composition of the Earth's mantle before the terminal bombardment. *Nature* **477**, 195-198.

Willis J. and Goldstein J. I. (1981) A revision of metallographic cooling rate curves for chondrites. *Lunar Planet. Sci.* **12B**, 1135–1143.

Wood J. A. (1967) Chondrites: Their metallic minerals, thermal histories, and parent planets. *Icarus* **6**, 1–49.

Worsham E. A., Bermingham K. R., and Walker R. J., Molybdenum and tungsten isotope evidence for diverse genetics and chronology among IAB iron meteorite complex subgroups. *Earth Planet. Sci. Lett.* In review.

Yin Q.Z., Jacobsen S.B., Yamashita K., Blichert-Toft J., Télouk P., and Albarède F. (2002) A short timescale for terrestrial planet formation from Hf–W chronometry of meteorites. *Nature* **418**, 949–952.

Yokoyama T., Rai, V.K. Alexander, C.M.O'D. Lewis, R.S., Carlson R.W., Shirey S.B., Thiemens M.H., Walker R.J. (2007) Osmium isotope evidence for uniform distribution of s- and r-process components in the early solar system. *Earth Planet. Sci. Lett.* **259**, 567–580.

Yokoyama T., Walker D. and Walker R. J. (2009) Low osmium solubility in silicate at high pressures and temperatures. *Earth Planet. Sci. Lett.* **279**, 165–173.

Van Orman J.A., Grove T.L., and Shimizu N. (2001) Rare earth element diffusion in diopside: influence of temperature, pressure and ionic radius, and an elastic model for diffusion in silicates. *Contrib. Mineral. Petrol.* **141**, 687–703.

Vockenhuber C., Oberli F., Bichler M., Ahmad I., Quitté G., Meier M., Halliday A.N., Lee D.C., Kutschera W., Steier P., Gehrke R.J., and Helmer R.G., 2004. New half-life measurement of [182]Hf: improved chronometer for the early solar system. *Phys. Rev. Lett.* **93**, 172501.

# Chapter 5: Summary and Future Work

## 5.1 Summary of Conclusions

The trace element and isotopic data reported here provide new constraints on the nature and timing of early planetary processes. Most of the planetary processes investigated appear to have been driven by internal heating of their respective parent bodies. Given the timing of these processes, within the first few Ma of Solar System history, the likely heat source was the decay of $^{26}$Al. By contrast, the formation of one sample investigated here was more likely driven by external heating, perhaps during near-surface impacts on the parent body.

The HSE abundances of the two ungrouped achondrites studied are consistent with earlier suggestions that a wide range of thermal conditions were experienced by diverse parent bodies at about the same time. These achondrites formed within ≤0.5 million years of each other, and within ~5 Ma of CAI formation, yet one body underwent extensive differentiation, while the other parent body underwent very limited melting. The nearly chondritic HSE abundances calculated for primitive achondrite NWA 6704 indicates that the parent body experienced thermal conditions that were insufficient to drive melting sufficient to allow metal segregation. By contrast, the highly depleted and fractionated HSE abundances of differentiated achondrite NWA 7325 indicate that its parent body experienced greater heating, resulting in complex planetary processes, including core formation, igneous processes, and late accretion. The difference in the extent of differentiation probably reflects a

size difference, as smaller parent bodies did not retain heat as efficiently as larger parent bodies, and therefore differentiation on smaller bodies was more limited.

Although they never melted, the H chondrites examined here originated from parent bodies that also experienced a wide range of thermal conditions. The parent bodies that produced the H chondrites studied here experienced relatively lower degrees of heating compared to the ungrouped achondrites, yet they nevertheless achieved sufficiently high temperatures to heavily metamorphose and partially equilibrate some H chondrites.

In order to investigate the Hf-W isotopic systematics of H chondrites, a new N-TIMS method was developed that can be used to measure $^{182}W/^{184}W$ and $^{183}W/^{184}W$ to precisions of ~±5 ppm, which is ~2-3x more precise than the most recently published method using N-TIMS that is capable of measuring $^{183}W/^{184}W$. The major advantage of this method, compared to the previous method utilized by the IGL (Touboul and Walker, 2012), is the capability to measure $^{183}W/^{184}W$, as variations in $^{183}W/^{184}W$ have been recently reported for some meteorites (e.g., Kruijer et al., 2014).

The HSE abundances and Hf-W isotopic systematics of H chondrites indicate that the thermal metamorphism they underwent did not fully chemically or isotopically equilibrate metals with silicates and oxides. However, the Hf-W isotopic systematics of silicates and oxides of some H chondrites form precise isochrons, indicating that silicates and oxides were in W isotopic equilibrium once the system cooled below their closure temperatures. In contrast to previous studies that supported an onion shell thermal model for the H chondrites, the new Hf-W data reported here for H4 and H5 chondrites are characterized by indistinguishable closure ages, which are inconsistent

144

with an onion shell thermal model. Instead, the data are consistent with disruption of the parent body before it cooled below ~800 ºC, the closure temperature of H4 chondrites (Kleine et al., 2008). The discrepancy between our observations and those of a previous study on Hf-W systematics of H chondrites (Kleine et al., 2008) is likely the result of a sampling bias.

The H5 chondrite Richardton has the lowest $\varepsilon^{182}$W of any H chondrite investigated here or by previous studies. Richardton must have originated from a parent body that was separate from the parent body of other H chondrites, given that the Mo isotopic composition of this meteorite differs from the Mo isotopic compositions of other H chondrites (Worsham et al., in review). Further, metal from Richardton has a $^{189}$Os isotopic composition that differs slightly from other H chondrites. Either this H chondrite formed on a parent body that experienced earlier thermal metamorphism, or it experienced a large flux of epithermal neutrons, which modified its W isotopic composition.

## *5.2 Further Research*

Collectively, the ungrouped achondrites may have sampled a large number of parent bodies that are underrepresented in our meteorite collections, and they are therefore an excellent resource for exploring an expanded variety of planetary bodies. Only a small fraction of ungrouped achondrites have so far been characterized for HSE and $^{187}$Re-$^{187}$Os isotopic systematics. Therefore, further projects characterizing the HSE and $^{187}$Re-$^{187}$Os systematics of ungrouped achondrites are needed to further

explore achondrite parent bodies that may have experienced widespread melting, core formation, igneous processes, and late accretion.

The Hf-W data for H chondrites indicates that metals did not achieve W isotopic equilibration with silicates during high degrees of thermal metamorphism (up to H6), although silicate phases appear to have reached W isotopic equilibration with each other. Prior studies have calculated model ages of metal segregation for iron meteorites, assuming that the metals and silicates achieved equilibration. Although the disequilibrium between metals and silicates in H chondrites reported here does not directly challenge this underlying assumptions of iron meteorite model ages, it does raise questions about the timing and extent of equilibration between metals and silicates during core formation.

To explore the nature of W equilibration between metals and silicates, an experimental study, similar to the Yokoyama et al. (2009) study for Os equilibration, could be performed. In such a study, pieces of a magmatic iron meteorite and a basalt could be heated and pressurized within experimental charges, and the degree of isotopic equilibration under different experimental conditions (time, temperature, and pressure) could be determined by measuring the isotopic compositions of experimental products. Alternatively, an investigation of the Hf-W isotopic systematics of a metal- and silicate-rich system that underwent melting and crystallization early in Solar System history could provide evidence for the nature of W equilibration. Ungrouped achondrite NWA 6704 would be a suitable candidate for such a study, because it was clearly melted and then crystallized, it contains abundant metal, and it has a nearly chondritic trace element composition, making it a good analogue for a chondritic parent body.

Metal from the H chondrite Richardton has an Os isotopic composition that is consistent with epithermal neutron capture, however the effect is small. Platinum isotopes have also been used previously as a cosmic ray dosimeter (Kruijer et al., 2013). Some isotopes of Pt ($^{192}$Pt and $^{194}$Pt) are more sensitive dosimeters than Os isotopes. Therefore, a study of the Pt isotopic composition of Richardton metal may provide clearer evidence for epithermal neutron capture.

*References for Chapter 5*

Kleine T., Touboul M., Van Orman J.A., Bourdon B., Maden C., Mezger K. and Halliday A., (2008) Hf–W thermochronometry: closure temperature and constraints on the accretion and cooling history of the H chondrite parent body. *Earth Planet. Sci. Lett.* **270**, 106–118.

Kruijer T.S., Fischer-Gödde M., Kleine T., Sprung P., Leya I., and Wieler R. (2013) Neutron capture on Pt isotopes in iron meteorites and the Hf–W chronology of core formation in planetesimals. *Earth Planet. Sci. Lett.* **361**, 162–172.

Kruijer T. S., Kleine T., Fischer-Gödde M., Burkhardt C. and Wieler R. (2014) Nucleosynthetic W isotope anomalies and the Hf-W chronometry of Ca-Al-rich inclusions. *Earth Planet. Sci. Lett.* **403**, 317–327.

Touboul M., and Walker R.J., 2012. High precision measurement of tungsten isotopes by thermal ionization mass spectrometry. *Int. J. Mass Spectrom.* **309**, 109–117.

Worsham E. A., Bermingham K. R., and Walker R. J., Molybdenum and tungsten isotope evidence for diverse genetics and chronology among IAB iron meteorite complex subgroups. *Earth Planet. Sci. Lett.* In review.

Yokoyama T., Walker D. and Walker R. J. (2009) Low osmium solubility in silicate at high pressures and temperatures. *Earth Planet. Sci. Lett.* **279**, 165–173.